Republic of Iraq

Quarterly Refereed Journal for Natural and Engineering Sciences

Issued by
Al-`Abbas Holy Shrine
International Al-`Ameed Centre for Research and Studies

Licensed by
Ministry of Higher Education
and Scientific Research

Fifth year, Nine volume, Issue 17 and 18
Ramadan 1440, Jun. 2019

Secretariat General
of Al-'Abbas
Holy Shrine

Al-Ameed Interna-
tional center
for Research and Studies

Print ISSN: 5721 – 2312
Online ISSN: 0083 – 2313
Consignment Number in the Housebook and Iraqi
Documents: 1996, 2014
Postal Code: 56001
Mailbox: 232

Al-Abbas Holy Shrine. International Al-`Ameed Centre for Research and Studies.

ALBAHIR : Quarterly Refereed Journal for Natural and Engineering Sciences \ Issued by Al-`Abbas Holy Shrine International Al-`Ameed Centre for Research and Studies. - Karbala, Iraq : Abbas Holy Shrine, International Al-`Ameed Centre for Research and Studies, 1436 hijri = 2015-

Volume : Illustrations ; 24 cm

Quarterly.- Fifth Year, Nine Volume, Issue 17 and 18 (June 2019)-

ISSN 5721-2312

Includes bibliographical references.

Text in English ; summaries in English and Arabic.

1. Science--Periodicals. A. title.

LCC : Q1.A1 A8365 2019 VOL. 9 NO. 17-18

DDC : 016.505

Cataloging Center And Information Systems / Library and House of Manuscripts of Al-Abbas Holy Shrine

Mobile: +9647602355555
+9647602323337
http://albahir.alkafeel.net
Email:albahir@alameedcenter.iq

Publication Conditions

In as much as Al-`Bahir- effulgent- Abualfadhal Al-`Abbas cradles his adherents from all humankind, verily Al-Bahir journal does all the original scientific research under the conditions below:

1. Publishing the original scientific research in the various scientific sciences keeping pace with the scientific research procedures and the global common standards; they should be written in English .
2. The research should not be published before under any means .
3. The research should adhere the academic commonalties; the first page maintains the title, researcher name /names, address, mobile number under condition that the name, or a hint , should never be mentioned in the context and keywords should be written in Arabic and English as there is an abstract in Arabic and English.
4. The Research studies should be delivered to us either via Journal website http://albahir.alkafeel.net , after filling the two standard format the first with the name of the researcher and the second without in Word .
5. The page layout should be (2)cm .
6. The font should be of (16 bold),Time New Roman, subtitles of (14 bold) and also the context.
7. The space should be single, indentation should not be, as 0 before, 0 after and no spacing, as 0 before, 0 after.
8. There should be no decoration and the English numeral should proceed to the last text.
9. Any number should be between two brackets and then measurement unit, for instance: (12) cm .
10. All sources and references should be mentioned at the end of the article and categorized in conformity with Modern Language Association (MLA), for instance : Name of Author/ Authors, Journal Name Volume Number, pages from - to, (year).
11. There should be a caption under a diagram in 10 dark, for instance: Fig(No.): Title or explanation. Similarly done with tables but over a diagram. for instance: Table(No.): Title or explanation.
12. Diagrams , photos and statics should be in colour with high resolution without scanning.

13. The marginal notes, when necessary, should be mentioned at the end of the article before the references.

14. Wherever there is the word “ figure” should be abbreviated as Fig. and table should be Table.

15. The pages never exceed 25 pages.

16- Rersearch chapers should be numbered as 1- Introduction and so on , if there is a subtile to the main tiltle , it is to be as 1.2 , 2.2 .

17. The Formulae should be written in Math Type.

18. All the ideas and thoughts reveal the mindset of the researcher not the journal and the article stratification takes technical standards.

19. All the articles are subject to the internet Turnitin , confidential reviewing to prove its academic merits , the processes are as follows :

20-

a- The researcher is notified that his paper is received within 14 days in maximum.

b- The article is to be sent to the researcher as soon as it does not meet the requirement of the publication conditions.

c- The researcher is notified that his article is accepted.

d- The articles need certain modification , as the reviewers state, are sent to the researchers to respond in a span of a month from the date of dispatch.

e- The researcher is to be notified in case the article is rejected.

f- The researcher is to be granted an edition containing his article.

21. Priorities are given in concordance to :

a. The articles participated in the conferences held by the publication institute.

b. The date of receiving.

c. The date of acceptance.

d. The importance and originality of the article.

e. The diversity of the fields the articles maintain in the meant edition.

22. The researchers should appeal to the modifications the language and scientific reviewers find in the articles.

23. The researcher should fill the promise paper having the publication rights of the Scientific Al-Bahir Journal and adhering to integrity conditions in writing a research study.

*Open Access publishing does have its cost; however, for this journal, no

In the Name of Allah

Most Merciful, Most Compassionate

Edition Word

Thanks to Allah for creating seven firmaments whose lowest part is of lenient waves and whose highest part goes with a saved heaven, it is alleviated high without a buttress, without a dowel to manage, then it is decorated with a beauty of planets and brilliant light. There are a moving lantern and a shining moon. Truly, peace and salute to the most honest prophet and messenger, the love of Him, the Evolver of the worlds, Muhammad and his immaculate progeny.

Now

Having exerted yourself to do something, you are called dexterous, and then having set people dumbstruck, you are called brilliant

As such the Bahir journal, peer reviewed, sets itself the task to expand the scientific scope of its interests to bring its specialized message into effect through various publications of scientific fields. In time, it cleaves itself to be prominent between other journals to serve the society; academicians, students and specialized researchers. All heartedly, the journal calls for engineering and sheer scientific articles to cull its highest mission.

Such an edition, newborn achievement, is a threshold to proceed in its pathway to solidify the scientific research orbits on scale of academic scientific standards.

A constellation of articles in engineering sciences, astronomy, chemistry, physiology and so forth. The current edition is the last one having two languages, Arabic and English, the coming ones, Insha'Allah, will be entirely in English, we do hope that such a shift gains heed of the researchers, which gives credence.

It is Him, success Guardian

Arabic Text Classification Using Maximum Weight Algorithm

*Zinah Abdulridha Abutiheen and **Ahmed H. Aliwy
**Kadhim S. Aljanabi
*Collage of Science, University of Kerbala, Iraq
**Collage of CS and Mathematic, University of Kufa, Iraq

Received Date: 5 / 2 / 2018
Accepted Date: 10 / 5 / 2018

الخلاصة

هناك العديد من خوارزميات التصنيف التي تطبق على قضايا تصنيف النصوص، الجزء الغالب هو تطبيقها على اللغة الانكليزية. على الجانب الاخر، قليل جدا من الباحثين طبق هذه الخوارزميات على اللغة العربية. اللغة العربية أصعب بكثير من اللغة الانكليزية وبالتالي معالجة اللغة العربية أكثر صعوبة وتحدي من اللغة الانكليزية. في هذا البحث خوارزمية Maximum Weight تطبق على النصوص العربية بعد المعالجة الاولية للنصوص حيث عدد النصوص (16757) ملفا عربيا نصيا يستخدم لأول مرة. بينت النتائج ان خوارزمية Maximum Weight يمكن ان تطبق على النصوص العربية حيث بلغت دقتها (83٪) بالمعدل، حيث تم استخدام 10-fold cross-validation لموثوقية نتائج هذا المصنف.

الكلمات المفتاحية

معالجة النصوص العربية، تصنيف النصوص، خوارزمية Maximum Weight

Abstract

Many algorithms of classification implemented to the issue of text categorization. A large portion of the work implemented in the English text. On the other hand, very few researchers implemented in the Arabic text. The nature of Arabic text is very different than English text, and the preprocessing of the Arabic text is extremely difficult and more challenging. In this paper, Maximum Weight (MW) algorithm applied after preprocessing on the Arabic dataset that consists of (16757) text files used for the first time. The results showed that MW is applicable to Arabic text, it reached about (0.83) on average. 10-fold cross-validation used to the reliability of the result.

Keywords

Exponentiated exponential Pareto distribution, reliability function, reversed hazard function.

1. Introduction

A huge amount of electronic texts is progressively accessible through the web and associations, making the process of retrieving data and information transforms into a genuine issue without great ordering and summarization of documents contents. Text or document classification is the solution for the issue. Numerous statistical learning technique implemented in the field of text classification. Text classification is the process of classifying text into predefined category belong to it depending on their contents. Text classification consists two phases: the first phase is preprocessing and the second phase is classification which cannot be applied without the first phase. In this paper, Maximum Weight applied on dataset after preprocessing that consists of Tokenization, Stop-words removal, Stemming, in addition to term weight[1].

Electronic text classification can significantly reduce human time and effort in arranging and organizing any type of electronic data.

Arabic corpus didn't as like as English corpus that commonly used such as Reuters dataset collection which has different versions. Arabic corpus lack of publicly available, for this reason,.a new corpus built from the Iraqi media consist of (16,757) documents manually classified into 5 different categories and can be used in future where it published on the internet.

Another difficulty is the nature of morphology Arabic that creates ambiguity in the text, the process of electronic text classification depends on the contents of documents. For this reason, Arabic documents classification is very difficult [2]. The Arabic language is very rich in its vocabulary where there is word has many of meanings, we can be extracted to one meaning using the stemming algorithm, and can be reduced of the dimensionality of the term space using feature selection.

There are many algorithms used for Arabic document classification as Decision Trees, K-Nearest Neighbor, Naïve Bayes, Maximum Entropy, and others which give good accuracy.

K Nearest Neighbor, Naïve Bayes, Multinomial Logistic Regression, and Maximum Weight on same data set. The results of these classifier for one test is (78.903%), (80.334%), (76.937%), (81.585%) respectively.

In this paper, Maximum Weight classifier implemented on the dataset collected after preprocessing phase.

The outline of this section as the following: in section 2 text classification, then section 2.1 preprocessing (first stage in text classification process) that consists four steps, classification using Maximum Weight in section 2.2, the data set that applied classifier on it in section 3, then implementation and result in section 4, and conclusion and future work in section 5.

2. text classification

Text classification (TC) (also known as text categorization, topic spotting, document categorization, or document classification) is an important part of text mining (TM) and natural

language processing (NLP) that tries to replace and save human effort required in performing manual classification. It consists of assigning and labelling documents using a set of pre-defined categories based on their content. Categories selected from a previously established taxonomy[1].

There are two approaches to text categorization: rule-based, and machine learning-based. The rule-based approach means that the classification rules defined manually and documents classified based on these rules. Machine learning approach means that classification rules or equations defined automatically using sample labelled documents[3].

Text classification consists of two phases: the first phase is preprocessing that contains tokenization, stop-words removal, stemming, in addition to term weight. The second phase is classification by classifier. It explained in Fig. (1) below:

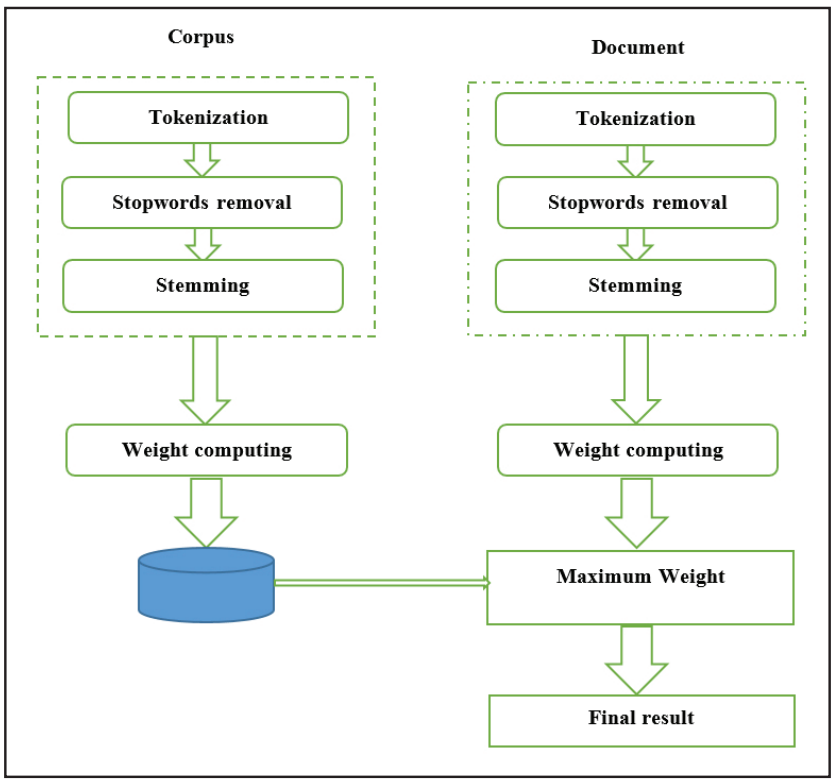

Fig (1): Methodology of Maximum Weight

2.1. preprocessing

Preprocessing represents the first step in TC. It is process prepared and format documents to be an input to machine learning techniques with high efficiency and accuracy. Documents should, firstly, be preprocessed which is an important stage in TC.

The aim of preprocessing is to reduce dimensions and to distinguish between the most important documents by selecting the significant or relative words and ignore the irrelevant words. This will convert the docu-

ments into the more suitable format can manipulate by computer.

The general idea of preprocessing explained in algorithm (1) below.

Algorithm 1: Preprocessing

Input: D: collection of documents

Output: V: collection of vectors

Step 1: for each document in D do:

- Tokenization
- Stop-Word Removal
- Stemming
- Calculate the weights of each word
- Add the vector of weights to V.
- End.

Algorithm (1): The general idea of preprocessing

Step 1: Tokenization

Tokenization is the first phase of preprocessing. It is the act of breaking up a sequence of strings into pieces such as words, keywords, phrases, symbols and other elements called tokens. In the process of tokenization, some characters like punctuation mark discarded. The tokens are the input for another process like parsing and text mining. Usually, tokens or words separated by white space, punctuation marks or line breaks that represent the boundary of words. All characters within contiguous strings are part of the token[4].

Step 2: Stop-Words Removal

Stop word removal is one of the most commonly used preprocessing steps across different NLP applications. The idea is simply removing the words that occur commonly across all the documents in the corpus and unimportant words that appear in a text such as an article or web page (i.e. pronouns, prepositions, conjunctions, etc.). Stop-word will be the word that sifted through earlier or after the handling of natural language processing (NLP). They are generally thought to be a "single set of words". It really can mean different things to different applications. For example, in some applications removing all stop words right from determiners (e.g. the, a, an) to prepositions (e.g. above, across, before) to some adjectives (e.g. good, nice) can be an appropriate stop word list. To some applications. However, this can be detrimental. For instance, in sentiment analysis removing adjective terms such as 'good' and 'nice' as well as negations such as 'not' can throw algorithms off their tracks. In such cases, one can choose to use a minimal stop list consisting of just determiners or determiners with prepositions or just coordinating conjunctions depending on the needs of the application. Finally, this phase consists of the following steps[5]:

i. Converting the documents into individual words stored in an array (Tokenization)

ii. Stop word removal. A comparison made

between the arrays received from step i and the array representing the stop word list, if a match is received, the word deleted from the array. Some fast search technique used by scanning the words array.

iii. Repeating step ii until all stop-words removed from the array.

This step can be speeded up by the used representation of stop list as a suffix tree.

According to this paper, the list of stop words is containing (16178) words that deleted from the text file, in addition to a list containing 169) words including correlatives, signal pronouns, prepositions, etc.

Step 3: Stemming

Different forms of a word often communicate essentially the same meaning. Stemming is the process for reducing inflected words to their word stem (base form) which can be removed any affixes (prefixes that added to the beginning of the word, infixes that added to the middle of the word, and suffixes that added to the ending of the word) from the words to reduce these words to their stems or roots under the assumption that words sharing the same stem. Thus, stemming process is merging those forms to the same stem. In other words, it is the process of reducing modulated words to their word stem, root or base. It is a hard stage in light of the fact that the word could have numerous determinations that change the stem itself, along these lines, it is difficult to recognize root letters and fasten letters[6].

There are two major approaches are very common in Arabic stemming: Light stemming (also called stem-based stemming) that removes prefixes and suffixes of words such as "Khoja stemmer" works well with this approach. And Root-based stemming (also called aggressive stemming) which reduces a word to its root [6].

In this, ISRI [7] has been used. It belongs to the Information Science Research Institute (ISRI) and shares many characteristics with Khoja stemmer, but it does not use a dictionary for word roots.

Step 4: Term Weight

There are many of methods for compute weight of feature subset selection are TF-IDF, Information Gain, Chi-Square, mutual information, and Gini index. In this paper, the method to select feature is TF-IDF where compute term frequency and inverse document frequency according to equation (1).

tf: Term Frequency $tf_{(t,d)}$ of term t in document d is defined as the number of times that t occurs in d.

idf: Inverse Document Frequency estimates the rarity of a term in the whole document collection. (If a term occurs in all the documents of the collection, its IDF is zero)

$$idf_i = log(\frac{\text{Number of documents}}{Number\ of\ documents\ that\ contain\ word\ i}) \quad \ldots(1)$$

TF-IDF combine the definitions of term frequency and inverse document frequency, to produce a composite weight for each term (t)

in each document that is calculated as follows:

$$\text{Weight}(t) = tf * idf \quad \ldots(2)$$

Each word with idf equal to zero is deleted when computing weights, thus reduces the size of the text file.

2.2. classification

After the preprocessing stage that mentioned in detail in the previous section, the data set is ready to input to the second stage from phases of text classification, which is techniques of classification that applying on the text. The classifier applies rules (may be learned from labelled data) on the input.

In this paper, Maximum Weight classifier has been used to classify Arabic text documents. The input for this classifier is the out-

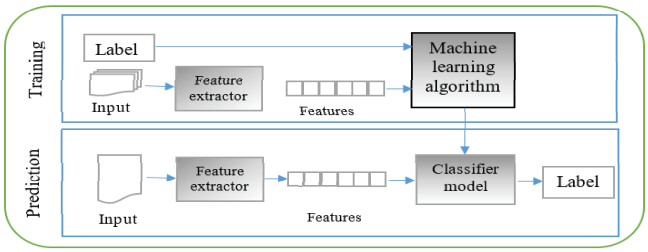

Fig (2): supervised classification

- **Maximum Weight**

Maximum Weight can be implemented simply where each feature will be related to one class not more, this help us where feature reduction is not matter for the same mentioned reason because each class has different subset of all features set and then feature reduction inclusively used. The algorithm (2) of this classifier is below:

algorithm 2: Maximum Weight

Input: set of classes C ={c_1,c_2 … c_n}; txtfwtr= dictionary of words and weight of it for traning data; txtfwts =test document

.**Output**: name of class

Step1: Let W_{imax}= maximum weight of the term i .among all these classes

Step2: Let C_{ij}= is a binary value which indicate the class j contain the maximum weight of the term i

Step3: **for** each word (w) in txtfwts **do**

for each class in C **do**

If (class contain w) **then**

Result=C_{ij} *W_{imax}

End for

Add result to dictionary

End for

.Name of class=argmax dictionary

Return name of class

.End

Algorithm (2): The algorithm of this classifier

3. corpus

Corpus used in this paper collected from Al Sabah newspaper. It is written in Arabic Language. It used for first time in machine learning. The corpus took a long of time to clean and arrangement and classified it manually. It consists of (16757) Arabic documents belong to 5 different categories (see Table (1)). Preprocessing implemented on it then MW classifier that is supervised learning; the

reform the corpus used for learning and evaluating the performance which is divided into two parts training and test data. (15080) documents (90%) is training data and (1677) documents is used for testing (10%).

Table (1): Dataset

Category	Total documents#	training documents#	testing documents #
Literature and Arts	2175	1957	218
Family and community	1017	915	102
Economy	3411	3070	341
Sport	8546	7691	855
Science and Technology	1608	1447	161
Total	16757	15080	1677

غياب أوين عن مانشستر يونايتد ستة أسابيع

16 /11 /2011 12:00 صباحا

بغداد –وكالات

أعلن نادي مانشستر يونايتد بطل الدوري الإنكليزي لكرة القدم في الموسم الماضي أن المهاجم مايكل أوين سيغيب عن الملاعب نحو ٦ أسابيع بداعي الإصابة.

وأوضح النادي أن أوين يaعاني من إصابة في ظهره تعرض لها خلال المباراة التي فاز فيها الفريق على غالاتي الروماني (٢-٠) قبل نحو أسبوعين ضمن مسابقة دوري أبطال أوروبا.وساهم أوين في صنع الهدف الأول بتمريرة جميلة إلى زميله الإكوادوري لويس انطونيو فالنسيا الذي وضعها في الشباك (٨).

من جانبه، قال المدرب الاسكتلندي أليكس فيرغوسون أن أوين الذي أصيب لدى قيامه بحركة صعبة للسيطرة على الكرة، «يعاني من تمزق عضلي وسيغيب ٦ أسابيع".

Fig. (3) Sample on Data Set

4. Implementation and Result

MW text classification algorithm on the new Arabic corpus after many stages from pre-processing (Tokenization, Stop-Words Removal, Stemming, Stop-Words Removal second time to reduce text file). In addition to compute weight of each term is calculated using.

The result of implement MW is (82.66%) in average where 10-fold cross validation to reliability of this classifiers. The result shown in Table (2). Below.

Table (2): Result of MW using 10-fold cross validation

Fold#	training files #	testing files #	MW
1	15080	1677	81.585%
2	15080	1677	83.13%
3	15080	1677	82.11%
4	15080	1677	74.84%
5	15080	1677	85.39%
6	15082	1675	83.363%
7	15082	1675	85.868%
8	15082	1675	83.304%
9	15082	1675	84.496%
10	15082	1675	82.469%

The accuracy of MW for 10 tests are explained in Fig. (4) below:

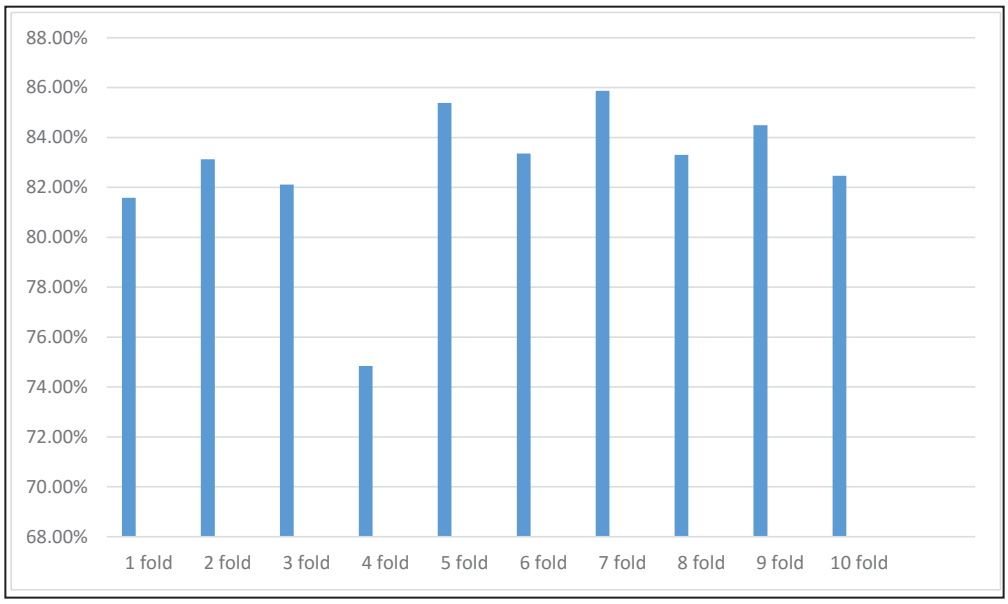

Fig. (4): Accuracy of Maximum Weight

5. Conclusion And Future Work

As we can see, the work focus on: (i) pre-processing Arabic text documents (ii) constructing a new Arabic corpus taken from Iraqi media which can be used by the researcher in the future, (iii) testing the corpus with a new classifier called Maximum Weight that proves efficiency and speedily.

In MW where each feature is relative to one class not more result in each class has its own features. In other words, each class has the different subset of all features set, and then feature reduction inclusively used. This algorithm tested with a new Arabic corpus. It can't be used for multi-class classification problems without modification.

It can be applied on anther dataset such as handwritten, social web, image, video, etc.

References

[1] A. Abu-Errub, "Arabic Text Classification Algorithm using TFIDF and Chi Square Measurements," International Journal of Computer Applications, vol. 93, (2014).

[2] A. Al-Badarenah, E. Al-Shawakfa, K. Al-Rababah, S. Shatnawi, and B. Bani-Ismail, "Classifying Arabic text using KNN classifier", (2016).

[3] P. Y. Pawar and S. Gawande, "A comparative study on different types of approaches to text categorization," International Journal of Machine Learning and Computing, vol. 2, p. 423, (2012).

[4] H. M. Dawoud, "Combining different approaches to improve Arabic text documents classification," MSc Thesis, Islamic University, (2013).

[5] J. K. Raulji and J. R. Saini, "Stop-Word Removal Algorithm and its Implementation for Sanskrit Language."

[6] A. S. A. Babiker, "Improving Stemming Algorithm for Arabic Text Search," Sudan University of Science and Technology, (2014).

[7] K. Taghva, R. Elkhoury, and J. Coombs, "Arabic stemming without a root dictionary," in Information Technology: Coding and Computing, 2005. ITCC 2005. International Conference on, pp. 152-157, (2005).

[8] S. Bird, E. Klein, and E. Loper, Natural language processing with Python: analyzing text with the natural language toolkit: " O'Reilly Media, Inc.", (2009).

Dielectrical Insulation of Polyvinyl Alcohol, Ethylene Glycol and Crushed Pomegranate Peel (PVA-EG-PP) Composite materials

Thamir Salman Bachari
Material Science Department, Polymer Research Centre, University of Basrah, Iraq.

Received Date: 18 / 5 / 2017
Accepted Date: 16 / 1 / 2018

الخلاصة

تم تحضير نماذج من مخلوط بولي فاينيل الكحول مع الأثلين كلايكول ومضاف مسحوق قشور الرمان المغربل. تم تشخيص مسحوق قشور الرمان والمخلوط باستخدام مطياف تحويلات فورير للأشعة تحت الحمراء. تم قياس قيم العزل الكهربائي. معاملات العزل الكهربائي مثل ثابت العزل، فقد العزل، سعة الفضاء الحر، المواصلة، التوصيل المتناوب والتوصيل المستمر. وجد ان نقص جدير بالاهتمام في فقد العزل الى 2.639 مع زيادة حجم حبيبات مسحوق قشور الرمان المغربل الى (600) مايكروميتر النموذج (4) ومختلف الدراسات اللاحقة لفاعلية انسجام مسحوق قشور الرمان مع البوليمرات. وجد زيادة في التوصيلية الكهربائية للنماذج (2) و (3) حجم حبيبات قشور الرمان (212) مايكروميتر و(300) مايكروميتر ونقص عند النموذج (4).

الكلمات المفتاحية

مخلوط، مضاف، تشخيص، عزل، السعة، الحث.

Vol. 9, No. 17 and 18, P. (23-36),Jun, 2019

Abstract

Samples are prepared from mixture of manufacture foam material polyvinyl alcohol with ethylene glycol (PVA-EG) and additive of crushed and sieved pomegranate peel (PP). Crushed pomegranate peel (PP) and the mixture are diagnosed by Fourier transforms infrared (FTIR) spectrophotometer. The electrical insulation parameters are measured. The dielectric parameters such as dielectric constant (ε′), dielectric loss factor (ε″), free space capacitance (Co), conductance (Gs), dependent conductivity (σac), and independent conductivity (σdc) have been investigation. There is a significant decrease in dielectric loss factor ε″ to 2.39 as the grain sizes of crushed and sieved (PP) increased to (600) μm sample (4), and various recent investigations of functionalization of PP fillers to improve compatibility with polymers. The electrical conductivities of composites are found to increase at sample (2) and (3) PP grain size (212) μm and (300) μm and decrease at sample (4).

Keywords

Mixture, Diagnosis, Insulation, capacitance, Inductance.

1. Introduction:

Applications of polymers have been increasingly used for many technical tasks, such as biopolymers, Copolymers and composites. Biopolymers may occur in natural or synthesis sources as proteins and carbohydrates and synthetically prepared as poly (lactic acid), polyvinyl alcohol (PVA), polyethylene glycol (PEG) etc. most natural biopolymers are degradable soon after treating to be used for industrial purposes [1]. Polymers composites have many lubricants, that can be used in various applications such as dielectric materials, Nano-sized conductor fillings, including grapheme nanoplatelets, can create a filter network inside the polymer matrix in low-weight part, while the presence of conductive nanoinclusions into a polymer matrix could alter the permittivity of the composite systems resulting in enhancement of their energy storing capability [2]. Pomegranate polyphenols are strong antioxidants and chemical protective factors but possess low availability and biological half-life. For example, punicalagin (PU), is the phenol in pomegranates, is not absorbed in its proper form and for those decomposed into ellagic acid (EA). The major polyphenols in pomegranate are decomposed to ellagic acid (EA) moieties and rapidly metabolized into short-lived metabolic product. A pomegranate contains many polyphenolic compounds with high antioxidant and free-radical-scavenging activity including flavonoids, condensed and hydrolyzed tannins, and hydrolyzed tannins (ellabitannins (ETs) and Gallo tannins). Encapsulation of ellagitannins (ETs) into biocompatible and biodegradable nanoparticles (NPs) may overcome their susceptibility to gastrointestinal hydrolysis, poor absorption, low systemic bioavailability and short half-life. The hypothesis that encapsulation of pomegranate polyphenols into biodegradable sustained release nanoparticles (NPs) may circumvent these limitations [3]. Chloroform is a volatile liquid has a molecular weight 119.38 with molecular formula $CHCl_3$ was supplied from Sd Fine chem.-limited, India. Polyvinyl alcohol (PVA) was hot water soluble supplied from HIMEDIA REF Laboratories Put ltd. India. PVA is a hydrophilic linear polymer, has molecular weight 89,000 to 98,000. Chemically and physically modified PVA with molecular formula -[CH_2-CHOH]- repeated unit, (C_2H_4O). Polymer systems have been developed due their high ionic conductivity and became main objectives in polymer research. Due to their potential applications as electrolytes in solid-state batteries, fuel cells, electrochemical display devices/smart windows, photochemical cells etc., according to their high conductivity, high energy density, wide electrochemical stability and easy process ability. The main advantages of polymer electrolytes are their mechanical behaviors, ease of fabrication of thin films of desirable sizes and their ability to form proper electrode/electrolyte in contact in electrochemical devices [4].

More over their studies of phase separation in thin films of binary mixtures is ef-

fective production and commercially important for different coatings and films, including insulating layers, photographic materials and paint systems. Film of polymer blends exhibit more desirable characteristics than individual homopolymer, many blends polymer components are also highly incompatible with each other, will remix and phase separate. The degree separation in polymer blends will greatly affect the resulting morphology, that can have adverse effects on the resulting film [5]. FTIR technique has attained high precision and accuracy in measurement to be sufficiently reproducible for most industrial; research and development purpose. Spectra from polymeric samples are usually relatively rapid and straightforward. Moreover, FTIR micro-spectroscopy combines the spatial specificity of microscopy with the powerful chemical specific of spectroscopy [6].

Ethylene glycol is a chemical commonly is used in many commercial and industrial applications including antifreeze in winter and coolant to reduce over heating in summer. The molecular formula of ethylene glycol is $HOCH_2OH$ or $C_2H_6O_2$ and its molecular weight is (62.067) g/mol, is a colorless, odorless, viscous dihydroxy alcohol. Bulk dielectric polymer film with an intrinsic ultralow dielectric constant at (10) kHz has been successfully synthesized based on a novel polyimide. More importantly, such outstanding dielectric properties remain stable up to (280) ^oC. The excellent ultra-low dielectric is mainly because of the large free volume (sub-nanoscale), that intrinsically exist in the amorphous region of polymeric materials [7]. The aim of the project is focused on the dielectric own quality of the composites, specifically the measurement of dielectric parameters and the dielectric properties are investigation.

2. Experiment Work

2.1. Manufacture of Foam Material of PVA

(10) gm of polyvinyl alcohol (PVA) powder supplied from HEMEDIA Laboratories, Ltd, India, has been weight by using Sartorius balance, Germany. (10%) concentration of PVA with (100) millimeter of distilled water have been emplaced into a bottom round flask was put into isomental heater and stirrer sort Heidolf, Germany is used to mix the mixture. The system operated with temperature has been raised between (92-98) ^oC as in Fig. (1). Each (15) minutes the system is stopped to measure the temperature by thermometer and the vapor steam is let out to avoid solidification of the material, continuation of the operating the system until a complete dissolve of PVA in time period one and half hour. The obtained product of foam material of PVA is collected in clean glass container as in Fig. (2).

Fig. (1): Setup of Manufacture foam material of PVA

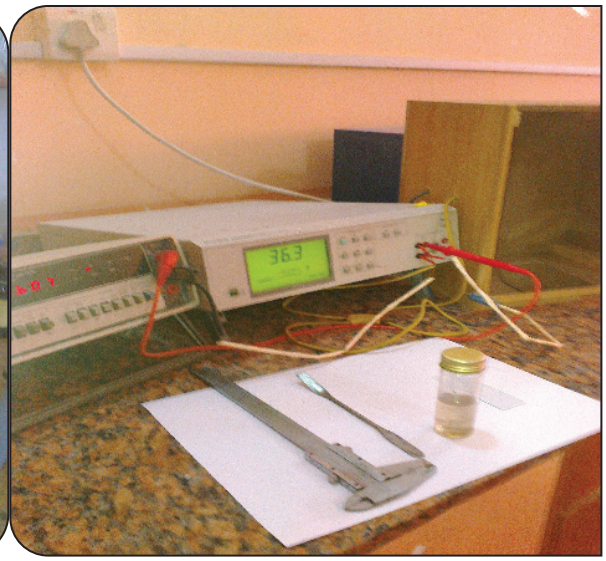

Fig. (2): Foam material of PVA and set up of measurements

2.2. Samples Preparation:

Glass substrates were emplaced in flask that is cleaned with distilled water for (10) minutes and was rinsed with acetone then is washed by distilled water. The glass substrates were put in vacuum furnace at (90) ^{o}C until they were dried. The furnace is put off and the clean glass substrate is left inside the furnace over night to let the temperature falls to room temperature and the clean glass substrates are taken out for use. Pomegranate peel (PP) was left to be dried in open air for two months. The dried pomegranate peel was crushed by stainless steel mortar and was kept in plastic container. The crushed PP. was sieved for different grains size, (75) µm, (212) µm, (300) µm, (600) µm and remaining from the last sieving is large than (600) µm grain size (2360) µm. Each weight (0.03) gm. of pomegranate peel particle size was dissolved in (0.025) mole of chloroform and mixed by spatula to ensure homogeneous solution; this is added and mixed with (0.092) mole polyvinyl alcohol (PVA). And (0.041) mole of ethylene glycol (EG) mixture, all the mixtures were deposited on the clean glass substrates as samples. Two copper electrodes were fastened at both ends of the films and left over night to be dried and to ensure the chloroform will be evaporated from the mixture. These specimens are subjected to dielectric measurements by using FLUKE PM (6303) RCL meter serial number 781003, Germany. The dimensions of the specimens and the cross sections of the tip vicinity have been measured with Vernier Caliper Certificate made in China. Table (1): indicates the samples preparation

Table (1): Samples preparation

PVA moles	EG moles	PP. grain sizes µm	Length of specimens .mm	Width of specimens .mm	Thickness of specimens .mm	Cross sectional area of the tip .vicinity mm^2
0.091	0.041	75	16.20	20.00	1.31	0.8
0.091	0.041	212	16.54	18.53	1.33	0.915
0.091	0.041	300	15.22	12.35	1.521	0.142
0.091	0.041	600	16.33	12.95	1.51	3.14
0.091	0.041	> 600	16.65	13.42	1.63	0.138

3. Calculations and Results:

3.1. Dielectrical Insulation

Dielectrical parameter measurements were included quality factor (Q), dissipation factor (D), impedance (Z), parallel resistance (Rp), series resistance (Rs), parallel capacitance (Cp), series capacitance (Cs) and phase shift (ϕ). Table (4) indicates the dielectric measurements and calculations. Dielectric constant (έ) and dielectric loss (ε̆) of samples were calculated using the following relations [8]:

$$'\varepsilon = Cs\frac{d}{\varepsilon oA} \qquad (1)$$

Where Cs: the series capacitance in pF

ε_o permittivity of free space $F.m^{-1}$. d: the thickness of sample mm.

A: cross sectional area of effective electrode area mm^2. Dielectric loss factor is given by [9]:

$$''\varepsilon = \frac{\varepsilon}{RpCpw} \qquad (2)$$

$$Rp = \frac{1}{DwCp} \qquad (3)$$

Where w: angular frequency 2πf. And f: frequency Hertz.

The free space capacitance

$$Co = \varepsilon o\frac{A}{d} \qquad (4)$$

Where ε_o: permittivity of free space $8.85*10^{-12}$ F m^{-1}.

A: electrode area mm^2

d: thickness of the electrode mm.

C_o is equal to $4.863*10^{-4}$ pF

Conductance is given by

$Gs = \varepsilon' Co\ \omega$ (5)

ac conductivity σac:

$\sigma ac = \varepsilon o\varepsilon'' w$ (6)

Total conductivity σt is:

$$\sigma t = Gs\frac{d}{A} \qquad (7)$$

3.2. Fourier Transforms Infrared (FTIR) Spectroscopy:

FTIR spectroscopy of crushed PP grain size (75) µm is carried out with kBr disc by using JASCO spectrophotometer (4200), serial No. C08176018, Japan. Spectra are

taken in wave number (400-4000) cm^{-1} as in Fig. (3). Band at (3410.98) cm^{-1} is the presence of stretching primary amines, band at (2928.76) cm^{-1} is due to secondary amines with corresponding vibration peak at (1615.57) and band at (1364.86) cm^{-1} corresponding to C-N stretching vibration aromatic group[10] and band at (1049.09) cm^{-1} is corresponding to C-H of alkanes, peak at (1445.39) cm^{-1} stretching vibration C-OH of protein and polyphenols and peak at (1731.760) cm^{-1} corresponding to C=O stretching vibration of flavonoids and amides[11], peak at (639) cm^{-1} alkenes[12]. Table (2) is the comparison of the obtained results with previous studies. FTIR spectroscopy of (PVA-EG-PP), for sample (1) at foam material of PVA (0.092) mole, EG (0.041) mole and crushed PP grain size (75) µm and 0.03 gm. in weight is dissolved in (0.025) mole of chloroform and added to the mixture (PVA-EG). The spectra have been carried out in wave number (400-4000) cm^{-1} as in Fig. (4) by using JASCO spectrophotometer (4200), serial No. (C08176018), Japan. Band at (3385.42) cm^{-1} attributed to OH [13], band at (2927.41) cm^{-1} related to the presence of –CH groups [14] and band at (1078.98) cm^{-1} is not noted and used as an indicator for PVA structure [15]. Peak (1727.42) cm^{-1} and peak (1616.54) cm^{-1} pomegranate peel powder [16] and peak (1364.39) cm^{-1} C-N complex reaction, Yang, et al [11]. Table (3) is the comparison of the obtained results with previous studies.

4. Results and Discussion:

FTIR test of pomegranate peel (PP) grain size (75) µm as shown in Fig. (3), have been investigated. Table (2) indicates the comparison between the obtained results with other studies, band (3410.98) cm^{-1} is primary amines, in comparison with Fig. (4); of PVA-EG-PP, Table (3) band (3385.42) cm^{-1} is determine OH. Peak at (1364.34) cm^{-1} for PVA-EG-PP is complex reaction took place between C-N. Table (4) Maximum calculated dielectric constant is ($2.47*10^3$) for sample (1) PP grain size (75) µm and minimum value is (16.301) for sample (4) PP grain size (600) µm. the dielectric constant decreases with increasing of PP grain size so that the giant dielectric constant is close to (75) µm of PP [17]. The maximum calculated dielectric loss factor is ($2.03*10^3$) for sample (1) and minimum value is (2.639) for sample (4). ε′ and ε″ are experimentally observable parameters and used to characterize dielectric dispersion over (1) kHz [18]. Dielectric constant measures the efficiency of an insulating material and is used to determine the ability of an insulator to store electric energy [19]. If a material is to be used for strictly insulating purposes, it would be better to have a lower dielectric loss. However, one of the major reasons for the choice of a particular dielectric material its dielectric constant. Those with high dielectric constant enable high values of capacitance to be achieved, each one having a different permittivity or dielectric constant. Free space capacitance Co value ($4.863*10^{-4}$) pF.

Maximum conductance is ($2.768*10^{-9}$) S for sample (1), and minimum ($4.97*10^{-11}$) S for sample (4), Maximum σac ($1.132*10^{-4}$) S m^{-1} for sample (1) and minimum ($1.46*10^{-7}$) S m^{-1} for sample (4). Maximum σdc is ($1.078*10^{-4}$) S m^{-1} samples (1) and minimum ($12.2*10^{-8}$) S m^{-1} Samples (4). Fig. (5) Indicates the relation between the dielectric constant ε′ and the series capacitance Cs, the decrease in Cs will cause decrease in ε′, consequently the larger relative permittivity is the larger resulting capacitance becomes as in sample (1) and (2), the important of the case is to maintain the conductance Gs. Fig. (6) Indicates the dependence of the ac conductivity on the dielectric loss factor ε″ according to the linear relationship the value of σac increase with increasing ε″. It is important to consider the losses in ac capacitors. The complex dielectric constant is usually defined as ε* = ε^'- jε''. The real part of permittivity ε′. It is a measure of how much energy from an electric field is stored in a material. ε″ is the imaginary part of permittivity. It is a measure of how dissipative or lossy a material is to an external field. The ratio (ε''/ϵ') is tanδ.[20]. Fig. (7), the dependant of the dielectric constant ε′ on PP grain size μm, the value of ε′ is decreased at sample (4) and alternatively cause decrease in values of Gs, σac and σdc. Fig. (8), the dependant of ε″ on PP grain size as the grain size increase ε″ decrease except at sample (4), is nearly the same as in Fig. (8). Fig. (9), indicates variation of the σac S m^{-1} with PP grain size μm, σac decreases as the PP grain size increases. Fig. (10), the variation of σdc S m^{-1} with particle size PP μm the variation gave a peak at sample (3), σdc is equal to ($8.58*10^{-4}$) S m^{-1} and electrical conductivity gradually decreases as the PP grain sizes increases, this is related to the complex dielectric constant, similarly complex AC conductivity consists of real and imaginary part [21]. Fig. (11) the variation of conductance Gs S with PP grain size μm, Gs decrease at sample (4) and (5) ($4.97*10^{-11}$) S and ($1.22*10^{-9}$) S. Fig. (12), the variation of total conductivity σt S m^{-1} with PP grain size μm there is increase at sample (3) (8.71*10-4 S m^{-1}). Capacitive reactance Xcs and inductive reactance X_L have been calculations. Generally, PP filler enhance the electrical conductivity and the polar behavior of PVA [22]. The dielectric behavior relates to the tendency for capacitance build-up, that is commonly involve electric polarization. The associated charge movement can be due to polar bond rotation, functional group movement etc. [23] the measurement of capacitance (as measured at 1 kHz) for the composites of the specimen's inclusion the effect of the two copper wires and the tip vicinity at the points of contact.

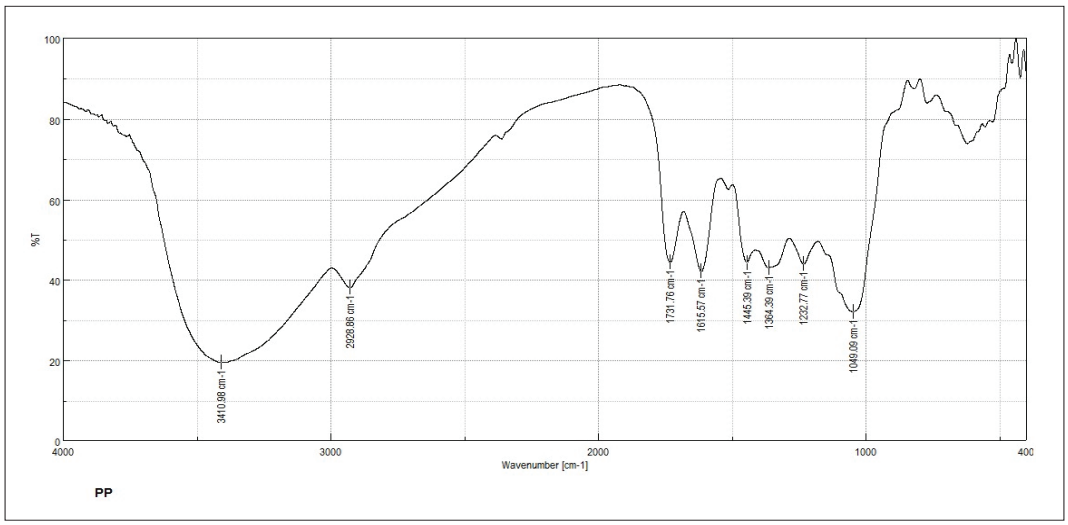

Fig. (3): FTIR spectroscopy of (75) µm Pomegranate Peel (PP)

Table (2): Comparison of the obtained results with previous studies

Functional group obtained results	Wave number cm^{-1}	Functional groups of reference	Wave number cm^{-1}
Primary amines	3410.98	Primary amines	ref.10,3371
Secondary amines	1615.57 ,2928.86	Secondary amines	ref. 10 ,2927
C-N stretching vibration aromatic groups	1364.86	C-N stretching vibration aromatic groups	ref. 10 ,1373
C-OH of alkenes	1049.09	C-OH of alkenes	ref. 11 ,1060
C-C stretching vibration of Aromatics	1445.39	C-OH stretching of protein and polyphenols	ref. 11 ,1616
C=O stretching vibrations of flavonoids	1731.76	C=O stretching vibrations of flavonoids	ref. 11 ,1724.90
Alkenes	639	Alkenes	ref, 12 ,698.23

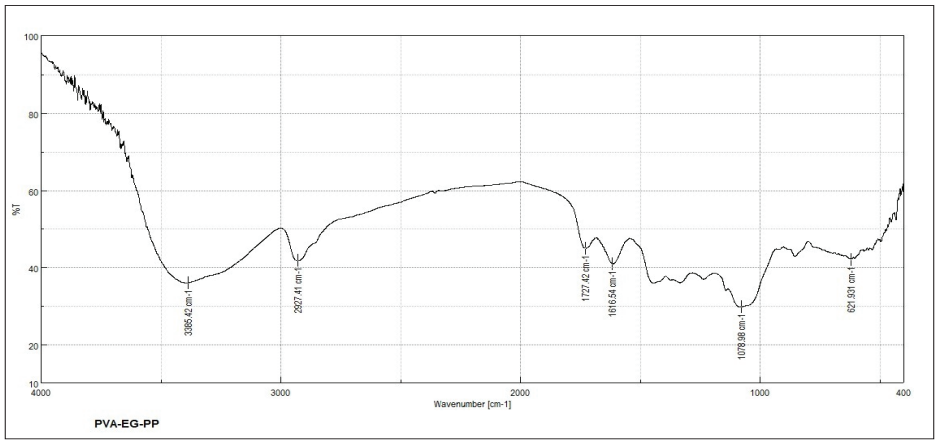

Fig. (4): FTIR of PVA-EG-PP

Table (3): The comparison of the obtained results with previous studies.

Functional groups of obtained results	Wave number cm^{-1}	Functional groups of references	Wave number cm^{-1}
OH	3385.42	OH	3391.21, ref. 13
-CH2 groups	2927.41	-CH2 groups	2940, ref. 14
Indicator for PVA structure	1078.98	Indicator for PVA structure	1150-1050, ref. 15
Pomegranate peel powder	1727.42, 1616.54	Pomegranate peel powder	1614, ref. 16
C-N complex reaction	1364.39	C-N complex reaction	1350.64, ref. 11

Samples	**Q**	**D**	**Rp MΩ**	**Rs MΩ**	**Z MΩ**	**Cp pF**	**Cs pF**	**Lp kH**	**Ls kH**
75µm PP.	1.07	0.847	33.32	36.3	71.95	5.8	4.9	7.4	3.038
212 µm PP.	1.24	0.912	28.8	22.6	73.6	6.9	8.9	7.42	2.382
300 µm PP.	1.07	1.01	788.2	-------	-------	0.2	0.3		
600 µm PP.	2.07	0.162	3278	-------	-------	0.3	0.3		
< 600 µm PP.	3.82	0.298	2673	--------	-------	0.2	0.3		
ε′	**ε″**	**Gs S**	**σac S m^{-1}**	**σdc S m^{-1}**	**σt S m^{-1}**	**Xcs MΩ**	**XL MΩ**	**ϕc**	**ϕL**
$9.06*10^{2}$	$10^{3}*2.03$	$10^{-9}*2.768$	$10^{-4}*1.132$	$10^{-4}*1.087$	$10^{-6}*4.532$	32.497	19.078	-69.9	68.0
$1.46*10^{2}$	$10^{3}*1.17$	$4.46*10^{-9}$	$6.5*10^{-5}$	$6.00*10^{-5}$	$6.65*10^{-4}$	17.891	14.958	-88.7	82.6
$3.6*10^{2}$	$10^{2}*2.44$	$8.81*10^{-9}$	$1.35*10^{-5}$	$10^{-4}*8.58$	$10^{-4}*8.71$	530	----	-84.2	------
16.301	2.639	$4.97*10^{-11}$	$1.46*10^{-7}$	$12.2*10^{-8}$	$2.39*10^{-8}$	530	----	-80.7	------
$3.99*10^{2}$	$10^{2}*1.18$	$10^{-9}*1.22$	$6.60*10^{-6}$	$0.78*10^{-5}$	$1.43*10^{-5}$	530	----	-76.2	------

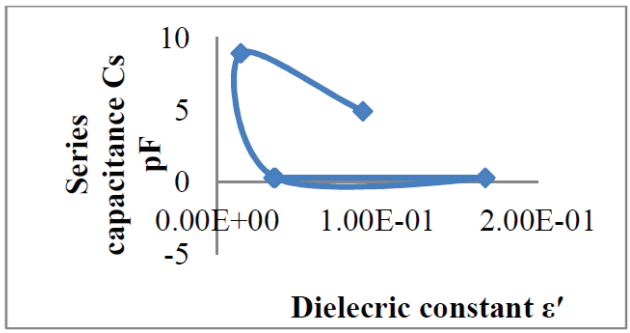

Fig. (5): the relation between the dielectric constant ε′ and Series capacitance Cs

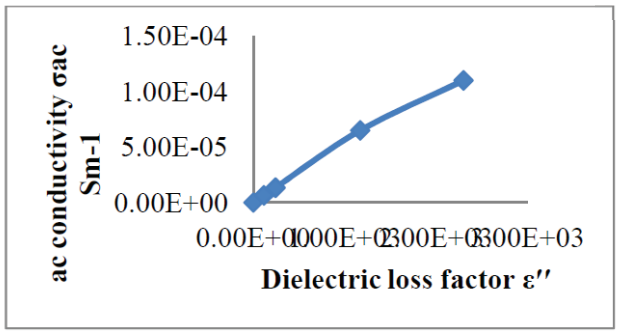

Fig. (6): the dependant of ac conductivity σac on the dielectric loss ε″ factors ε″

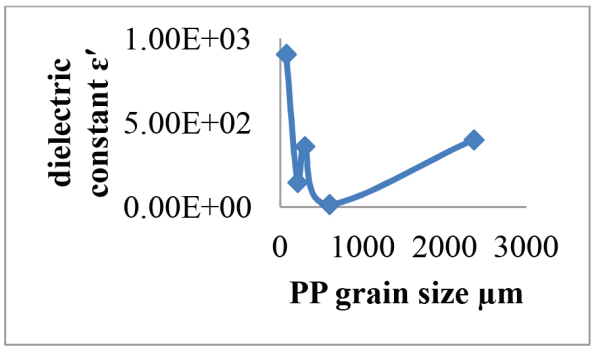

Fig. (7): the dependant of dielectric constant ε′ on PP grain size µm

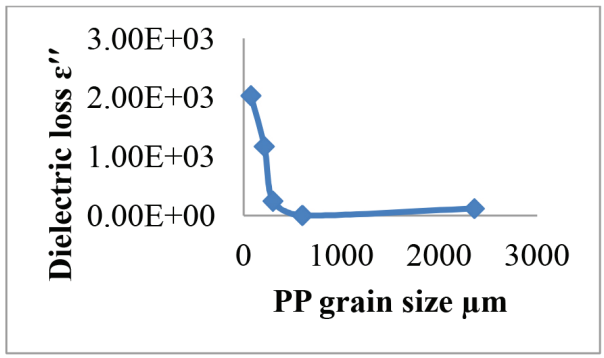

Fig. (8): the dependant of dielectric loss ε″ on PP grain size µm

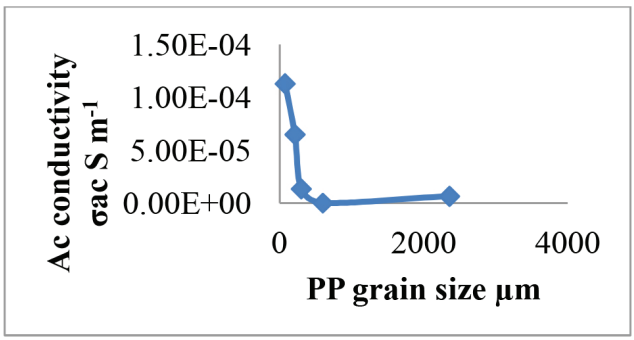

Fig. (9): the variation of AC conductivity σac S m^{-1} with PP grain size µm

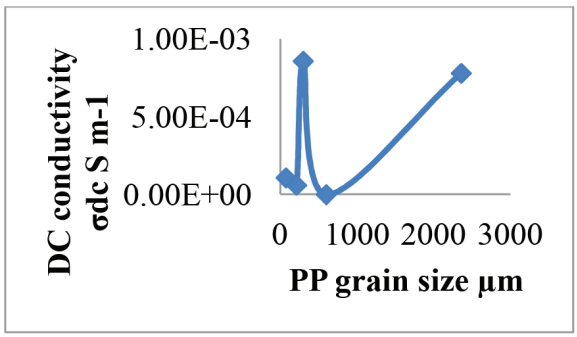

Fig. (10): the variation of Dc conductivity σdc S m^{-1} with PP grain size µm

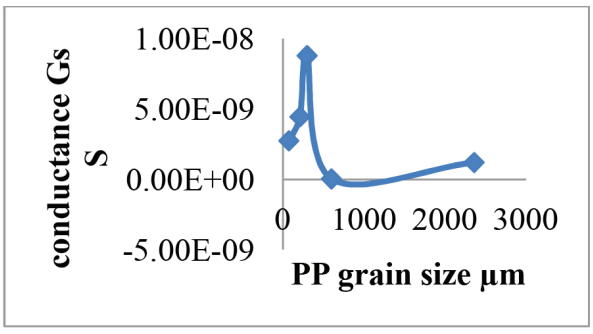

Fig. (11): Variation of conductance Gs S with PP grain size µm

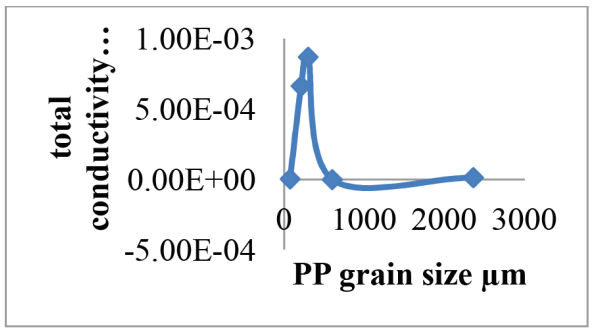

Fig. (12): Dependant of total conductivity σt S m^{-1}on PP grain size µm

5. Conclusions:

1- Decrease in the dielectric loss factor is due to the dielectric material changes polarity and in specimen (4) is due to increase particle size of PP. to 600 μm.

2- The volume of capacitor depends on the dielectric material that was chosen.

3- Capacitors are used for a wide variety of purposes and made of different materials and in different styles. They will consider three board types, that is, capacitors made for ac, dc and pulse applications. ac case is the most general since ac capacitors will work (or at least survive) in dc and pulse applications and the reverse may not be true.

4- Losses in ac capacitor one is due to a conduction loss represent the actual freightage flow in the dielectric and the other is a dielectric loss due to movement or rotation of the atoms or molecules in an alternating electric field.

5- Dielectric loss refers to the energy that is lost to heating of an object that is made of dielectric material if a variable voltage is applied to it. This loss happen because as the material changes polarization 6- Ideal capacitor is a purely reactive device, containing absolutely zero resistive (power dissipation) effects.

7- Dependent frequency ac conductivity can be calculated from the equation and.

8- Composites, the wonder materials are becoming an essential part of today's materials due to the advantages such as low weight, corrosion resistance, high fatigue strength and faster assembly. They are extensively used as materials in making aircraft structure, electronic packaging to medical equipment and space in extensive composite polymers with an appropriate weight, appropriate electric conductivity and/or appropriate impact value for use with practical articles.

References:

[1] Q. M. Jebur, A. Hashim and M. A. Habeeb, The Effect of Biomaterial on Optical properties of polymer Blend and their Applications, journal of Chemical and Pharmaceutical Sciences, Volume 10, issue 1, pp. 728-731, (2017).

[2] I. Tantis, G. C. Pasarras, D. Tasis, Functionalized Graphine-poly (Vinyl Alcohol) Nanocomposites: physical and dielectric properties, eXPRESS polymer letters, Vol. 6, No. 4, pp. 283-292, (2012).

[3] A. B. Shirode, D. j. Bharali, S. Nallanthighal, J. K. Coon, S. A. Mousa and R. Reliene, Nanoencapsulation of Pomegranate Bioactive Componds Breast Canser Chemoprevention, International Journal of Nanomedicine 10: pp. 475-484, (2015).

[4] A. Hashim, M. Husain, J. H. Ghazi, H. Hakim, Characterization of (polyvinyl Alcohol-Polyacrylamide-Pomegranate Peel) Composites as Biocompositeso Materials, Universal Journal of Physics and Application (3): pp. 242-244, (2013).

[5] F. A. Jasim, A. Hashim, A. G. Hadi, F. Lafta, S. R. Salman and H. Ahmed, Preparation of (Pomegranate Peel-Polystyrene) Composires and Study their Optical Properties, Advance in Physics Theories and Applications, Vol. 18, pp.22-27, (20 11).

[6] R. Bhargava, S-Q. Wang and J. Koenig, FTIR Microspectroscopy of polymers Systems, Ava Polymer Sci, 163, pp. 137-191, (2003).

[7] Y. Liu, C. Qiant, L. Qut, Y. Wu, Y. Zhang, X. Wu, B. Zou, W. Chen, Z. chen, Z. Chi, S. Liu,

X. Chen and J. Xu, A Bulk Dielectric Polymer Film with Intrinsic Ultralow Dielectric Constant and Outstanding Comprehensive Properties, Chemistry of Materials, ACS Publications, 27 (19), pp. 6543-6549, (2015).

[8] O. Gh. Abdullah, B. K. aziz and A. O. Saeed, Kaolin Light Concentration effects on The Dielectric Properties of Polyvinyl Alcohol Films, International Journal of Science and Advanced Technology, Volume 2. No. 1, pp. 65-69, (2011).

[9] B. Hussien, The D.C and A.C Electrical Properties of (PMMA-Al2O3) Composites, European Journal of Scientific Research, Vol. 52, No. 2, pp.236-242. (2012).

[10] M. Shanmugavadivu, S. Kuppsang and R. Ranjithkumar, Synthesis of Pomegranate Peel Extract Mediated Silver Nanoparticlesand Its Antibacterial Activity, American Journal of Advance Drug Delivery, AJADD [2][2]:174-182, (2015).

[11] H. Yang, Y. Ren, T. Wang and C. Wang, Preparation and Antibacterial activity of A/Ag+/Ag3+ nanoparticles composites Made by Pomegranate rind extract, Result in Physics, volume 6, pp. 299-304, (2016).

[12] M. S. Cheyad and T. A. Salman, Characterization and Study the Inhibition Activity of Pomegranate Peel Extraction for α-Brass Corrosion in H2SO4 Solution, Oriental Journal of Chemistry, Vol. 33, No. 3, pp. 1241-1251, (2017).

[13] N. S. Labidi and A. Djebaili, Studies of The Mechanism of Polyvinyl Alcohol Adsorption on The Calcite/Water in The Presence of Sodium Oleate, Journal of Minerals & Materials Characterization & Engineering, Vol. 7, No. 2, pp. 147-16, (2008).

[14] M. U. Mihas, M. Ahmad, l. Ali and M. Sohail, Synthesis of Chemical Cross-Linked Polvinyl Alcohol-CO- Poly (Methyacrylic Acid) Hydrogels by Copolymerization; A Potential Graft-Polymeric Carrier for Oral delivery of 5-Flourouracil, Daru Journal of Pharmaceutical Sciences, 21 (1); 44, (2 013).

[15] A. K. Elbadawy, S. K. El-Refai, T. M. Tamer, M. A. El-Meligy and M. S. Mohy Eldin, Poly (vinyl Alcohol)-Alginate Physically Crosslinked Hydrogel Membranes for Wound Dressing Applications: Characterization and Bioevaluation, Arabian Journal of Chemistry, Volume 8, Issue 1, pp. 38-47, (2015).

[16] P. H. F. Pereira. T. I. S. Oliveira, M. F. Rosa, F. L. C. Icante, G. K. Moates, N. Welle, K. w. Waldro and H. M. C. Azeredo, Pectin extraction from pomegranate Peels with cetric Acid, International Journal of Biological Macromolecules, 88, pp. 373-379, (2016).

[17] L. Wei, Z. Lin-Li and Z. Xiao-Jing, grain Size effect on Electrical Conductivity and Giant Magnetoresistance of Bulk Magnetic Polycrystals, Chin. Phys. Lett, Vol. 26, No. 11, pp. 117502-(1-4), (2009).

[18] A. O. Musa, M. A. Al-Amber and F. Sh. Hashim, Determined the Energy Gap and Activation Energies of Some Transition Metal Complexes of Liquid Crystalline Shiff Base, National Journal of Chemistry, Volume 30, pp. 323-329, (2008).

[19] T. S. Velayutham, A. B. Ahmad, W. H. Abd Majid and G. S. Neon, properties of polyurethane Graphite Composites, Journal Fizik Malaysia, Vol. 29, No. 1&2, pp. 25-28, (2008).

[20] P. Barber, S. Balasubramanian, Y. angchamy, S. Gong, A. Wibowo, H. Gao, H. J. Ploehn and H-C zur Loye, Polymer Composites and Nanocomposites Dielectric Materials for Pulse Power Energy Storage, Materials, 2, pp. 1967-1733, (2009).

[21] B. P. Prasnna, H. B. Muralihara and M. Revanasiddappa, Synthesis, Characterization and Enhance Dielectric Constant of Polyaniline-Exfoliated Graphite Flakes Composites, IJLTEMAS, international Journal of Latest Technology in Engineering, Management &

applied Science, Vol. III, Issue V, pp.55-60, (2014).

[22] O. GH. Abdullah, S.A. Hussen and A. Alani, Electrical Characterization of Polyvinyl Alcohol Films Doped with Sodium Iodide, Asian Transactions on science & Technology, Volume 01, Issue 04, pp. 1-4, (2011).

[23] A. Wang and D. D. Chung, Dielectric and Electrical Conduction Behavior of Carbon Paste Electrochemical Electrodes, with Decoupling of Carbon, Electrolyte and Interface Contribution, Carbon 72, pp. 135-151, (2014).

The Association Between Periodontitis and Coronary Artery Atherosclerosis Patients in Iraqi Population

Adel Ateyah AL-Nasrawy
Genetic Engineering and Biotechnology Institute for Postgraduate studies-Baghdad University,
College of Dentistry - Kerbala University, Iraq.

Received Date: 26 / 7 / 2017
Accepted Date: 22 / 12 / 2017

الخلاصة

مرض القلب التاجي هو تضيق الشرايين التاجية للقلب بسبب تجمع المواد الدهنية وبناء البلاكات او الاغشية الحية على جدرانها، هذا المرض يسبب نقصان ورود الدم الغني بالأوكسجين لعضلة القلب، ويعاني مرضى القلب التاجي من الم شديد وعدم الراحة وهو ما يعرف بالذبحة الصدرية. ان ازدياد الادلة الخاصة بالعلاقة الوثيقة بين مرضى (التهاب اللثة وما حول الاسنان) واصابتهم بأمراض القلب الوعائية تم تمييزها وملاحظتها خلال السنوات الاخيرة. والدليل الاساسي المتوفر هو اكتشاف تواجد الحامض النووي (الدنا) الخاص بالجراثيم المرضية المسببة لالتهاب اللثة وما حول الاسنان في البلاكات او الاغشية الحية على جدران الشرايين التاجية المتصلبة والذي يعتبر الخطوة الاولى لتوضيح العلاقة الاساسية بين هاتين الحالتين المرضيتين.

الكلمات المفتاحية

أمراض الشريان التاجي: تصلب الشرايين ، التهاب اللثة ، PCR ؛ بورفيوموناس اللثة 16S الريبوسوم RNA والأنماط الجينية fimA.

Abstract

Background: Coronary heart disease is a narrowing of coronary arteries due to accumulation of fatty materials (plaque) build-up on its walls. This disease will decrease the oxygen-rich blood supply. Coronary heart disease patients will suffer from pain and discomfort known as angina. Increasing evidence regarding the potential association between periodontal diseases and cardiovascular diseases has been identified in recent years. The available evidence underlines the importance of detecting DNA of periodontal pathogens on atheromatous plaques as the first step in demonstrating the causal relationship between these two conditions.

Keywords

Ccoronary artery diseases: Atherosclerosis, Periodontitis, PCR; Porphyromonas gingivalis 16S ribosomal-RNA and fimA genotypes.

a. Materials and Methods

Atheromatous plaques from coronary arteries were achieved by diagnostic and therapeutic catheterization, homogenized, and bacterial DNA was extracted. To obtain a critical "keystone periodontal pathogen (Porphyromonas gingivalis), two amplifications of the eubacterial (16S ribosomal-RNA gene) and fimA genotypes were carried out for each sample with specific primers for the target bacteria and performed by a conventional monoplex and multiplex polymerase chain reaction (PCR) technique. Statistical analysis test included the x2test.

b. Results

Seventy four coronary artery atheromatous plaque samples were analyzed. Most of them)54/74((73%) were positive for the target bacterium Porphyromonas gingivalis according to genus and species level due to presence of eubacterial 16S ribosomal-RNA gene and species specific fimA genotypes in coronary artery atheromatous plaque samples, the simultaneous presence of several and various P. gingivalis fimA genotypes within the same atheromatous plaque specimen was a common observation.

Conclusions: This study was conducted to investigate the presence of a particular DNA from the most common periodontitis-associated bacteria P. gingivalis both at genus and species level in coronary artery atheromatous plaques retrieved by endarterectomy, this finding is provide an additional evidence that supports the potential association between chronic periodontitis and cardiovascular diseases, in which the periodontal P. gingivalis can access to the systemic circulation (bacteremia), colonize at distant sites, and thus, might influence the pathophysiology of coronary artery atherogenesis.

1. Introduction

Cardiovascular disease is a common cause of death in industrialized countries, accounting for (29%) of deaths worldwide. Atherosclerosis is the principal cause of all cardiovascular diseases; it is responsible for (50%) of all mortality in the United States, Europe, and Japan [1]. More than 50 prospective cohort and case control studies undertaken during the past 25 years demonstrated evidences for an association between periodontitis and cardiovascular diseases like, atherosclerotic vascular disease, including stroke, myocardial infarction, peripheral vascular disease, abdominal aortic aneurysm, coronary heart disease, and cardiovascular death [2,3].

Coronary heart disease is a narrowing of coronary arteries due to accumulation of fatty materials (plaque) build-up on its walls. This disease will decrease the oxygen-rich blood supply. Coronary heart disease patients will suffer from pain and discomfort known as angina [4].

Atherosclerosis is the major event in the pathophysiology of cardiovascular diseases, in which large- to medium-size muscular and large elastic arteries become occluded with fibrolipidic lesions, known as atheromas. These atheromatous plaque are responsible for end-stage complications or events associated with cardiovascular diseases, such as coronary thrombosis, acute myocardial infarction, and stroke [5].

Periodontitis is a chronic inflammatory disease caused by bacterial colonization, which results in destruction of the tissues between the tooth surface and gingiva, loss of connective tissue attachment, erosion of alveolar bone, and tooth loss, periodontitis is common and increases with age, in a United States of America survey, about half of adults aged (>30) years have some periodontitis and almost 10% have severe disease [6].

Several studies have demonstrated that the presence of oral bacteria in atherosclerotic plaques is implicated in the pathogenesis of cardiovascular diseases, and that atherosclerosis and cardiovascular diseases are both accelerated by periodontal disease [3, 7]. A link between periodontitis and cardiovascular disease has been proposed, periodontal disease and cardiovascular disease are highly prevalent in the modern community. Both pathologies are chronic inflammatory disorders, like periodontitis, atherosclerosis is a complex condition with a suspected microbial etiology in which *P. gingivalis* is attracting increasing attention for its possible role in accelerating disease progression [5, 8].

Porphyromonas gingivalis, an anaerobic Gram-negative coccobacillus which belongs to the Bacteroidaceae family. In the natural environment, *P. gingivalis* is a constituent of the multispecies biofilm, It considered the main periodontal pathogen involved in onset and progression of various forms of periodontal diseases [9]. *P. gingivalis*, is a keystone pathogen in chronic periodontitis, it has been found to associate with remote body organ inflammatory pathologies, and it has the ability

to evade the host immune response and access nutrients in the microenvironment which is directly related to its survival, proliferation, and infection.

More recent analyses from large-cohort studies suggest new onset, and prevalent periodontitis, as well, is associated with increased cardiovascular diseases like Myocardial Infarction, Atherosclerosis [10], Diabetes Mellitus [11], Rheumatoid Arthritis [12], Preeclampsia with low birth weight [13], Orodigestive Cancers Mortality [14], and Alzheimer's Disease[15].

The systemic inflammatory or immune response to periodontal infection may increase cardiovascular risk. Also, pathogens from the mouth can enter atherosclerotic plaques via the blood stream, and this could promote an inflammatory or immune response within the atherosclerotic plaque. Adverse ranges of oral bacterial pathogens and bacterial DNA have been detected in atherosclerotic plaque [16].

Despite for heterogeneity of the studies, overall results of epidemiological studies suggest for a modest but significant association between periodontal infections and cardiovascular disease that is independent on the effects of confounders. Scientific evidence supporting a possible role of oral bacterial species in atherosclerosis relies to a large extent on the detection and identification of bacterial DNA in human arterial wall tissues or atherosclerotic plaque in cross-sectional study designs [17]. DNA from *P. gingivalis*, a major periodontal pathogen, has been detected in coronary atherosclerotic plaques and atherosclerotic vessels [18].

An association between oral bacteria and atherosclerosis has been postulated. A limited number of studies have used 16*S RNA gene* sequencing based metagenomics approaches to identify bacteria at the species level from atherosclerotic plaques in arterial walls [19]. Because of the high prevalence of periodontitis in humans, and because cardiovascular diseases are the main cause of death in developed countries, an increasing interest was raised in the scientific community to identify the potential links between both entities [20].

Therefore, the aim of this investigation was to detect DNA from periodontitis-associated bacteria *P. gingivalis* at the genus and species level in coronary artery atheromatous plaque recovered from patients using strict sample procurement and laboratory procedures. Our hypothesis was that bacterial DNA from periodontopathic bacteria would be present in the retrieved atherosclerosis samples, and this presence would be related to the oral health status of the patients.

2.Materlals and methods

2.1. Collection of Specimens

After clinical diagnosis of coronary artery atherosclerotic patients, atheromatous plaque thrombosis samples from diagnostic catheterization and therapeutic catheterization or both for seventy four coronary artery atherosclerotic patients (who received endarterec-

tomies because of various manifestations of ischemic vascular disease) aged between (29 to 73) years who admitted to the Heart and Arteries catheterization Unit (Cardiology) in AL-Hussein Educational Hospital in Kerbala City during the period from July 2016 to April 2017. A pool of (24) diagnostic catheterization tissue specimens were taken from clinically non-atherosclerotic areas of coronary artery from subjects was obtained as a control group. Then, the atheromatous plaque samples were rapidly transferred into (1.5) ul polypropylene microcentrifuge tube contained 500 ul of (0.9%) sterile normal saline solution, and subjected to the laboratory for molecular bacteriology detection.

Detection of *P. gingivalis* by Essential Genes

2.2.DNA Extraction

Isolation of DNA from atherosclerotic plaques samples were done using Genomic DNA Mini Kit (Geneaid, Korea) / Tissue using a protocol in accordance with the manufacturer's instructions, each atherosclerotic plaque sample (coronary artery plaque tissue of the catheter tip) with (500) ul of (0.9%) sterile normal saline was used for DNA extraction, extracted DNA aliquots were measured with Q5000 UV-Vis Spectrophotometer, (20-25) nanogram /microliter of extracted DNA aliquots were used for microbiological and molecular detection.

Molecular detection of *P. gingivalis* was performed by monoplex PCR of (16*S rRNA* gene) amplification according to [21] and multiplex PCR of species specific *fimA* gene amplification according [22]. Using the following amplification primers in Table (1): and according to the amplification reaction programs of (Tables 2, 3).

Table (1): The Primers used in molecular detection of P. gingivalis

Gene	´Duplexing primers 5´- 3	Product size (bp)	Reference
P. gingivalis 16Sribosomal RNA	F AGG CAG CTT GCC ATA CTG CG R ACT GTT AGC AAC TAC CGA TGT	404	[23]
Type I *fimA*	F CTG TGT GTT TAT GGC AAA CTTC R AACCCC GCT CCC TGT ATT CCGA	392	[24]
Type Ib *fimA*	F CAG CAG AGC CAA AAA CAA TCG R TGT CAG ATA ATT AGC GTC TGC	271	[22]
Type II *fimA*	F ACAACTATACTT ATG ACA ATG G R AACCCCGCT CCC TGT ATT CCG A	257	[24]
Type III *fimA*	F ATTACACCTACA CAG GTG AGG C R AACCCCGCT CCC TGT ATT CCG A	247	[24]

Type IV *fimA*	F CTATTCAGG TGC TAT TAC CCA A R AACCCCGCT CCC TGT ATT CCG A	251	[24]
Type V *fimA*	F AACAACAGTCTC CTT GAC AGT G R TATTGG GGG TCG AAC GTT CTG TC	462	[25]

Amplification Reaction programs:-

Table (2): Cycling parameters for monoplex PCR of 16S rRNA gene amplification

No. of cycles	Stage	Temperature °C	Time
1	Initial denaturation	95	5 min.
35	Denaturation	94	30 Sec.
	Annealing	60	30 Sec.
	Elongation	72	1 min.
1	Final extension	72	10 min.

Table (3): Cycling parameters for multiplex PCR of species specific fimA gene amplification

No. of cycles	Stage	Temperature °C	Time
1	Initial denaturation	95	5 min.
35	Denaturation	94	30 Sec.
	Annealing	58	30 Sec.
	Elongation	72	30 Sec.
1	Final extension	72	7 min.

2.3. Agarose Gel Electrophoresis

A concentration of (1,2%) Agarose gel used for PCR products electrophoresis. Which, accomplished with the use of two types of DNA ladder (Accu Ladder 100 bp Bioneer/Korea) and (50 bp DNA Step Ladder Marker Promega/ USA).

2.4. Statistical Analysis

The collected data were analyzed using the statistical system and Chi-Square ($\chi 2$) test, with P-value of (≤ 0.05).

3.Results and discussion

There are (3,000) years of history suggesting the oral influence, particularly of periodontitis on the general health of human subjects [26]. In periodontitis, *P. gingivalis* represents a keystone pathogen causing microbial and immune dysbiosis [27]. *P. gingivalis* has an arsenal of potent virulence factors, can invade periodontal, atherosclerotic, and brain tissue, thereby avoiding immune surveillance and maintaining its viability, it may act as the main organism in periodontitis and in related

systemic diseases and other remote body inflammatory pathologies including dementia [15], atherosclerotic plaques of patients with cardiovascular diseases[16], [18].

More recent analyses from large-cohort studies suggest new onset, and prevalent periodontitis, as well, is associated with increased coronary heart disease risk [28] and there is a graded association between tooth loss and stroke, cardiovascular death, and all-cause mortality in patients with stable coronary artery disease [29].

The prevalence of the most Periodontal pathogen *Porphyromonas gingivalis* in the total 74 coronary artery atherosclerosis plaque Patients were 73%))54/74() distributed in (36/ 66.7%) (54) in males and (1833.3%) (54 /) in females and (3361%) (54 /) in coronary artery atherosclerosis plaque Patients with 29-60 years and 2139%) 54 /) in atherosclerosis plaque Patients with >60 years, more than in control group (520.83%) (24 /) as demonstrated in table no.1

Table (1): Distribution of Periodontal Porphyromonas gingivalis in coronary artery atherosclerosis plaque Patients and control groups.

Porphyromonas gingivalis in Subject					
Variable No, Percentage(+)		Atherosclerosis group		Control group	
		(-) No, Percentage	(+) No, Percentage	(-) No, Percentage	
Gender	Male	36 (66.7%)	12 (16.2%)	3 (12.5%)	14 (58.33%)
	Female	18 (33.3%)	8 (10.8%)	2 (8.33%)	5 (20.83%)
Age	29-60 years	33 (61%)	14 (70%)	2 (8.33%)	13 (54.17%)
	> 60 years	21(39%)	6 (30%)	3 (12.5%)	6 (25%)

On the other hand, detection of *P. gingivalis* in coronary artery atherosclerosis plaque patients and control groups was achieved by monoplex PCR of 16*S rRNA* gene amplification and multiplex PCR of species specific *fimA* gene amplification, all atherosclerosis plaque samples were positive for the genus specific level according to 16*S rRNA* gene as demonstrated in figure no.1 and various species specific level according to *fimA* genotypes that were represented by *fimA* genotypes I, II, III, 1V and V as demonstrated in figures (2 and 3), these results indicate confirmatory diagnosis of the highly virulent periodontal pathogen *P. gingivalis* in atherosclerosis plaque samples of coronary artery disease patients, furthermore, interpret the ability of this potent bacterium to use its arsenal virulence factors in attaching different types of body tissues, establishing various complications, these results were agreed with multiple previous similar studies revealed that in addition to local in-

flammation at the initial site of infection, *P. gingivalis* has the ability to disseminate from ulcerative periodontal tissues to circulate and interact with the heart, liver, and other body tissues, therefore, *P. gingivalis* play an important role in periodontitis-associated systemic diseases, such as atherosclerosis [30].

Furthermore, presence of multiple *fimA* genotypes I, II, III, 1V and V in coronary artery atherosclerotic plaque samples in the present study is compatible to other scientific evidence supporting a possible role of oral bacterial species in atherosclerosis relies to a large extent on the detection and identification of bacterial DNA in human arterial wall tissues or atherosclerotic plaque in cross-sectional study designs [31]. Most importantly, Kozarov *et al.* demonstrated that viable *P. gingivalis* and *A. actinomycetemcomitans* could be isolated from atherosclerotic plaque [32].

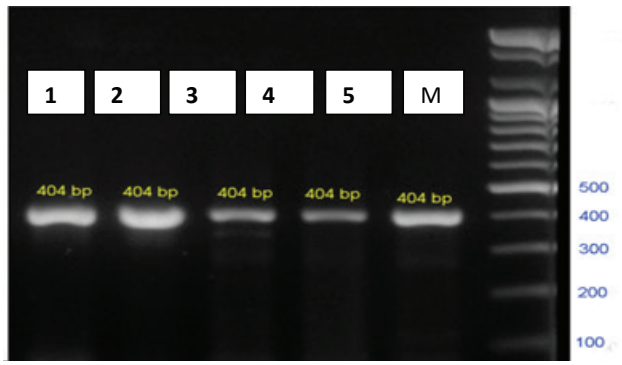

Fig. (1): positive results of coronary artery atherosclerosis plaque samples with 16S rRNA gene amplification. Lanes (1, 2, 3, 4, and 5): 404 bp. amplicon, and lane M: DNA 100 bp. molecular weight marker.

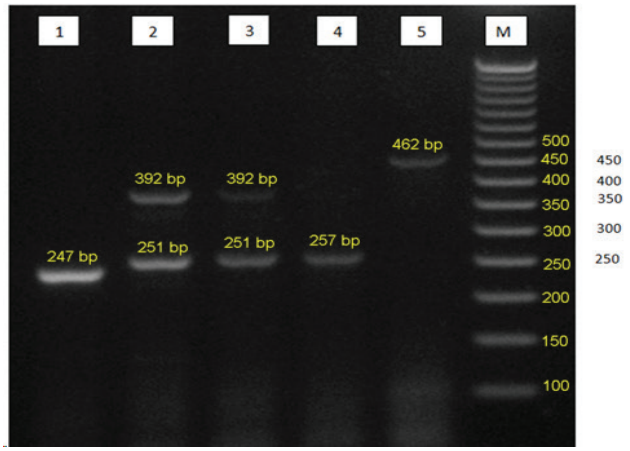

Fig. (2): P. gingivalis positive coronary artery atherosclerosis plaque samples for fimA genotypes lane (1) fimA genotype (III) 247 bp., lanes (2, 3) fimA genotypes (1V) 251bp., and fimA genotype (I) 392 bp., lane (4) fimA genotype (II) 257 bp., lane (5) fimA genotype (V) 462 bp., and lane M= DNA Ladder (50 bp).

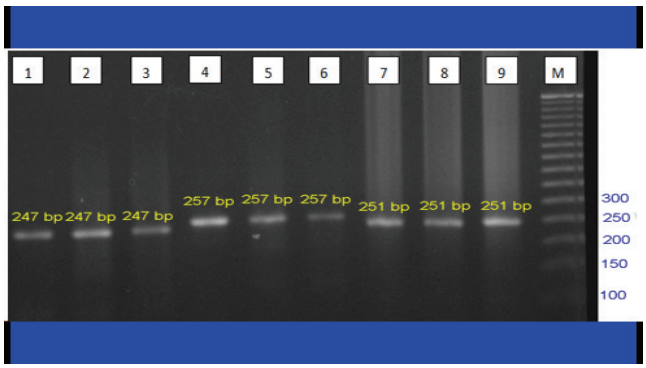

Fig. (3): positive coronary artery atherosclerosis plaque samples for P. gingivalis fimA genotypes. Lanes (1, 2, 3) fimA genotype (III) 247 bp., lanes (4, 5, 6) fimA genotype (II) 257 bp., lanes (7, 8, 9) fimA genotypes (IV) 251 bp., and lane M= DNA Ladder (50 bp.).

The present study demonstrated the presence of DNA from periodontal bacteria *P.gingivalis* in atheromatous plaque retrieved from patients who received endarterectomies of various manifestations of ischemic coronary artery vascular diseases was (54/74)

73%)), this prevalence was approximately to many previous investigations revealed that the prevalence of the most commonly periodontal virulent pathogen *P.gingivalis* in patients who received similar clinical cardiovascular manifestations was (3378.57%) (42 /) in carotid artery atheromatous plaques samples [33]., as well as previous clinical, epidemiological and molecular study indicated that *P.gingivalis* was by far the most abundant species, representing nearly (80%) of nearly 600 known oral bacterial species in artery tissues were obtained from patients with atherosclerotic cardiovascular disease who underwent coronary or femoral artery bypass surgery [34], and more than the concomitant detection of DNA from *P.gingivalis* observed in (61.90%) followed by *A. actinomycetemcomitans* (66.67%) of atheromatous samples [33]. As well many other authors identified *P.gingivalis* and *A. actinomycetemcomitans* as the most prevalent DNA from bacteria in atheromatous plaque from coronary arteries [35].

Another related study revealed a diverse range of oral bacterial pathogens and bacterial DNA has been detected in atherosclerotic plaque [16]. Etiologically, the chronic presence of periodontal microbes can lead to atherogenesis via two pathways: (1) direct invasion of the arterial wall and (2) the release, in response to infection, of systemic inflammatory mediators with atherogenic effects [36]. These pathogens, especially *P. gingivalis*, have demonstrated the ability to interact with the endothelial surface and to induce smooth-cell proliferation, causing damage and impairing the vasomotor functionality of the endothelial cells [37], indeed, in animal models, infection with *P. gingivalis* increases atherosclerotic plaque volume with the accumulation of cholesterol esters and inflammatory mediators [30], [38].

In large cohort studies it has been suggested that pathogenesis of atherosclerosis is associated with both innate and adaptive immune responses. Maekawa *et al.* 2011 claimed that oral infection with *P. gingivalis* accelerates atheroma formation by shifting the lipid profile of the host [39], and higher antibody titers against *P. gingivalis* have been detected in patients with cardiovascular disease and stroke [40], atherosclerosis [41], and myocardial infarction than in controls [42].

Furthermore, many up to (30%) of coronary artery atherosclerotic plaque samples exhibited (2-3) fimA genotypes in the same site and single fimA genotype in the control group enrolled in the current study, these investigations were suggested various explanations, such as the presence of several different P. gingivalis fimA genotypes colonizing the same atherosclerotic site, and a higher intra individual heterogeneity of P. gingivalis which established and showed allelic variation in the P. gingivalis housekeeping genes indicating genetic recombination and genetic variability, resulted different clones of P. gingivalis fimA genotypes colonizing the same atherosclerotic plaque site as demonstrated in P. gingivalis fimA genotypes colonizing

the same periodontal pocket [43], [44], Other investigation demonstrated that the recognition of genes linked to chromosome 9p21, and related to transforming growth factor beta regulation, predisposes to periodontitis, and to coronary artery disease, as well, provides further evidence that common pathophysiological pathways are important for the two diseases [45]. Indeed, previous support study indicated that severe periodontal disease is associated with a (25%) to (90%) increase in risk for cardiovascular diseases after adjustment of other risk factors [46], if causal, these associations would be of great importance because of the potential that preventing or treating periodontal disease could reduce the risk of major adverse cardiovascular events [3].

4. Conclusions and recommendations:

Within the limitations of this investigation, we have identified periodontitis-associated bacterial DNA in coronary artery atheromatous plaque retrieved by endarterectomy, These findings provide additional evidence that supports the potential association between periodontitis and cardiovascular diseases, in which a keystone periodontal P. gingivalis which access to the systemic circulation (bacteremia), colonize at distant sites, and thus, might influence the pathophysiology of atherogenesis.

However, the mere presence of bacterial DNA in these atheromatous plaque did not imply that live bacteria were present within the plaque, and therefore, further investigations are warranted. These studies should seek microbiologic data from atheromatous plaque and gingival crevicular fluid (GCF) and serum from the same patients, thus being able to confirm this likely direct relationship between periodontitis and cardiovascular diseases.

Confirmatory studies are thus needed to determine the number and abundance of more virulent pathogenic species present in atherosclerotic plaque and clinically periodontitis patients for activation of vaccination programs or protocols in order to minimize or get rid of these two chronic, problematic, related dangerous syndromes.

References

[1] Lusis A. J.," Atherosclerosis". Nature; 407:233–41. [PubMed: 11001066], (2000).

[2] Leng WD, Zeng XT, Kwong JS, Hua XP., "Periodontal disease and risk of coronary heart disease: an updated meta-analysis of prospective cohort studies." Int. J. Cardiol.; 201:469–472, (2015).

[3] Ralph Stewart, MD; Malcolm West, MD., "Increasing Evidence for an Association Between Periodontitis and Cardiovascular Disease" American Heart Association, Inc. Article: 133: P. 549-551, (2016).

[4] Sayols-Baixeras, S., Lluis-Gannela, C., Lucas, G. and Elos ua, R., "Pathogenesis of Coronary Artery Disease: Focus on Genetic Risk Factors and Identification of Genetic Variants" Appl Clin Genet., vol. 7, pp. 15–32, (2014).

[5] Paquette DW, Brodala N, Nichols TC., "Cardiovascular disease, inflammation, and periodontal infection". Periodontol 2000;44:113-126, (2007).

[6] Eke PI, Dye BA, Wei L, Thornton-Evans GO, Genco RJ; CDC.. "Periodontal Disease

Surveillance workgroup". J. Dent. Res.; 91:914–920, (2012).

[7] Dimitry A., Chistiakov, Alexander N., Orekhovd ,Yuri V., and Bobryshev. "Links between atherosclerotic and periodontal disease" Experimental and Molecular Pathology. Elsevier Inc. 100: 220–235, (2016).

[8] Miyauchi S, Maekawa T, Aoki Y, Miyazawa H, Tabeta K, Nakajima T, et al. "Oral infection with Porphyromonas gingivalis and systemic cytokine profile in C57BL/6.KOR-ApoE shl mice" J. Periodontal Res.; 47: 4028, (2012).

[9] M Hernández, N. Dutzan, and J. García Sesnich, "Host-Pathogen Interactions in Progressive Chronic Periodontitis," J Dent Res, vol. 90, pp. 1164–70, (2011).

[10] Rydén L., Buhlin K., Ekstrand E., de Faire U., Gustafsson A., Holmer J., Kjellström B., Lindahl B., et al. Periodontitis increases the risk of a first myocardial infarction. A report from the PAROKRANK Study. Circulation;133:576–583 ,(2016).

[11] Pınar Gümüş and Nurcan Buduneli. DIABETES MELLITUS AND PERIODONTITIS: SIGNS OF A BIDIRECTIONAL RELATIONSHIP. EMJ Diabet., 1:30-36, (2013).

[12] Koziel J, Mydel P and Potempa, J,."The link between periodontal disease and rheumatoid arthritis" Current Rheumatology Report,v16,article 408, (2014).

[13] Perez-Chaparro P, Gracieux P, Lafaurie G, Donnio P, and Bonnaure Mallet M.. Genotipic characterization of Porphyromonas gingivalis isolated from subgingival plaque and blood sample in positive subjects with periodontitis. J Clin Periodontol., 35: 748-53 ,(2008).

[14] Jiyoung Ahn, Stephanie Segers and Richard B. Hayes.. "Periodontal disease, Porphyromonas gingivalis serum antibody levels and orodigestive cancer mortality". Carcinogenesis, 33(5):1055–1058 ,(2012).

[15] Olsen, Ingar, Martin A. Taubman, and Sim K. Singhrao.."Porphyromonas gingivalis suppresses adaptive immunity in periodontitis, atherosclerosis, and Alzheimer's disease" REVIEW ARTICLE Journal of Oral Microbiology 8(1): 1-13, (2016).

[16] Fernandes CP, Oliveira FA, Silva PG, Alves AP, Mota MR, Montenegro RC, Burbano RM, Seabra AD, Lobo Filho JG, Lima DL, Soares Filho AW, and Sousa FB. "Molecular analysis of oral bacteria in dental biofilm and atherosclerotic plaques of patients with vascular disease". Int J Cardiol;174:710–712, (2014).

[17] Clifford A and Hoffman GS. "Evidence for a vascular microbiome and its role in vessel health and disease|". Curr Opin Rheumatol. ;27(4):397–405, (2015).

[18] Stephani Dwiyanti1, a), Yuniarti Soeroso1, Hari Sunarto1, Basuni Radi2"Relationship between Quantitative Measurement of Porphyromonas gingivalis on Dental Plaque with Periodontal Status of Patients with Coronary Heart Disease"AIP Conf. Proc. 1817, 030003-1–030003-6, (2017).

[19] Mougeota,J-L. C., Stevensa,C. B., Paster B. J. Brennana, M. T., Lockhart, P. B. and Mougeota, F. K. B. "Porphyromonas gingivalis is the most abundant species detected in coronary and femoral arteries" ORIGINAL ARTICLE. JOURNAL OF ORAL MICROBIOLOGY, VOL. 9, NO. 1, pp 1-9 ,(2017).

[20] Bouchard P, Boutouyrie P, D'Aiuto F, et al. "European workshop in periodontal health and cardiovascular disease consensus document". Eur Heart J Supp;12(Suppl. B):p13-22 ,(2010).

[21] Lyons SR, Griffen AL and Leys EJ.. Quantitative real-time PCR for Porphyromonas gingivalis and total bacteria, J Clin Microbiol., 38:2362–5 ,(2000).

[22] Martin FE, Nadkarni MA, and Jacques NA, et al.. "Quantitative microbiological study of human carious dentine by culture and real-time PCR: association of anaerobes with histopathological

changes in chronic pulpitis". J Clin Microbiol., 40: 1698–704 ,(2002).

[23] Lee ZM, Bussema C 3rd and Schmidt TM. rrnDB. Documenting the number of rRNA and tRNA genes in bacteria and archaea, Nucleic Acids Res., 37:489–93, (2009).

[24] [24] Nelson KE, Fleischmann RD, DeBoy RT, Paulsen IT, Fouts DE and Eisen JA, et al.. Complete genome sequence of the oral pathogenic bacterium Porphyromonas gingivalis strain W83, J Bacteriol., 185: 5591-601 ,(2003).

[25] Fumiko Hayashi, Mitsugi Okada, Yuki Oda, Taro Kojima and Katsuyuki Kozai1.. Prevalence of Porphyromonas gingivalis fimA genotypes in Japanese children, Journal of Oral Science, 54(1):77-83 ,(2012).

[26] Seymour GJ, Ford PJ, Cullinan MP, Leishman S, Yamazaki K. "Relationship between periodontal infections and systemic disease". Clin Microbiol; 13(Suppl 4): 310 ,(2007).

[27] Hajishengallis G, Darveau RP, Curtis MA. "The keystone pathogen hypothesis". Nat Rev Microbiol; 10: 71725 ,(2012).

[28] Yu YH, Chasman DI, Buring JE, Rose L, Ridker PM.. "Cardiovascular risks associated with incident and prevalent periodontal disease". J Clin Periodontol. V. 42: PP. 21–28 ,(2015).

[29] Vedin O, Hagstrom E, Budaj A, Denchev S, Harrington RA, Koenig W, Soffer J, Sritara P, et al. "Tooth loss is independently associated with poor outcomes in stable coronary heart disease" (published online ahead of print December 16, 2015). Eur J Prev Cardiol. Accessed December 24, 2015, (2015).

[30] Jie Yang a,b, Juan Wu A , Rui Zhang a, b , Min Yao a,b, Yu Liu a, Leiying Miao c , Weibin Sun. "Porphyromonas gingivalis oral infection promote T helper 17/Treg imbalance in the development of atherosclerosis." Journal of Dental Sciences 10.003.P 1-10, (2016).

[31] Clifford A, Hoffman GS.."Evidence for a vascular microbiome and its role in vessel health and disease." Curr Opin Rheumatol.; 27(4):pp. 397–405, (2015).

[32] Kozarov EV, Dorn BR, Shelburne CE, et al. "Human atherosclerotic plaque contains viable invasive Actinobacillus actinomycetemcomitans and Porphyromonas gingivalis. Arterioscler Thromb Vasc Biol. ; 25(3):e17– 8, (2005).

[33] Elena Figuero,*Marıa Sanchez-Beltran, Susana Cuesta-Frechoso, Jose Marıa Tejerina, Jose Antonio del Castro, Jose Marıa Gutie rrez, David Herrera,* and Mariano Sanz. "Detection of Periodontal Bacteria in Atheromatous Plaque by Nested Polymerase Chain Reaction" J Periodontol;82(10): pp.1469-1477, (2011).

[34] Mitra S, Drautz-Moses DI, Alhede M, et al. In silico analyses of metagenomes from human atherosclerotic plaque samples. Microbiome. 2015 ;3:38 ,(2015).

[35] Gaetti-Jardim E Jr., Marcelino SL, Feitosa AC, Romito GA, Avila-Campos MJ. "Quantitative detection of periodontopathic bacteria in atherosclerotic plaques from coronary arteries." J Med Microbiol. 58: 1568-1575, (2009).

[36] Mehak Hussain, Cordola M. Stovar, and Aline Dupount Porphyromonas gingivalis in Periodontal disease and Atherosclerosis scenes of action for antimicrobial peptides and complement" Frontires in Immunology Molecular Innate Immunity. Volume 6 Article 45 pp.1-6 ,(2015).

[37] Chun YH, Chun KR, Olguin D, and Wang HL. "Biological foundation for periodontitis as a potential risk factor for atherosclerosis. J Periodontal Res;40: 87-95, (2005).

[38] Hayashi C, Viereck J, Hua N, Phinikaridou A, Madrigal AG, Gibson FC3rd, Hamilton JA, Genco CA. "Porphyromonas gingivalis acceler-ates inflammatory atherosclerosis in the innominate artery of ApoE deficient mice. Atherosclerosis.; 215:52–59, (2011).

[39] Maekawa T, Takahashi N, Tabeta K, Aoki

Y, Miyashita H, Miyauchi S, et al. Chronic oral infection with Porphyromonas gingivalis accelerates atheroma formation by shifting the lipid profile. PLoS One; 6: e20240, (2011).

[40] Pussinen PJ, Alfthan G, Jousilathi P, Paju S, Tuomilehto J., Systemic exposure to Porphyromonas gingivalis predicts incident stroke. Atherosclerosis; 193: 222-228, (2007).

[41] Seymour GJ, Ford PJ, and Cullinan MP, et al. "Relationship between periodontal infections and systemic disease.Clin Microbiol Infect. 13(Suppl 4):3–10, (2007).

[42] Pussinen PJ, Alfthan G, Tuomilehto J, Asikainen S, and Jousilahti P. "High serum antibody levels to Porphyromonas gingivalis predict myocardial infarction". Eur J Cardiovasc Prev Rehabil .11: 408–411, (2004).

[43] Enersen M, Olsen I, Kvalheim O and Caugant D. fimA Genotypes and Multilocus Sequence types of Porphyromonas gingivalis from patients with periodontitis, J Clin Microbiol., 46: 31-42, (2008).

[44] Morten Enersen.. Porphyromonas gingivalis: a clonal pathogen (Diversities in housekeeping genes and the major fimbriae gene). Journal of Oral Microbiology 3: 8487-8489, (2011).

[45] Schaefer AS, Richter GM, Groessner-Schreiber B, Noack B, Nothnagel M, El Mokhtari NE, Loos BG, Jepsen S, and Schreiber S. "Identification of a shared genetic susceptibility locus for coronary heart disease and periodontitis."PLoS Genet. 5: e1000378, (2009).

[46] Beck J, Garcia R, Heiss G, Vokonas PS, and Offenbacher S. "Periodontal disease and cardiovascular disease. J Periodontol; 67:1123–37, (1996).

Circumstances Around Pediatric and Teenager's Diabetic in The South of Iraq

*Makarim M. Ali and Najim A. AL-Awwadi
**Ali B.Roomi, Fatima Assad
***Hadyel Kamel
*College of Pharmacy, Thi-Qar University, Iraq
**General Directorate for Education, Thi-Qar, Iraq
***College of Nursing, Thi-Qar University, Iraq

Received Date: 11 / 8 / 2017
Accepted Date: 28 / 12 / 2017

الخلاصة

تم التخطيط لهذه الدراسة لتقدير الظروف المحيطة لانتشار مرض السكري في الأطفال والمراهقين، وأقل 18 خلال فترة (أكتوبر 2012 – مايو 2013) في مدينة الناصرية، وفقا للسن والجنس والمنطقة، بداية المرض، عدد الأزمات، عوامل الخطر الجينية، ومستوى اقتصادي للأسرة، المظاهر السريرية، مكونات الدم.

المواد وطرق العمل: (100) من الأطفال والمراهقين، وتتراوح أعمارهم ما بين (1–18) سنة، من الذكور والإناث تم تشخيصهم سابقا وكانوا مصابين بمرض السكري نوع الأول (DM-1) بما لا يقل عن (3) أشهر.

النتائج: في هذه الدراسة تم استنتاج ان مرض السكري يؤثر بنسبة (34%) من عمر 1 يوم الى 1 سنة، و(44%) من المرضى في سن (1-5) سنوات و (69%) من المرضى تكون أسرهم لديها مستوى اقتصادي معتدل والغالبية العظمى من العينات بنسبة (53%) لم يتعرضوا الى الأزمات. أظهرت غالبية العينات بنسبة (68%) غير مرتبطة بعوامل جينية.

الكلمات المفتاحية

داء السكري، مرض السكري من النوع الأول (DM-1)، الأطفال والمراهقون.

Vol. 9, No. 17 and 18, P. (51-62),Jun, 2019

Abstract

The aim of This study was planned to estimate the conditions surround the prevalence of diabetes mellitus in children and adolescents, less than18 years of age throughout the period of (October 2012 - May 2013) in the Nasiriya city.

Materials and methods: (100) children and adolescents, the ages range between (1-18) years, male and female previously diagnosed for at least (3) months with Type 1 diabetes (DM-1), according to age, gender, area, onset of disease, crises number, genetic risk factors, family economical level, clinical features, blood parameters were included in the study.

The results: In the present study, diabetes mellitus affects(34%) at age of 1 day to 1 year, and(44%_ of the patients at the age of (1-5) years and(69%) of family's patients have a mild economical level, and the majority of samples that didn't found crisis(53%). Showed the majority of the samples non genetic related risk factors(68%).

Keywords

Diabetes Mellitus, Type 1 diabetes (DM-1), Children and Adolescents.

1. Introduction

Diabetes Mellitus-1 is widely understood to be caused by an autoimmune process that destroys the insulin-secreting beta-cells in the pancreatic islets [1]. While it is accepted that genetic factors play a key role in its development, environmental and nutritional factors are believed to be modifiers [2-4], as only ~(5%) or fewer subjects with genetic susceptibility to Diabetes Mellitus-1 develop the clinical disease [5]. In Australian children, Diabetes Mellitus-1 incidence increased significantly between 2000-2004, from 19 to 24 new cases per 100,000 of the children's population [6], a trend that is reflected globally [7]. There are a major regional and between-country differences in the incidence of Diabetes Mellitus-1 [8], and even between high income OECD (Organization for economic cooperation and development) countries the incidence varies by a factor of more than (2) [9].

In the 19th century, diabetes was uncommon and the incidence of childhood diabetes was relatively low and Table until the middle of the twentieth century. There has been an upturn in the incidence of Diabetes Mellitus-1. The rise has been too rapid for the explanation to be purely genetic. The causes are not yet completely understood, although various factors have been proposed such as rapid growth in early childhood, early exposure to certain food constituents (e.g. Cow's milk hypothesis), enter virus infection, chemicals and reduced exposure in early childhood to infective agents that contribute to the development of a healthy immune system (the 'hygiene hypothesis') [10]. Diabetes Atlas, fifth edition: www.diabetesatlas.orgNote: These figures are based on what countries report, and the figures will depend on screening strategies. Although numerous studies have documented worldwide increases in diabetes, [11]. Few data exist on the population prevalence of diabetes among ways to estimate the conditions surround the prevalence of diabetes mellitus in children and adolescents in Iraq. Early exposure to dairy proteins increases the in- cadence of diabetes in BB rats (2). Controversy exists over the possible protective effect of breast- feeding on the risk of insulin-dependent diabetes mellitus (IDDM) in humans [3,4]. The incidence of childhood IDDM in Finland is the highest in the world [5]. There for we were deciding to do this study, which aimed to estimate the conditions surround the prevalence of diabetes mellitus in children and adolescents, less than18 years of age throughout limited period.

2. Materials and methods:

A descriptive study (cross-sectional design) was conducted in (2) observational centre Bint al-Huda educational hospital and Diabetic and Endocrine glands centre in Nasiriya city. Non –Probability (purposive) sample of (100) children and adolescents, the ages range between (1-18) years, male and female previously diagnosed for at least (3) months with DM-1. They visited the diabetic centre for check –up and get their medicine. The data are collected

through the use of semi-constructed questionnaire, which consists of 17-items medical test items. Reliability of the questionnaire is determined through a pilot study and the validity through a panel of (18) experts. The data were described statistically and analysed through the use of the descriptive and inferential statistical analysis procedures (SPSS).

3. The results:

The findings of the present study indicate that the diabetes mellitus affects (34%) at age of (1) day to (1) year, and (44%) of the patients at the age of (1-5) years that's mean (78%) of our study's sample are children under than 5 years old Table (1). Our study showed that the most samples (69%) of family's patients have a mild economical level, and the majority of samples that didn't found crisis (53%)

Also this study showed the majority of the samples non genetic related risk factors (68%). The results showed the higher range of the patient's fasting blood sugar (200-349) mg/dl were (47%) of the patient sample, and the majority of patient's random blood sugar were (48.7%) in the range (200–349) mg /dl. The blood urea was (43%) of selected patients in the range (20–24) mg/dl urea. And our results showed the majority of the patient's (98%) serum creatinine were in the range (0.6 –3) (mg/ l, but the cholesterol is (63%) of the patients in the range (125 – 174) mg/dl.

Table (1): Date of the onset of disease

Date of the onset of disease	Patient's number	% Percentage
Day – year	34	% 34
Year – 5year	44	44%
5year – 10 year	20	20%
10year – 12year	2	2%

Table (2): Descriptive Statistics for the Practice items of Juveniles who effected by DM-1 (MS) Mean of Score, (SD) Standard Deviation, and (RS) Relative Sufficiency of the Diabetes Mellitus Diseases

The practices of Juveniles who affected by diabetes (Type 1)		.No	.M.S	.S.D	.R.S	.Ass
3	Reaction of adolescent care of singe and Symptoms					
3-1-1	Body energy	100	1.18	0.52	39.33	F

3-1-2	Prevent hypoglycaemia	100	2.12	0.86	70.67	P
3-1-3	Fruits and leafy vegetables	100	1.72	0.82	57.33	F
3-1-4	Amount of fluid	100	1.21	0.56	40.33	F
3-2	Dental Care					
3-2-1	Oral hygiene	100	1.45	0.69	48.33	F
3-2-2	Teeth and gum infected	100	1.13	0.37	37.67	F
3-2-3	Examine my teeth	100	1.33	3.01	44.33	F
3-3	Injection method					
3-3-1	Store	100	2.37	0.88	79.00	P
3-3-2	Dose	100	2.30	0.92	76.67	P
3-3-3	Check up the vial	100	1.10	0.36	36.67	F
3-3-4	Hand clean	100	1.17	0.49	39.00	F
3-3-5	Shake the vial	100	1.89	0.93	63.00	F
3-3-6	Sterilization	100	1.54	0.82	51.33	F
3-3-7	Avoid the inflammation	100	1.20	0.57	40.00	F
3-3-8	Injection places sterilization	100	1.38	0.74	46.00	F
3-3-9	Air bubbles	100	2.39	0.87	79.67	P
3-3-10	Amount of insulin	100	2.38	0.90	79.33	P
3-3-11	Grasp	100	1.19	0.53	39.67	F
3-3-12	Angle	100	1.38	0.75	46.00	F
3-3-13	Syringe units	100	2.20	0.94	73.33	P

Table (2): Container

The practices of Juveniles who affected by diabetes (Type 1)		.No	.M.S	.S.D	.R.S	.Ass
3-3-14	Pressure on skin after injection	100	1.12	0.41	37.33	F
3-3-15	Measurement glucose	100	1.39	0.68	46.33	F
3-3-16	Change the injection	100	1.24	0.59	41.33	F
3-4	Foot care					
3-4-1	Skin cleanness	100	1.16	0.49	38.67	F

3-4-2	Examine my feet	100	1.24	0.61	41.33	F
3-4-3	Family	100	1.72	0.89	57.33	F
3-4-4	Feet hygiene	100	1.20	0.59	40.00	F
3-4-5	Change socks	100	1.15	0.46	38.33	F
3-4-6	Shoes	100	1.31	0.61	43.67	F
3-4-7	Warm water	100	1.55	0.83	51.67	F
3-4-8	Nails	100	1.12	0.38	37.33	F
3-4-9	Rub	100	1.21	0.56	40.33	F
3-4-10	Skin ointment	100	1.27	0.65	42.33	F
3-4-11	Walking	100	1.17	0.51	39.00	F
3-4-12	Hot is exposed	100	1.28	0.59	42.67	F
3-4-13	Washing with hot or cold water	100	1.20	0.43	40.00	F

Table (3): Showed the number of families.

Number of family	Patient's number	Percentage %
5 - 3	15	% 15
10 – 6	61	61%
15 - 11	17	17%
20 – 16	7	7%

Table (4): Frequency of family economical level.

Family economical level	Patient's number	Percentage %
Good	19	19%
Mild	69	69%
Poor	12	12%

Table (5): Frequency of fund of crisis.

Found of crisis	Patient's number	Percentage
Crisis	47	47%
No crisis	53	53%

\

Table (6): Show the frequency of clinical features.

Clinical features	Patient's number	Percentage
Weight loss	46	46%
Polyphagia	61	61%
Polyurea	89	89%
Polydepsia	78	78%
Blurred vision	42	42%

Table (7): Frequency of the area.

Area	Patient's number	Percentage%
Urban	56	56%
Ruler	44	44%

Table (8): Frequency of gender.

Sex	Patient's number	Percentage%
Male	55	55%
Female	45%	45%

Table (9): Frequency of genetic risk factors.

Causes	Patient's number	Percentage
Genetic	32	32%
Non genetic	68	68%

Table (10): Frequency of weight risk factors.

Weight	Patient's number	Percentage%
Thin	46	46%
Normal	43	43%
Overweight	11	11%

Table (11): Frequency of education, level of the mother.

Education level of mother	Patient's number	Percentage%
Illiterate	23	23%
Read and write	14	14%
Primary school	26	26%
Secondary school	20	20%
Diploma	9	9%
Bachelors	8	8%

Table (12): Frequency of patient's fasting blood sugar.

Fasting blood sugar mg/dl	Patient's number	Percentage
50 – 99	8	12.12%
100 – 149	10	15.15%
150 – 199	7	10.6%
200 – 249	7	10.6%
250 – 299	12	18.18%
300 –349	12	18.18%
350 – 400	6	9%
More than 400	4	6%

Table (13): Patient's random blood sugar test.

Random blood sugar	Patient's number	Percentage
100 – 149	5	14.8%
150 – 199	5	14.7%
200 – 249	9	26.4%
250 – 299	2	7.8%
300 – 349	8	14.5%
350 – 400	2	13.8%
More than 400	3	8.82%
Total	34	100%

Table (14): Frequency of patient's random blood urea.

Blood urea mg/dl	Patient's number	Percentage
20 – 24	43	67%
25 – 29	34	53%
30 – 34	22	29%
More than 35	1	1%
Total	100	100%

Table (15): Frequency of the patient's serum creatinine.

Serum creatinine	Patient's number	Percentage
0.6 – 3	98	98%
More than 3	2	2%
Total	100	100%

Table (16): Frequency of patient's serum cholesterol.

Serum cholesterol	Patient's number	Percentage
95 – 124	25	25%
125 – 174	63	63%
175 – 200	11	12%
Total	100	100%

4. Discussion:

Our study a descriptive (cross-sectional design) was conducted in (2) observational centre Bint al-Huda educational hospital and Diabetic and Endocrine glands centre in Nasiriya city, and this study started from October 2012 to April 2013 and included the ages of the patients (1-18) years. The results revealed that the majority of samples from school age in which there is no super advice and because as showed by the results the low educational level of the patients' mothers or family, so the uncontrolled nutritional system by the children represented by the increase amount of candy intake lead to hyperglycaemia and may be overweight. Table (1) showed the sudden onset or susceptible age affected by diabetes in children are from (year to 5 years) represented *(*44%*)* of the patients.

This result agrees with the study of [12] which referred to the incidence of DM-1 is increasing in children and youth by about (3%) (range about 2–5%) per annum, with the greatest rate of rise in the under 4-yr-old age group [12]. Our results also supported by a prospective data collection in Kuwait between 1992 and 1997 showed an incidence in children under the age (5) years rising dramatically to (20.9) per (100 000) (5) years later. The rise was particularly steep in those aged (5–9) years [13]. In Table (2) there are no any significant differences between the mothers age categories. There is an enormous gap between knowledge and practice of optimal diabetes care, and a major factor in this gap is lack of care organization and the disease knowledge. Regarding to the family members' number (6-10) is a higher than other number's categories and the majority of the patient's family have a mild economical level as described in forms and Tables (4). The increase of diabetes is closely related to socioeconomic and environmental factors together with a genetic influence. There was a 10-fold difference between the different countries, with higher rates in the diabetes, and those from low incidence countries, as well as those from families of a lower socioeconomic status [22]. The described changing patterns of pre-sanitation of diabetes have also changed the incidence and severity of DKA in children [21]. Although

more than)85%(of DM-1 occur in individuals with no previous first degree family history, the risk among first degree relatives is about 15 times higher than in the general population. About the crisis, the statistical Table (5), showed the patients did not have crisis were higher than the patient has a crisis. The development of complications is related to the duration of diabetes, and youth with diabetes represent a population at high risk for developing these complications. Indeed, persons diagnosed with diabetes before (20) years of age have a markedly lower life expectancy than the general population without diabetes [23]· According to the area, the statistical Table (8), so the majority of patient were urban According to the gender, the statistical Table (9) shows the male sex was higher than female sex. Between 10- to 19-year-old youth, we found a higher prevalence among female youth (compared with male youth) in (3) of the (5) racial/ethnic groups (black, API, and AI). A study found an excess prevalence of female youth among black youth, but not among NHW youth [19]. Regarding to the genetic risk factor, the statistical Table (10), showed the patients did not have genetic risk factor were higher than genetic risk factor as only ~(5%) or fewer subjects with genetic susceptibility to DM-1 develop the clinical disease [5]. According to the weight risk factor the statistical Table (11), showed the thin patient riskier than other weights. Although children with type 1diabetes are typically not overweight, the population of many countries is becoming more overweight. It is estimated that as many as a quarter of children with DM-1 in these countries may be overweight at the time of diagnosis [15].

Regarding the investigations in the Table (13), there is an increase in threading of fasting blood sugar in the range (250-299) mg\dl were 12 patients (18.18%) of the total number of patients (66), that's who made fasting blood sugar test and range (300-349) mg\dl so on. Patients who made random blood sugar they were (n=34) patients. Most read recurrent from (200-249) mg\dl in Table (14). And other investigation, routinely made for diabetic patient, such as blood urea there is increasing over the normal range. Most recurrent reading was at the range (20-24) mg\dl and (p=67%) in the Table (15). At the serum creatinine more patient's serum creatinine was *(*98%*)* of the range (0.6-3) mg\dl in Table (16). And serum cholesterol greater reading was at the range (125-174) mg\dl were (n=63), (p=63%). We conclude with these results the age of patients, age of the patient's mother, number of family, economical level of family and education level of the mother was effected to the onset of disease.

References

[1] Knip M, Virtanen SM, Seppa K, et al., Ilonen J, Savilahti E, Vaarala O, Reunanen A, Teramo K, Hämäläinen AM, Paronen J, Dosch HM, Hakulinen T, Akerblom HK; Finnish TRIGR Study Group. Dietary intervention in infancy and later signs of beta-cell autoimmunity. N Engl J Med.;363(20):1900-8, (2010).

[2] Akerblom HK, Knip M. Putative environmental factors in Type 1 diabetes. Diabetes Metab Rev.14(1):31-67, (1998).

[3] Variation and trends in incidence of childhood diabetes in Europe. Eurodiab ACE Study Group. Lancet.355(9207):873-6, (2000).

[4] Atkinson MA, Eisenbarth GS. Type 1 diabetes: new perspectives on disease pathogenesis and treatment. Lancet.358(9277):221-9, (2001).

[5] Virtanen SM, Knip M. Nutritional risk predictors of beta cell autoimmunity and type 1 diabetes at a young age. Am J ClinNutr.78(6):1053 -67, (2003).

[6] Australian Institute of Health and Welfare. Incidence of Type 1 diabetes in Australian children 2000-2008. Diabetes series no. 13. Cat. No. CVD 51. Canberra: AIHW, (2010).

[7] Onkamo P, Vaananen S, Karvonen M, Tuomilehto J. Worldwide increase in incidence of Type I diabetes--the analysis of the data on published incidence trends. Diabetologia.42(12):1395-403, (1999).

[8] Joner G, Stene LC, Sovik O. Nationwide, prospective registration of type 1 diabetes in children aged <15 years in Norway 1989-1998: no increase but significant regional variation in incidence. Diabetes Care.27(7):1618-22 (2004).

[9] Karvonen M, Viik-Kajander M, Moltchanova E, et al. Incidence of childhood type 1 diabetes worldwide. Diabetes Mondiale (DiaMond) Project Group. Diabetes Care.23(10):1516-26, (2000).

[10] GALE EAM. The rise of childhood type 1 diabetes in the 20thcentury. Diabetes: 51: 3353–3361, (2002).

[11] Onkamo P, Vaananen S, Karvonen M, Tuomilehto J. World- wide increase in incidence of type I diabetes: the analysis of the data on published incidence trends. Diabetologia.42: 1395–1403, (1999).

[12] International diabetes federation (IDF) world atlas of diabetes. (available from www.eatlas.idf.org), (2006).

[13] Shaltout AA, Moussa MAA, Qabaard D M et al; For the Kuwait diabetes study group. Further evidence of the rising incidence of childhood type 1 diabetes in Kuwait. Diabet Med: 19: 522–525, (2002).

[14] American diabetes association. Type 2 diabetes in children and adolescents. Diabetes Care: 23: 381–389, (2000).

[15] Dunger DB, SperlIng MA, Acerini CL et al. ESPE/ LWPES consensus statement on diabetic ketoacidosis in children and adolescents. Arch Dis Child. 89: 188–194, (2004).

[16] Delli AJ, Larsson HE, Ivarsson SA et al. Type 1 diabetes, in Holt RIG, Cockram CS, Flyvbjerg A et al (Ed.) Textbook of diabetes, 4edition. Oxford: Wiley Blackwell, (2010).

[17] Dean HJ, Moffatt M. Prevalence of diabetes mellitus among Indian children in Manitoba. Arctic Med Res.

[18] Oeltmann JE, Liese AD, Heinze HJ, Addy CL, Mayer-Davis EJ. Prevalence of diagnosed diabetes among African-American and non-Hispanic white youth, 1999. Diabetes Care.26: 2531–2535, (2003).

[19] Allen PJ, Vessey JA. Primary Care of the Child with a Chronic Condition. 4th ed. St Louis, MO: Mosby, (2004).

[20] Dean HJ, Moffatt M. Prevalence of diabetes mellitus among Indian children in Manitoba. Arctic Med Res.

[21] [21] Oeltmann JE, Liese AD, Heinze HJ, Addy CL, Mayer-Davis EJ. Prevalence of diagnosed diabetes among African-American and non-Hispanic white youth, 1999. Diabetes Care.26: 2531–2535, (2003).

[22] Edwards TR. Incidence, prevalence, and mortality of diabetes mellitus in Wadena, Marshall, and Grand Rapids, Minnesota: The Three-City Study. Diabetes Care.9:343–350, (1986).

[23] Lee JM, Herman WH, McPheeters ML, Gurney JG. An epidemiologic profile of children with diabetes in the US. Diabetes Care.29:420–421, (2006).

[24] Libman I, Songer T, Laporte R. How many people in the US have IDDM? Diabetes Care. 16: 841–842, (1993).

On Bi-domination in Graphs

(Manal Naji) M. N. Al-Harere and Athraa T. Breesam
Department of Applied Sciences, University of Technology, Baghdad, Iraq.

Received Date: 14 / 6 / 2017
Accepted Date: 1 / 11 / 2017

الخلاصة

المجموعة المهيمنة هي المجموعة ذات الهيمنة المزدوجة في الرسم البياني ، إذا كان كل قمة في هذه المجموعة، تسيطر تمامًا على رأسين لا ينتميان إلى المجموعة المهيمنة. في هذا العمل ، تم تقديم خمسة تعريفات جديدة للهيمنة، وهي عبارة عن صيغ معدلة للهيمنة المزدوجة: «هيمنة ثنائية مستقلة ؛ الهيمنة الثنائية الكاملة ، الهيمنة الثنائية المتصلة، الهيمنة المقيدة ، شجرة تكميلية ثنائية الهيمنة «. يتم تحديد الحدود العليا والدنيا لحجم الرسوم البيانية التي تحتوي على هذه المعلمات.

الكلمات المفتاحية

ثنائية الهيمنة ، مجموعة ثنائية الهيمنة مستقلة ، مجموعة ثنائية الهيمنة الكلي ، مجموعة ثنائية الهيمنة المتصلة ، شجرة تكميلية ثنائية الهيمنة، هيمنة ثنائية مقيدة.

Abstract

A dominating set is a bi-dominating set in a graph, if every vertex in this set, dominates exactly two vertices that, do not belong to the dominating set. In this work, five new definitions of domination have been presented, which they are a modified versions of bi-domination: "independent bi-domination; total bi-domination, connected bi-domination, restrained domination, and complementary tree bi-domination". Upper and lower bounds are determined for the size of graphs having these parameters.

Keywords

bi-domination, independent bi-dominating set, total bi-dominating set, connected bi-dominating set, complementary tree bi-domination, restrained bi-domination.

Mathematical subject classification: (05C69)

1. Introduction

Let G=(E,V) be a graph with a set V(G) of vertices of order n and a set E(G) of edges of size m. The "degree of a vertex v∈ V(G)", of any graph G is defined as the number of edges incident on v. It is denoted by deg(v). The "minimum and maximum degrees of vertices in G denoted by δ(G) and Δ(G) respectively ". The "open neighborhood "N(v) is the set of vertices adjacent to v, and the "closed neighborhood" N[v]=N(v)∪{v}." The subgraph of G induced by the vertices in D is denoted by G[D],[2].

O. Ore is the first one who introduced the term "domination number" and "dominating set "[5]. A set D "⊆" V is a "dominating set " in G, if every vertex in V – D is adjacent to a vertex in D, that is N[D]=V. The minimum cardinality over all dominating set in G is the "domination number γ(G)"[7]. In recent years, many types of domination-related parameters have been studied. For a historical reference in this regard see books written by Haynes et al [3, 4, 6].

A dominating set D is an "independence dominating set" in G if [D] ,doesn't has edges, and where a set D is a "total dominating set" in G if G[D] , has no isolated vertex and, if G[D] is connected, then this is known as a "connected dominating set" in G, if G[D] is connected, also set D known as a "restrained dominating set" where, "every vertex doesn't belongs to dominating set D, is adjacent to a vertex in D and, to another vertex not in D"[3]. A set D is a "complementary tree dominating set" if, G[V-G] is a tree [8]. Finally, the new definition is the "bi-domination" where a dominating set D is a "bi-dominating set" in G, if every vertex in set D dominates exactly two vertices in V-D [1].

Here, the definitions of the parameters of some types of bi-domination like "independent bi-dominating set, total bi-dominating set, connected bi-dominating set, complementary tree bi-dominating set and restrained bi-dominating set" are introduced, this study includes the bounds of the size of any graph has these types of domination.

1.1. Definition [1]

"For any graph G(V,E) which is finite and simple undirected graph without isolated vertex, a subset D ⊂ V(G) is a bi-dominating set if every vertex in D dominates exactly two vertices in V-D, such that |N(v) ∩ V-D| = 2. The minimum cardinality of bi- dominating set is denoted by γ_{bi} (G). The domination number of G, denoted γ_{bi} (G) is a minimum cardinality over all bi-dominating set in G".

1.2. Observation [1]

For any finite simple graph G(n,m) with a bi- dominating set D and bi-domination number γbi(G). We have

The order of G is n ≥ 3.

δ(G) ≥1 , Δ(G) ≥2.

Every v ∈ D, deg(v)≥ 2.

Every support vertex v,v∈ D.

$\gamma(G) \leq \gamma_{bi}(G)$.

2. Independent bi-dominating set

2.1. Definition

"A subset D⊂ V(G) is an independent bi-dominating set in graph G if, D is a bi-dominating set such that, the induced subgraph <D> has no edges, while the minimum cardinality of an independent bi-dominating set is denoted by $\gamma_{bi}^{i}(G)$".

2.2. Theorem

If graph G(n,m) has an independent bi-domination number $\gamma_{bi}^{i}(G)$ then

$$2\,\gamma_{bi}^{i}(G) \le m \le \frac{n^2 - n + (\gamma_{bi}^{i}(G))^2 - 2n\,\gamma_{bi}^{i}(G) + 5\,\gamma_{bi}^{i}(G)}{2}$$

Proof.

The proof requires two cases and as follows: let D be a γ_{bi}^{i} - set of G.

Case 1. To prove the lower bound $2\,\gamma_{bi}^{i}(G) \le m$:

By the definition of independent bi-dominating set, G[D] is a null graph, and there exist exactly two edges incident to, every vertex in D. Let G[V-D] be a null graph. So G contains as few edges as possible and G[V-D] will not violate the definition of independent bi-domination. Therefore, the number of edges is $2|D| = 2\,\gamma_{bi}^{i}(G)$. Thus, in general $m \ge 2\,\gamma_{bi}^{i}(G)$.

Case 2. To prove the upper bound:

Since set D is independent then, all vertices of G[D] are isolated and since, the number of edges of G[V-D] does not affect vertices of set D then, let G[V-D] be a complete induced subgraph. Let m_1 be the number of edges of G[V- D] Therefore,

$$m_1 = \frac{|V-D||V-D-1|}{2} = \frac{(n-\gamma_{bi}^{i}(G))(n-\gamma_{bi}^{i}(G)-1)}{2}$$

Since, D is a bi-dominating set, so let $m_2 = 2|D| = 2\,\gamma_{bi}^{i}(G)$,so $m = m_1 + m_2$.

$$\text{Hence, } m = 2|D| + \frac{|V-D||V-D-1|}{2} = 2\,\gamma_{bi}^{i}(G) + \frac{(n-\gamma_{bi}^{i}(G))(n-\gamma_{bi}^{i}(G)-1)}{2}.$$

3. Total bi-dominating set

3.1. Definition

"A subset D⊂V(G) is, a total bi-dominating set in G if set D is a bi-dominating such that, <D> has no isolated vertex, $\gamma_{bi}^{t}(G)$ is the minimum cardinality of a total bi-dominating set in G".

3.2. Theorem

Let G(n,m) be a graph having a total bi-domination number $\gamma_{bi}^{t}(G)$ then

$$3\,\gamma_{bi}^{t}(G) \le m \le \frac{n^2 - n}{2} + (\gamma_{bi}^{t}(G))^2 - n\,\gamma_{bi}^{t}(G) + 2\,\gamma_{bi}^{t}(G)$$

Proof.

Let set D be a γ_{bi}^{t}-set of G.

Case 1. To prove the lower bound $3\,\gamma_{bi}^{t}(G) \le m$:

This case occurs when the induced subgraph G[V-D] is a null graph, and since D is a total dominating set, so every vertex in D has at least a degree equal to 3. Therefore, the number of edges is $m = 3|D|$ so $3\,\gamma_{bi}^{t}(G) \le m$.

Case 2. To prove the upper bound, this case occurs where, the two induced subgraphs G[D] and G[V-D] are complete, so let m_1 and m_2 be the number of edges of G[D] and G[V- D] respectively. Therefore,

$$m_1 = \frac{|D|\,|D-1|}{2} = \frac{\gamma_{bi}^{t}(G)(\gamma_{bi}^{t}(G)-1)}{2}$$

$$m_1 = \frac{|D|\,|D-1|}{2} = \frac{\gamma_{bi}^t(G)(\gamma_{bi}^t(G)-1)}{2}$$

And according to the definition of bi-domination set we have m_3 edges between G[D] and G[V-D] where, $m_3=2|D|=2\,\gamma_{bi}{}^t(G)$, so in this case $m=m_1+m_2+m_3$.

Hence,

$$m = 2|D| + \frac{|D|\,|D-1||}{2} + \frac{|V-D||V-D-1|}{2} = 2\gamma_{bi} + \frac{\gamma_{bi}^t(G)(\gamma_{bi}^t(G)-1)}{2} + \frac{(n-\gamma_{bi}^t(G))(n-\gamma_{bi}^t(G)-1)}{2}.$$

In general, $m\leq m_1+m_2+m_3$.

4. Connected bi-dominating set

4.1. Definition

"Let D be a subset of V(G) then D is a connected bi-dominating set in G if, D is a bi-dominating set, such that, <D> is a connected induced subgraph. $\gamma_{bi}{}^c(G)$ is the minimum cardinality of a connected bi-dominating set"

4.2. Theorem

The size of graph G(n,m) has connected bi-domination number $\gamma_{bi}{}^c(G)$ is

$$3\,\gamma_{bi}^c(G) - 1 \leq m \leq \frac{n^2-n}{2} + \gamma_{bi}^c(G)^2 - n\,\gamma_{bi}^c(G) + 2\,\gamma_{bi}^c(G)$$

Proof.

We prove the required by two cases that depend on the bounds as follows: Let set D be a γ_{bi} - set of G

Case 1. To prove the lower bound $3\gamma_{bi}-1\leq m$.

Based on a Theorem 2.3 the number of edges is $m_1= 2\,|D|=2\gamma_{bi}$ since D is a bi-dominating set. Moreover, the induced subgraphs G[D] should contain as few edges as possible to be a connected. Thus, the minimum number of edges is $m_2=(D-1)=(\gamma_{bi}{}^c(G)-1)$ thus, $m=m_1+m_2=2\,\gamma_{bi}{}^c(G)+(\gamma_{bi}{}^c(G)-1)=3\,\gamma_{bi}{}^c(G)-1$. In general, $m\geq m_1+m_2$.

Case 2. The same proof in Theorem 3.2 (case 2).

5. Restrained bi-dominating set

5.1. Definition

"A bi-dominating set is a restrained bi-dominating set D in a graph G, such that G[V-D] has no isolated vertices. The minimum cardinality of a restrained bi-dominating set, is the restrained bi-domination number of G, is denoted by $\gamma_{bi}{}^r(G)$."

5.2. Theorem

The size of graph G(n,m) has restrained bi-dominating set $\gamma_{bi}{}^r(G)$ is

$$2\,\gamma_{bi}^r(G) + \left\lceil\frac{n-\gamma_{bi}^r(G)}{2}\right\rceil \leq m \leq \frac{n^2-n}{2} + \gamma_{bi}^r(G)^2 - n\,\gamma_{bi}^r(G) + 2\,\gamma_{bi}^r(G)$$

Proof.

Let D be a $\gamma_{bi}{}^r$ - set of G, so the number of edges is calculated from the two following cases.

Case 1. To prove the lower bound $2\,\gamma_{bi}^r(G) + \left\lceil\frac{n-\gamma_{bi}^r(G)}{2}\right\rceil \leq m$:

This case occurs where the induced subgraph G[D] is a null graph, and since D is a bi-dominating set then the number of edges is $m_1= 2\,|D|=2\,\gamma_{bi}{}^r(G)$. Additionally the graph G[V-D] should be containing as few edges as possible to be a graph with isolated vertices. Thus, the number of edges is $m_2 = \left\lceil\frac{|V-D|}{2}\right\rceil = \left\lceil\frac{n-\gamma_{bi}^r(G)}{2}\right\rceil$, so in this case $m=m_1+m_2$. Hence, $m = 2\,\gamma_{bi}^r(G) + \left\lceil\frac{n-\gamma_{bi}^r(G)}{2}\right\rceil$ .In general, $m\geq m_1+m_2$.

Case 2. The same proof in Theorem 3.2 (case 2).

6. Complementary tree bi-dominating set

6.1. Definition

"The complementary tree bi-dominating set D is, a bi-dominating set such that, the induced subgraph <V-D> is a tree. The minimum cardinality of a complementary tree bi-dominating set, is denoted by $\gamma_{bi}^{ct}(G)$ ".

6.2.Theorem

Let G(n,m) has complementary tree bi-dominating set $\gamma_{bi}^{ct}(G)$, then

$$\gamma_{bi}^{ct}(G) + n - 1 \leq m \leq \frac{n^{\prime} - n}{2} + (\gamma_{bi}^{ct}(G))^2 - n\,\gamma_{bi}^{ct}(G) + 2\,\gamma_{bi}^{ct}(G)$$

Proof.

Let D be a γ_{bi}^{ct}- set of G, so we prove the required by two cases that depend on the boundaries as follows:

Case 1. To prove the lower bound $\gamma_{bi}^{ct}(G)+n-1\leq m$.

Depending on a definition of bi-dominating set the number of edges is $m_1= 2\ |D|= \gamma_{bi}^{ct}(G)$. Moreover, the induced subgraph G[V-D] should contain as few edges to be a tree graph so the number of these edges is $m_2=|V-D|-1=(n- \gamma_{bi}^{ct}-1)$. So, in this case, $m=m_1+m_2=2\ \gamma_{bi}^{ct}+(n- \gamma_{bi}^{ct}-1)$. Hence,$m\geq \gamma_{bi}^{ct}+n-1$.

Case 2. The same proof in Theorem 3.2 (case 2).

Reference

[1] M. N. Al-harere and Athraa T. Breesam , Inverse bi-domination in graphs, accepted in International Journal of Pure and Applied Mathematics, 2017.

[2] F. Harary, Graph Theory, Addison - Wesley, Reading Mass, 1969.

[3] T. W. Haynes, S.T. Hedetniemi and P. J. Slater, Fundamentals of domination in graphs, Marcel Dekker, Inc., New York ,1998.

[4] T. W. Haynes, Michael A. Henning, Ping Zhang, A survey of stratified domination in graphs, Discrete Mathematics 309, 5806-5819,2009.

[5] O. Ore., Theory of graphs, American Mathematical Society, Provedence, R.I., 1962.

[6] A. A. Omran, M.N. Al-Harere, Variant types of domination in triangular graph, The 23rd Specialized Scientific Conference of College of Education, University of Mustansiriya, April, 2017.

[7] E. Sampathkumar and P. S. Neeralagi, The neighborhood number of a graph, Indian J. Pure and Appl. Math.16 (2) ,126 - 132,1985.

[8] E. Sampathkumar and H.B. Walikar, The connected domination number of a graph, J. Math. Phys. Sci., 13,607-613, 1979.

Experimental and Numerical Evaluation of Impact Strength for Carbon/ E-Glass/ Epoxy Composite Plate

*Abdul Kareem Abdul razzaq Al-Humdany
** Jawad Talib Abodi
*Salah Mahdi Ali
*Mechanical Engineering Department, College of Engineering, University of Karbala، Iraq
**Civil Engineering Department, College of Engineering, University of Karbala، Iraq.

Received Date: 2 / 8 / 2017
Accepted Date: 15 / 3 / 2018

الخلاصة

في هذا البحث تم استخدام برنامج الأنسس لتحليل الاجهادات الناتجة عن اصطدام رصاصه عيار (9) ملم بالصفائح المركبة الهجينة. المواد المستخدمة في هذا البحث هي ألياف كربونية ذات اتجاه واحد والياف زجاجية مع الايبوكسي. التجارب العملية في هذا البحث تتضمن تصنيع صفائح هجينه من الألياف الكربونية والزجاجية مع الايبوكسي وبسمك مختلف وإطلاق الرصاص عليها بسرعه (371) م\ث ومن مسافة (5) م. لإثبات النتائج المتحصل عليها من برنامج الأنسس تم مقارنة سرعة خروج الرصاصة واقل سرعة لازمة لاختراق هذه الألواح والطاقة الممتصة من قبل الالواح مع النتائج العملية. وقد بينت النتائج أن إجهاد القص والانفعال يكون في أعلى قيمة في الطبقات الأولى بينما إجهاد الشد يكون في أعلى قيمة له في الطبقات الأخيرة وان اقل سرعة لازمة لاختراق لوح من الالياف الكربونية والزجاجية والايبوكسي بسمك (5) ملم هو (371) م\ث، استخدام الالياف الزجاجية مع الالياف الكربونية يقلل الكلفة ويحسن امتصاص الطاقة ويزيد من مقاومة الصدمة.

الكلمات المفتاحية

برنامج الأنسس، بالصفائح المركبة الهجينة، مقاومة الصدمة.

Vol. 9, No. 17 and 18, P. (69-83),Jun, 2019

Abstract

In this work finite element ANSYS program is used to analyze the impact stresses of (9) mm bullet impact on hybrid composite plate using explicit dynamic and autodyne code. The material used in this work is unidirectional carbon fibers and plain weave E-Glass with epoxy as matrix. The experimental work includes manufacturing composite plates made from Carbon/E-Glass/Epoxy with different thicknesses subjecting these plates to impact by 9mm bullets at speed of (37) m/s from (5) m distance. The numerical results were proved by comparing the bullets residual velocity, the ballistic limit, and the energy absorption with the results from the experiment work. The results show that the shear and strain are maximum in the front layers while the tensile stress is maximum at the rear layers. The hybrid plates have good ballistic limit, and using E-Glass fibers with carbon fibers reduce the cost and improving the energy absorption and the impact resistance.

Keywords

ANSYS program, Hybrid composite plate, Impact resistance.

1. Introduction

Impact studies are so important in many fields like military, airspace and motivate the researchers to conduct more experiments and studies to get clear picture to the impact behavior. This search analysis and study the impact stresses of striking bullets on composite plate, and a unidirectional Carbon Fiber Reinforced polymer (CFRP), plain weave E-Glass fibers, with epoxy as matrix were used in this work. The high mechanical properties of composite material such as the high strength and low density compared to conventional material gave it important role in aerospace, automotive, and military manufacturing such as helmets and body armor. Harpreet and Puneet [1] conducted numerical and experiment analysis to find the impact damage of the composite materials using ABAQUS/Explicit. The material used in this work is graphite/epoxy and)6.5(g steel bullet with different speeds. The authors concluded that the numerical result in prediction the composite

damage matches well with the experiment results. V. Narayanamurthy et al. [2] performed numerical simulation to analyze the impact of steel bullets on steel target using ANSYS LS DYNA software and the authors proved this software can efficiently have calculated the impact parameter such as the damage, bullet residual velocity, and bullet displacement. Rimantas and Ausra [3] conducted a series of numerical analysis to prove that by using LS-DYNA software the bullet residual velocity can be accurately calculated. The authors have used Twaron textile in modeling the target and lead in modeling the bullet. The authors concluded that the residual velocity can be accurately calculated by using LS-DYNA software.

In this work impact stress analysis of Carbon/E-Glass/Epoxy composite plate is performed using ANSYS 16.1 software and the results proved by comparing the bullets residual velocity, the ballistic limit, the energy absorption with the experiment work. The result shows good agreement between the numerical and experimental work also shows hybrid plate with(5)mm thick can resist (9) mm bullet with speed of (371)m/s.

2. Projectile energy balance:

According to the conservation of the total energy, the projectile kinetic energy (KE_P) can be obtained by summing the projectile residual kinetic energy (KE_r) and the total energy absorbed by the target at that instant (KE_{abs}) which can be represented as follows [12]:

$$\mathbf{KE_P = KE_{abs} + KE_r} \quad \text{..... (1)}$$

3.The Hybrid Fabrication:

In order to integrate the best characteristics of both carbon and glass fibers reinforcement composite hybrid composite are introduced. Carbon fibers make the specimen stronger and the glass fibers preventing the material from collapsing [12], this does not mean that there is no internal damage but the carbon fibers retain in their place by the strengthening effects of nearby glass fibers. The hybrid laminates were fabricated using a unidirectional carbon

fiber type (sikawrap-230C), plain weave E-glass type (EWR600), and (sikadure-330) epoxy as matrix. The laminates were fabricated with volume fraction of (40%) fibers and epoxy volume fraction of (60%). In manufacturing the hybrid, the first ply was carbon fibers oriented in direction, the second ply was E-glass fibers in direction, the third ply was carbon fibers in direction and so on as in Table (1). All E-glass fibers plies placed in direction and carbon fibers ply alternating between and because according to [9] the ballistic limit and the energy absorption are maximum for the (0/90) lay-up laminate. The mechanical properties of the Carbon/Epoxy and E-glass/ Epoxy were calculated according to the manufacturer data sheet and the lamination theory as in Table (2) and (3).

Table (1): The hybrid layup

E-Glass fibers
Carbon fibers
E-Glass fibers
Carbon fibers
E-Glass fibers
Carbon fibers

Table (2): Carbon/Epoxy properties

Density	1.49 g/
E_{11}	97.9 GPa
E_{22}	7.4 GPa
E_{33}	7.4 GPa
G_{12}	2848.71 MPa
G_{23}	2607.971 MPa
G_{13}	2848.71 MPa
ν12	0.27
σT	1768.6 MPa
εT	0.018

Table (3): E-Glass/ Epoxy properties

Density	1.584 g/
E_{11}	9.14 GPa
E_{22}	9.14 GPa
E_{33}	5.15 GPa
G_{12}	1823.124 MPa
G_{23}	1215.277 MPa
G_{13}	1215.277 MPa
ν12	0.112
σT	162.7 MPa
εT	0.034

4. Impact Testing:

The experimental test was created according to the guidelines given by the National Institute of Justice (NIJ) standards (MIL-STD-662E, NIJ standard 0108.01) which is the most reliable test that widely used by agencies and armor manufacturers for product acceptance test [10]. The schematic of ballistic set-

up of (NIJ) test are shown in Fig. (1). The test weapon used was (9) mm handgun and fixed on stand to insure that the bullets are fired in strait line with the target and the chronograph also laser beam is used to help in aiming as shown in Fig. (2), and in order to determine the velocity of the bullet a Caldwell chronograph was used which is shown in Fig. (3). The test procedure used to test the composite plates was done using specimens of different thicknesses. The test specimens were perpendicular to the line of bullet flight at the point of impact, and one bullet was fired on each specimen. The bullet used in this test has flat ended and conical nose, the core was made from lead and the jacket from copper, the bullet length was (15.38) mm and the diameter (9) mm, and its weight 8g. Fig. (4) shows a tested hybrid plate 5mm thick consisting of (6) layers of carbon fibers and (6) layers of E-Glass fibers.

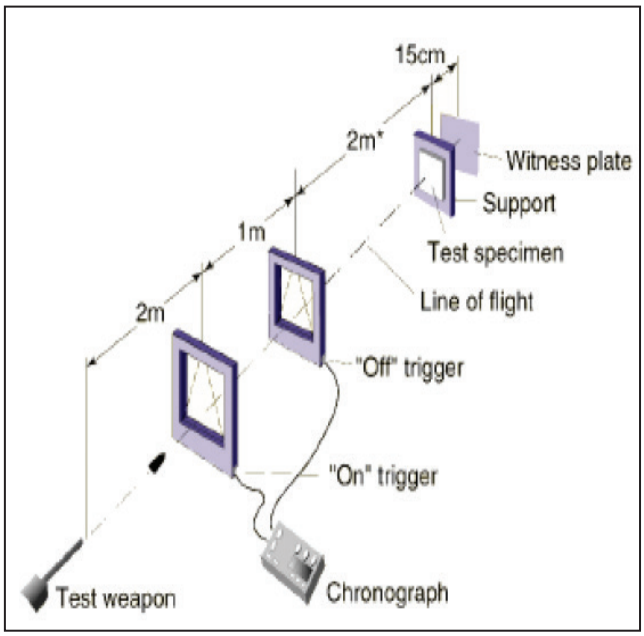

Fig. (1): The ballistic testing [10]

Fig. (2): Gun fixing mechanism

Fig. (3): The ballistic chronograph

Fig. (4): The front face of hybrid plate (5)mm thick [6 layers E-Glass and 6 layers Carbon fibers]

5. Projectile modeling:

For modeling the (9) mm bullet it has been used the lead metal as core and copper metal to encase the lead core as in Fig. (5). Jonson cook failure low is used in modeling the lead and copper metal [11]. The lead and copper metal properties are taken from ANSYS (16.1) engineering data sources- explicit materials. The projectile was modeled in detail according to the projectiles used in the experiments and in order to save computation time the planer symmetry condition in a quarter models is used as in Fig. (6), and in meshing the projectile a mesh of size 1 mm is used as in Fig. (7). The numerical analyzes is done by setting the bullet initial velocity of (371) m/s as it obtained from the experiments and due to the lack of thermal material data for the target material the heat generated during the impact is neglected.

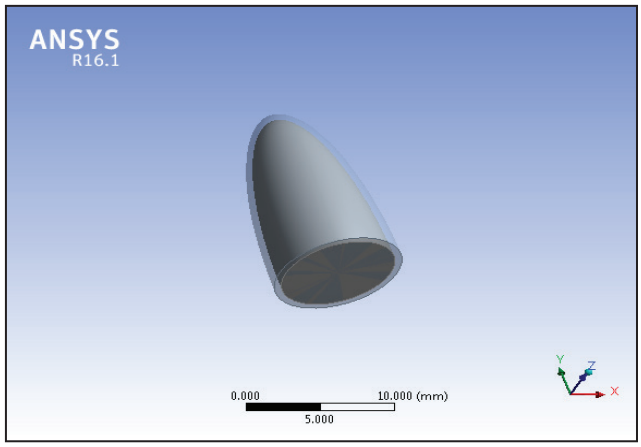

Fig. (5): Bullet modeling in ANSYS

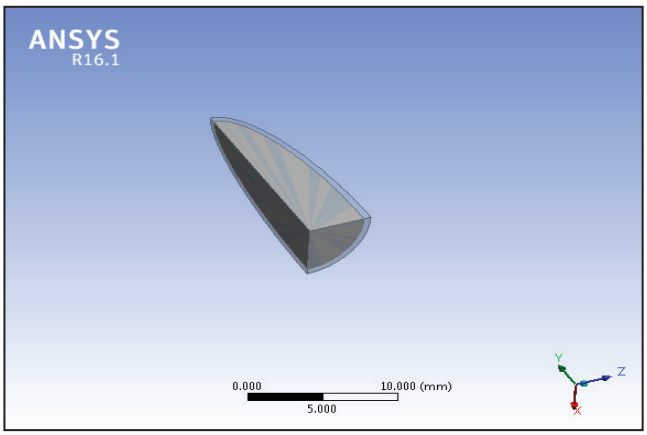

Fig. (6): Bullet symmetry

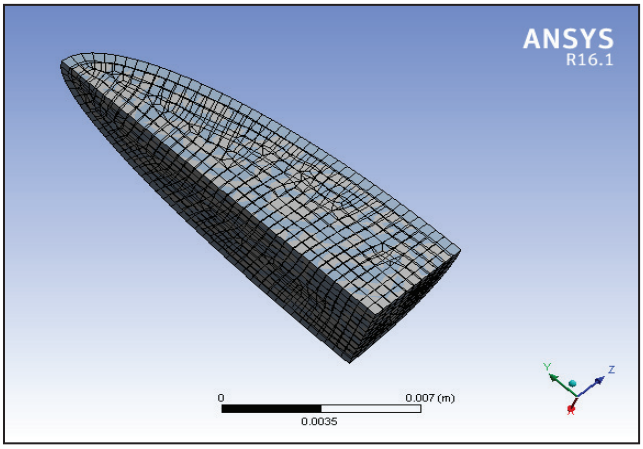

Fig. (7): Bullet meshing

6. Hybrid modeling:

In modeling of the hybrid composite plate the plies are layup in the same way that used in the experiment work. Ply to ply contact for the composite were defined using automatic contact, that because in the experimental work all the layers are fully bonded to each other, and the friction between the bullet and plate is set (0.2) [12]. All the plates are modeled in the same size and details as in experiment with (15)cm length, (15) cm width, and different thicknesses, and meshed with size of (1) mm. The boundary condition that has been used

is fixing the four edges of the plate. In this work the numerical analysis of the stresses of the impact is made using ANSYS 16.1 and a comparison with the experimental work were made. Symmetry boundary condition of (and are used to save time as shown in Fig. (8).

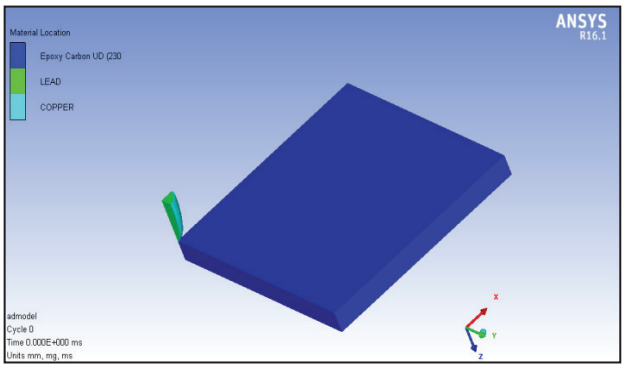

Fig. (8): Quarter model with symmetry condition X=Y=0.

7. Comparison between the Numerical Solution and the Experiment Work Results:

Fig. (9) shows the change in the residual velocity with plate thickness for the hybrid plate in both experimental and analytical solution. The residual velocity decreases with plate thickness increment and reaches zero at (5) mm thickness. The numerical solution shows reducing in the error with increasing plate thickness to reach zero in (5) mm case, that because the bullet temperature and the weather condition has been neglected due to the lack of data available, and this effects the bullet residual velocity.

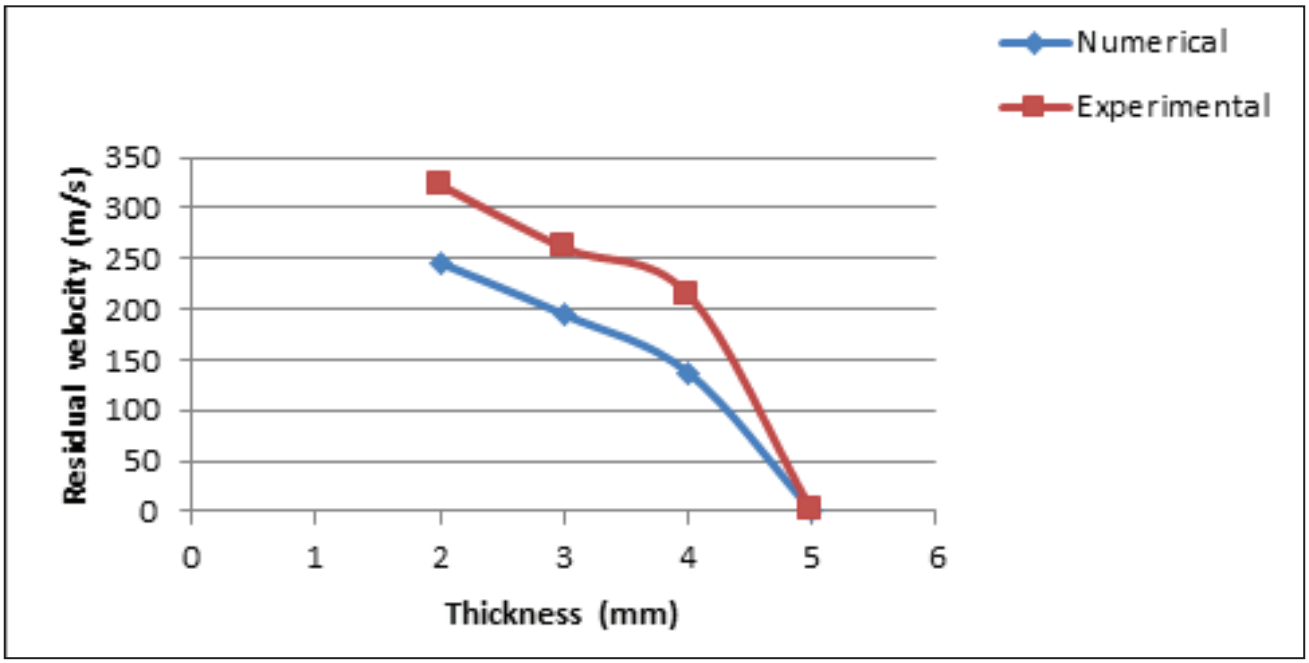

Fig. (9): The change in the residual velocity with plate thickness for the hybrid plates in both experimental test and numerical solution.

Fig. (10) shows the change in the bullet residual kinetic energy with plate thickness for the hybrid composite in both the experiment and the numerical work. Both the residual kinetic energy curves are decreasing with thickness and reach zero at (5) mm plate thickness that because with increasing the thickness the plates become stronger and therefore absorb higher energy.

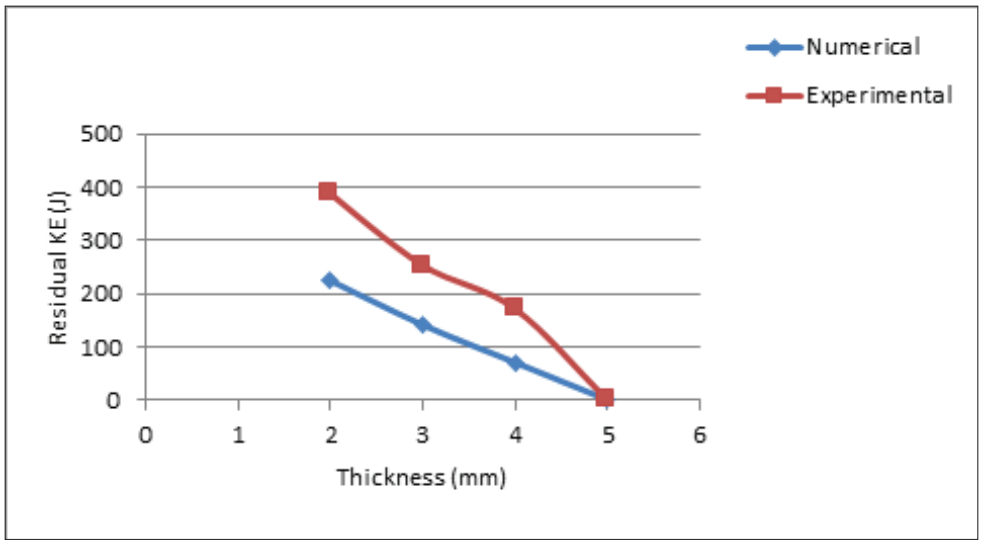

Fig. (10): The change in the bullet residual KE with plate thickness for the hybrid composite plate

Fig. (11) shows the change in the bullet energy absorbed with plate thickness in both the experiment and the numerical work. Both energy absorbed curves in this Fig. shows increasing with plate thickness until absorbed all the bullet energy at (5) mm plate thickness.

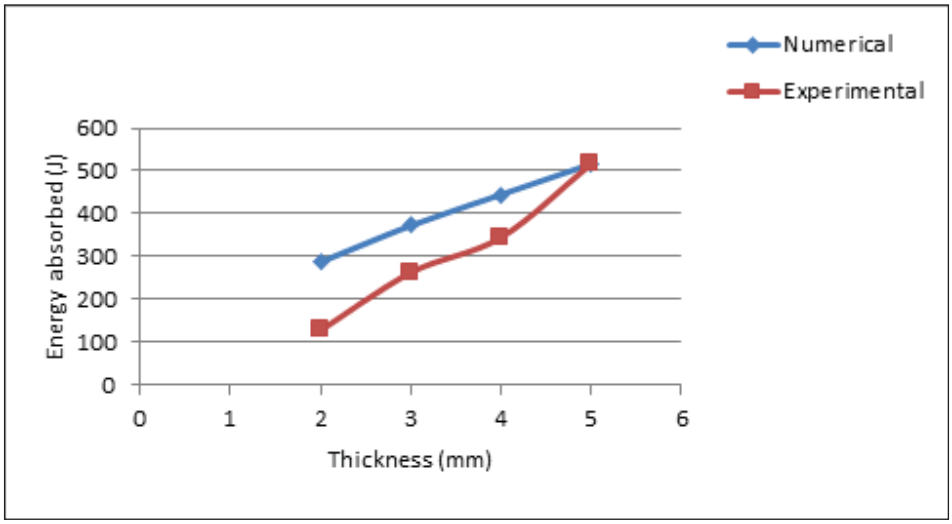

Fig. (11): The change in the energy absorbed with plate thickness for the hybrid composite plate

Fig. (12) shows comparison in ballistic limit for the hybrid plate (5) mm thick between experimental work and the numerical solution. The ballistic limit in the experimental work is (371) m/s and the experimental and numerical solution shows good agreement.

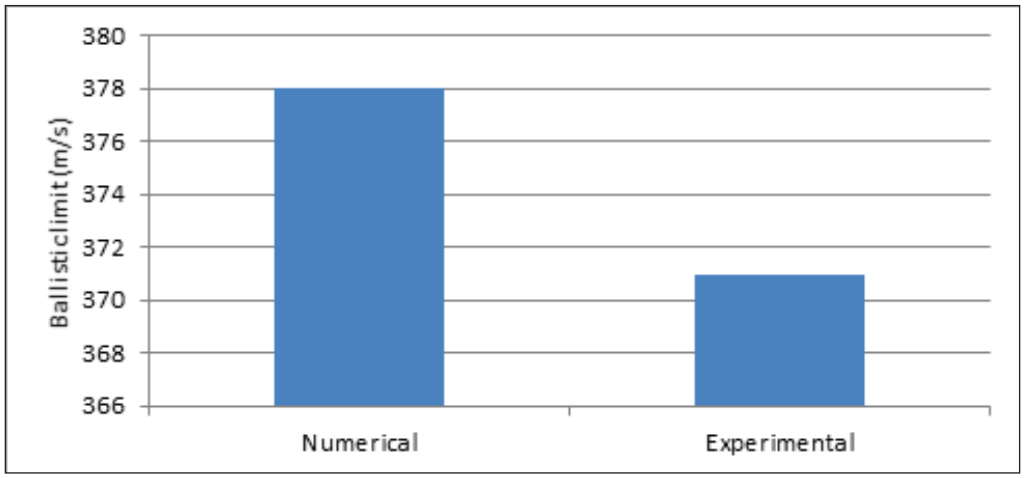

Fig. (12): Comparison in the ballistic limit for the hybrid plate (5) mm thick impacted by (9) mm bullet.

8. ANSYS Results of the Hybrid Models:

8.1. The Directional Deformation Result:

Fig. (13) shows the directional deformation in Z-direction for the hybrid plate)4(mm thick impacted by (9) mm bullet. The Fig. shows complete penetration to the hybrid plate, also it shows conoid formation and the maximum directional deformation is (0.035173) m. Fig. (14) shows the change in the directional deformation with time. The maximum directional deformation curve increasing with time and reach maximum at the end of impact setting time.

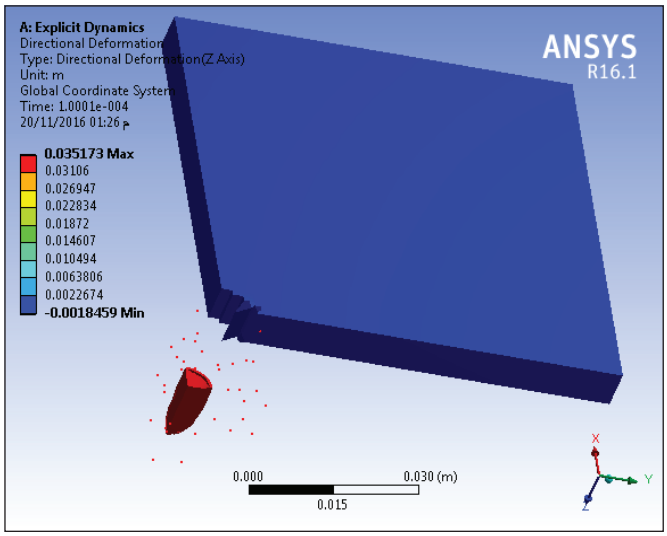

Fig. (13): The directional deformation in Z-direction

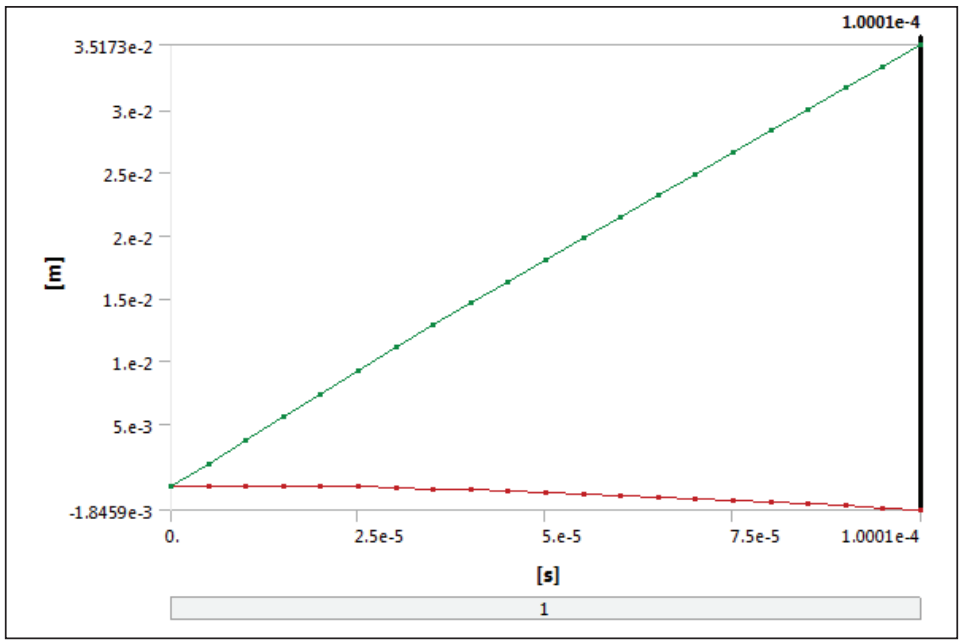

Fig. (14): The change in the directional deformation with time

8.2. The Maximum Principal Stress Result for The Hybrid Composite Plate:

Fig. (15) shows the stress distribution in hybrid plate at 0.0001s and the maximum principal stress at this time is 9.5536×10^{7}Pa. Fig. (16) shows the change in the stress with time. The maximum principal stress curve increases with time to reach maximum value 2.2791×10^{8}) Pa at (1.5×10^{-5}s. After that time the stress decreases because of the failure in the hybrid layers.

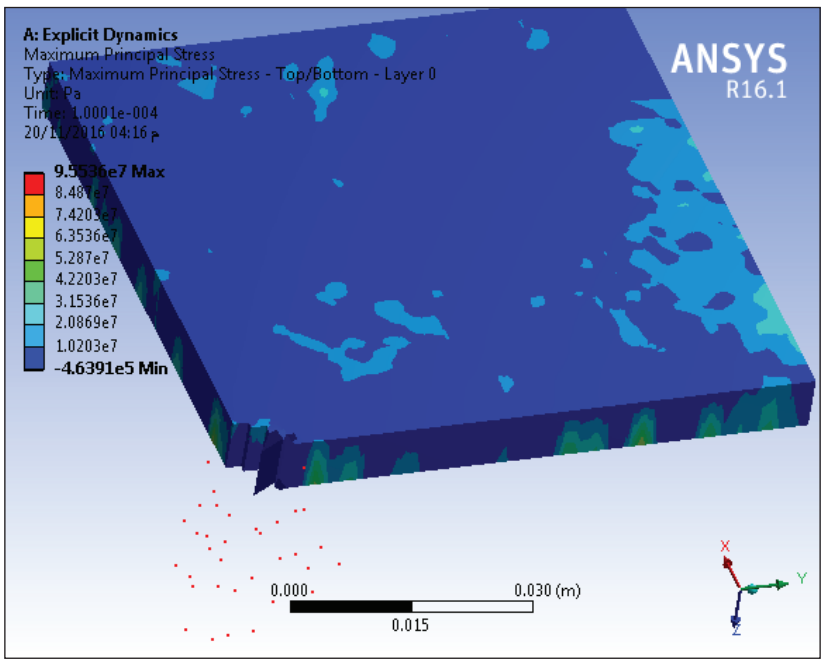

Fig. (15): The maximum principal stress distribution

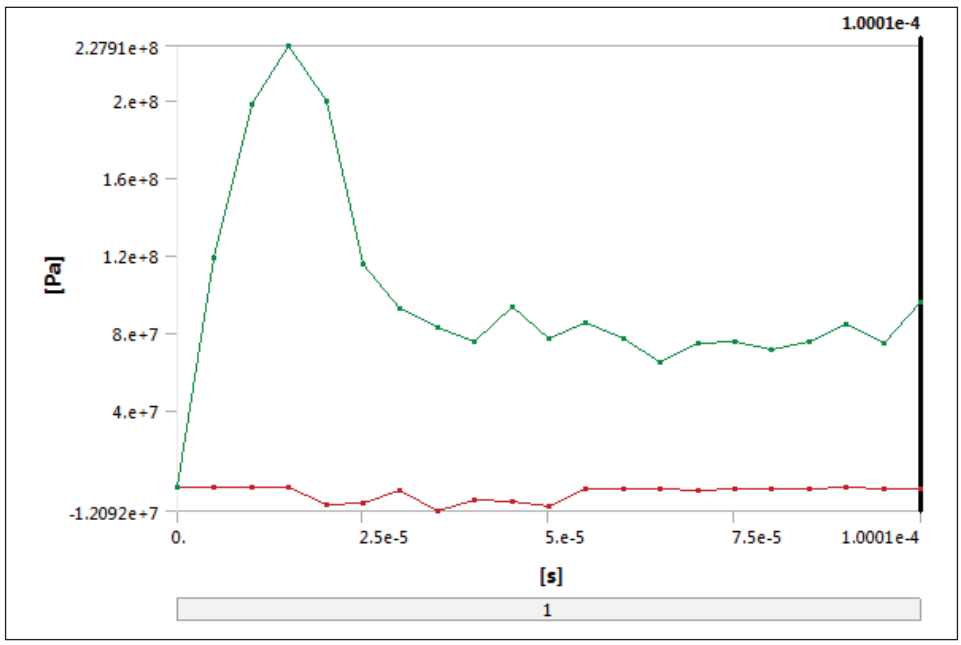

Fig. (16): The change in the maximum principal stress with time

8.3. The Maximum Principal Stress Result for The 9mm Bullet:

Fig. (17) shows the stress distribution in the bullet at the time 0.0001s and the maximum principal stress at this time is (1.129) Pa. The Fig. also shows deformation in the front end and the middle of the bullet, and the copper jacket has slide backward. Fig. (18) shows the change in the stress with time. The maximum principal stress increases with time reaching its maximum value (5.31 Pa at (2.5s. After that time the bullet are begins to leave the hybrid plate and therefore the stress is decreasing.

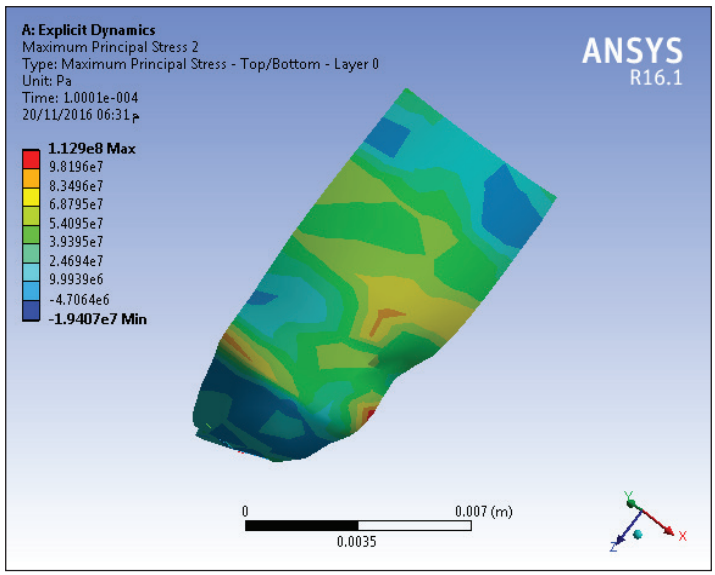

Fig. (17): The maximum principal stress for the 9mm bullet

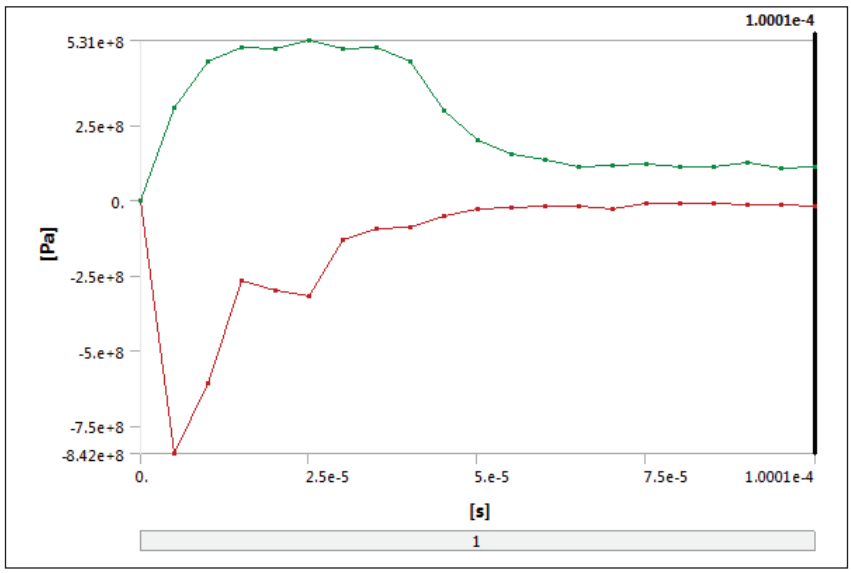

Fig. (18): The change in the stress with time for the 9mm bullet

8.4. The Maximum Shear Stress Result:

Fig. (19) shows the shear stress distribution in the hybrid plate at the time (0.0001)s and the maximum shear stress at this time is (4.8015 $\times 10^{-5}$) Pa. Fig. (20) shows the change in the shear stress with time. The maximum shear stress curve are increasing with time to reach maximum (1.201 $\times 10^{8}$) Pa at the time (1.5 $\times 10^{7}$s). After that time the hybrid layers start failing and therefore the shear stress carve decreases.

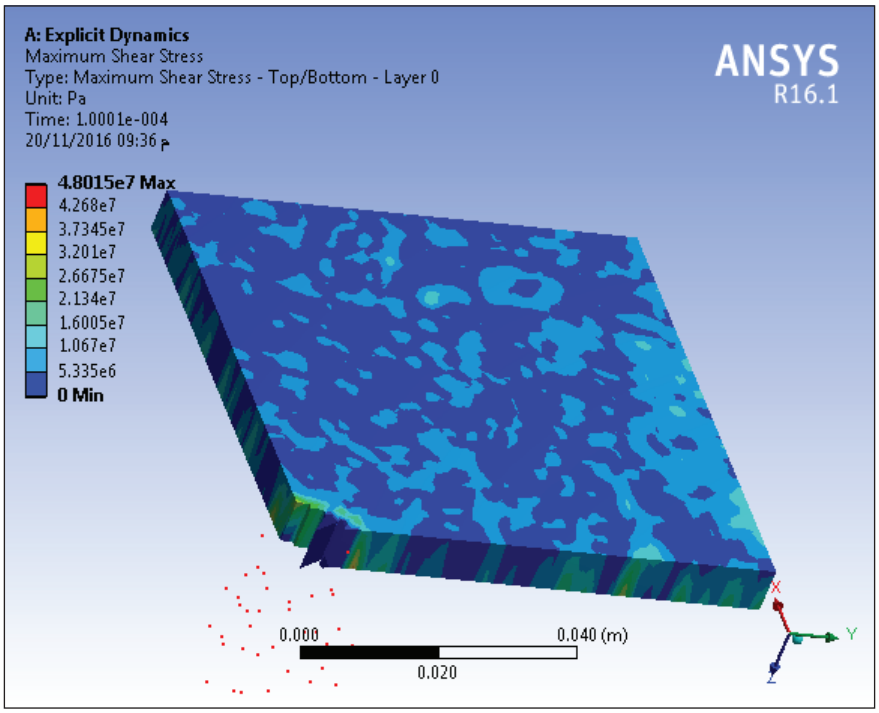

Fig. (19): The maximum shear stress distribution

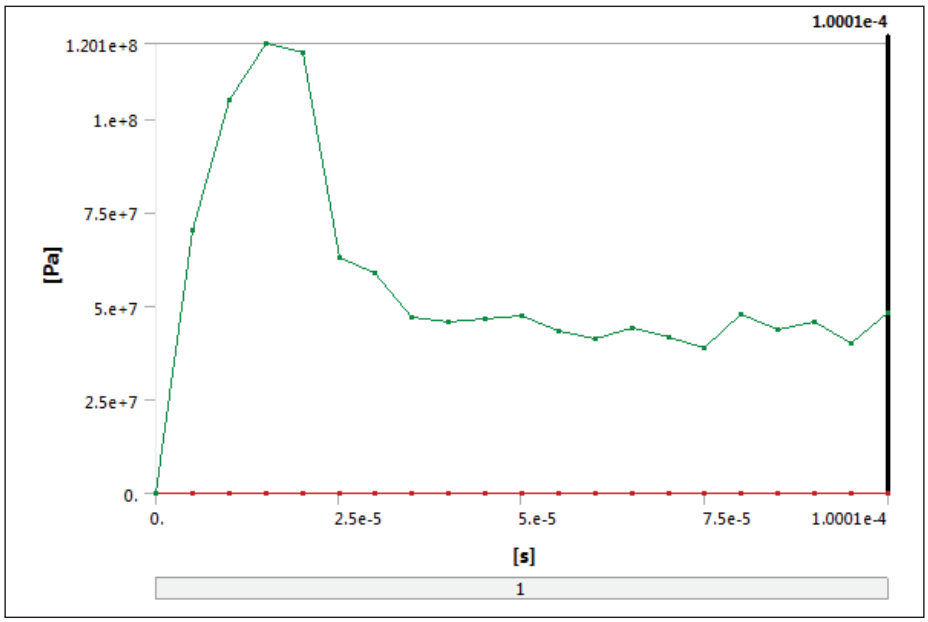

Fig. (20): The change in the maximum shear stress with time

8.5. The Maximum Principal Strain Result:

Fig. (21) shows the strain distribution in the hybrid plate at the time 0.0001s and the maximum principal strain at this time is (4.2696%). Fig. (22) shows the change in the strain with time. The maximum strain curve shows increasing with time to reach maximum at the end time.

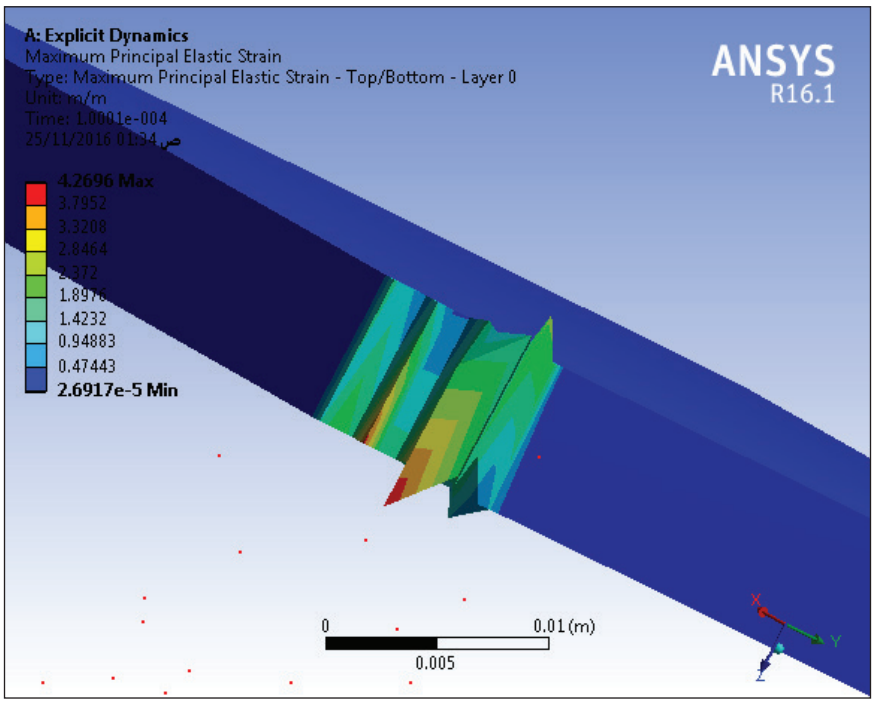

Fig. (21): The maximum principal strain

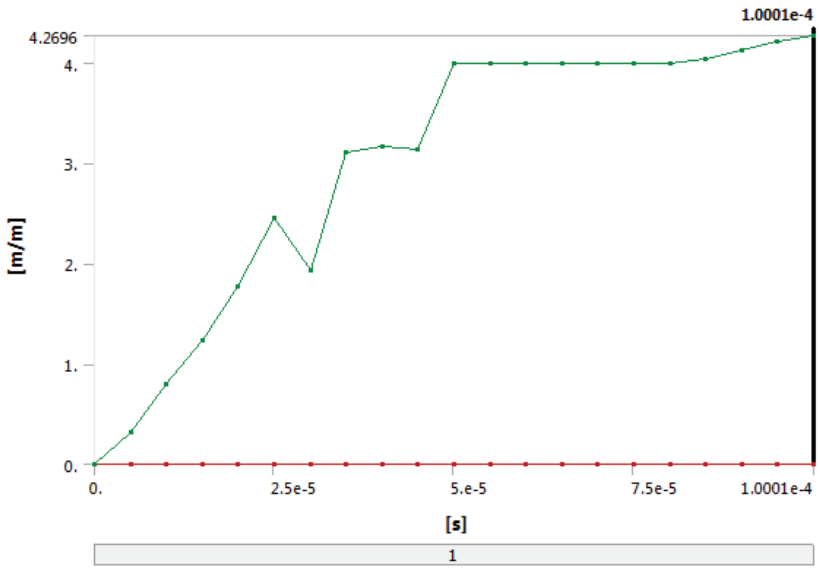

Fig. (22): The change in the maximum principal strain

8.6. The Internal Energy Result:

Fig. (23) shows the change in the internal energy with time for the hybrid plate. Both E-Glass/Epoxy and Carbon/Epoxy shows increasing in the internal energy with time until (0.0264) s. after that time the bullet start to exit the hybrid plate therefore both curves show fluctuation because of the stress waves acting on the plate until the time (0.0496) Ms. After that time the bullet is completely exit the plate therefore sharp decreasing in the internal energy happen.

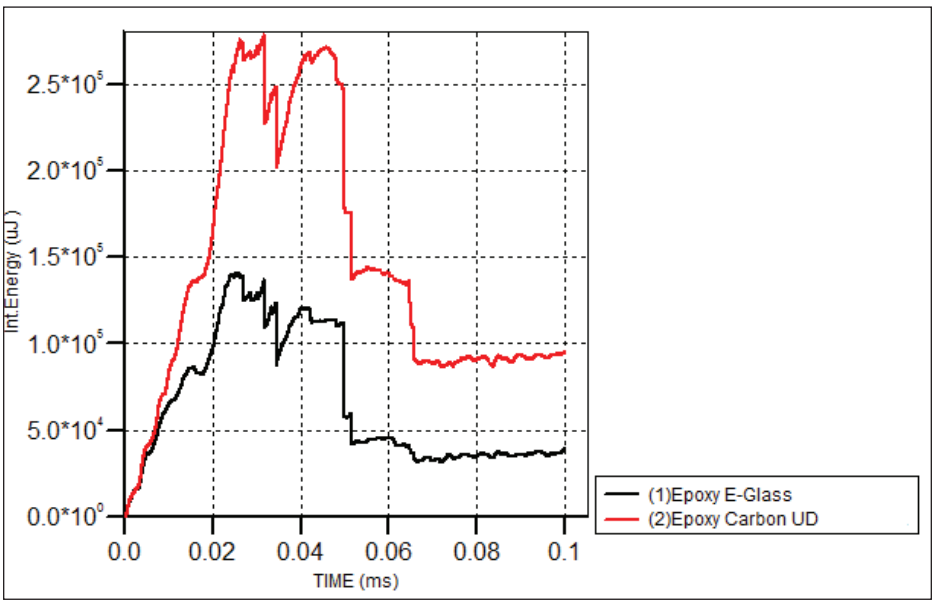

Fig. (23): The change in the internal energy with time

9. Conclusions:

1. The absorbed impact energy is increasing with the increase in the plate thickness.

2. In all cases for the bullet velocity which are above the ballistic limit the damaged area are decreasing with the increase of the bullet velocity.

3. In all cases for the bullet velocity which are below the ballistic limit the damaged area are increasing with the increase of the bullet velocity.

4. In all cases the damage was more towards the exit side of the laminates than the entry surface.

5. Adding E-Glass fibers to the carbon fibers increase the energy absorption and reduce the co

References:

[1] Harpreet, S., and Puneet, M., "Modeling Damage Induced Plasticity for Low Velocity Impact Simulation of Three Dimensional Fiber Reinforced Composite", Elsevier, J. Composite Structure 131 290-303, (2015).

[2] V. Narayanamurthy., C. Lakshmana, R., and B. N. Rao., "Numerical Simulation of Ballistic Impact on Armor Plate with a Simple Plasticity Model", Defense Science Journal, Vol. 64, No. 1, PP. 55-61, (2014).

[3] Rimantas, B., and Ausra, A., "Computational Analysis of a Bullet Against the Multilayer Fabrics in LS-DYNA", International Journal of Impact Engineering 34 1286-1305, (2007).

[4] Robert M. Jones.,"", Edition, Taylor & Francis Inc., (1999).

[5] Valery V. Vasiliev and Evgeny V. Morozov.,"", Edition, Elsevier Ltd., (2007).

[6] F. C. Campbell., "Structural Composite Materials", Structural Composite Materials., ASM International., www.asminternational.org., (2010).

[7] Bryan Harris.,"", Edition, The Institute of Materials, London., (1999).

[8] Istvan, M., Istvan, O., and Andras, S., "", Typotex Publishing House., ISBN 978-963-687-1., (2012).

[9] Rahul, S, S., R. Velmurugan., and N. K. Gupta., "Influence of Orientation and Thickness on The Response of Glass/Epoxy Composites Subjected to Impact Loading", Elsevier., J. Composite Part B 60 627-636, (2014).

[10] Elias, R., Rizal, Z., Dayang, L, M., Nawal, A., Ramin,V., and Ramin, A., "The Effect of Staking Sequence Layers of Hybrid Composite Materials in Energy Absorption Under High Velocity Ballistic Impact Condition", J. Engineering and Technology, (2013).

[11] A. A. Ramadhan., A. R. Abu Talib., A.S. Mohd., and R. Zahari., "Experimental and Numerical Simulation of Energy Absorption on Composite Kevlar 29/Polyester Under High Velocity Impact", J. Advanced Science and Engineering Research., Vol. 2, PP. 52-67, (2012).

[12] X. Chen., "", Elsevier., Woodhead Publishing., www.elsevier.com., (2016).

The Adomıan Decomposıtıon Technıques to Solve The Second Kınd Inhomogeneous Fredholm Integral Equatıon

Ali yasir Hammood Altameemi
Department of Nasiriyah, Directorate of Education in Dhi-Qar, Ministry of Education, Iraq.

Received Date: 13 / 9 / 2017
Accepted Date: 22 / 2 / 2017

الخلاصة

من البديهي القول ان معادلات فريدهولم التكاملية لها تطبيقات كثيرة في مختلف العلوم لذلك أثارت هذه المعادلات انتباه الكثير من العلماء والباحثين في ميدان علم الرياضيات.

في هذا البحث سنقدم طريقة جديدة وموثوقة لحل معادلة فريدهولم التكاملية الغير متجانسة من النوع الثاني وتسمى هذه الطريقة (Adomian Decomposition Method) وسيتم شرح آلية عمل هذه الطريقة بصيغتها الاصلية وصيغتها المعدلة في الحل من خلال مجموعة متنوعة من الامثلة.

الكلمات المفتاحية

معادلات فريدهولم التكاملية، طريقة تحليل أدوميان، طريقة التحليل المعدلة.

Abstract

It is arbitrary that, Fredholm Integral Equations have got many variable applications in different scientific domains. So, such brand of equation has attracted many scientists' and researchers' attention in mathematics science.

Then, in this research, the researcher will produce new authentic method to solve the second kind inhomogeneous Fredholm Integral Equation whose name is Adomian Decomposition Method. The procedural steps of this method will be produced and explained with its original as well as its modified modes in terms of solution process through multiple kinds of examples.

Keywords

Fredholm Integral Equations, Adomian Decomposition Method, Modified Decomposition Method.

1. Introduction

It is evident that, Fredholm Integral Equation exists in many fields of scientific applications. For example, Newton's law, stating that, the rate of change of the momentum of a particle is equal to the force acting on it, can be translated into mathematical language as a differential equation. Similarly, problems arising in electric circuits, chemical kinetics, and transfer of heat in a medium can all be represented mathematically as differential equations. These differential equations can be transformed to the equivalent integral equations of Fredholm types.In mathematic field of science, Fredholm came to the prominence as a Swedish scientist who established the brand of (Integral Equation) in the applications mathematical domain.

In this sense, this scientist was enabled to convert the boundary value problems into integral Equations which coined lately by his name. In the last years of previous century, this mode of equation (Fredholm Integral Equations) was employed effectively in variable fields of physical and chemical problems, accodingly. Consequently, the scientific contribution of such Equation engaged many researchers to study it deeply.

The researcher will produce the method to solve these problems which is termed Adomian Decomposition Method. This method was discovered by the scientist Adomian in 1990.

It is well known that, Adomian Decomposition Method has been used by many scientists and engineers in order to solve highly nonlinear integral equations which can not be solved by other methods. But this method has been used globally to solve the second kind from Volterra integral equations and Fredholm integral equations and it is impossible to be used regardimg to solve the first kind from these two equations.

Haifa Ali and Fawzi Abdelwahid have been published a scientific article under a title (Modified Adomian Techniques Applied to Non-Linear Volterra Integral Equations) in (Open Journal of Applied Sciences) in 2013 to explain Adomian Decomposition Method to solve Volterra integral equations. On the other hand, I explained the mechanism and procedures this method regarding to deal with Fredholm integral equations.

2. Basic Definitions

It is understood that, some definitions have been selected in order to help us to understand integral equations and their types generally as well as to understand Fredholm integral equations, specificly.

Definition 1. [1]An integral equation is an equation that involves the unknown function $u(x)$ that appears inside of an integral sign. The most standard type of an integral equation in $u(x)$ is of the form

$$u(x)=f(x)+\lambda\int_{g(x)}^{h(x)}K(x,t)u(t)dt \quad (2.1)$$

Definition 2. [2] If the function $f(x)=0$ in equation (2.1), then equation (2.1) is called homogeneous. Otherwise it is called inhomogeneous.

Definition 3. [3] If the limits of the integral in equation (2.1) are fixed so, is called a Fredholm integral equation.

These types of equations are classified into two types, the general form of Fredholm integral equation of the first kind is

$$f(x)=\lambda\int_{a}^{b}K(x,t)u(t)dt \quad (2.2)$$

where, the unknown function $u(x)$ appears inside the integral sign.

The second kind given by

$$u(x)=f(x)+\lambda\int_{a}^{b}K(x,t)u(t)dt \quad (2.3)$$

where, the unknown function $u(x)$ appears inside and outside the integral sign.

3. The Adomian decomposition method

Polyanin and Manzhirov conclude that, this method arises to work for linear, nonlinear integral equations, differential equations and integro-differential equations.

We shall explain the technique of this method by expressing $u(x)$ in equation (2.3) in the form of a series

$$u(x)=\sum_{n=0}^{\infty}u_n(x) \quad (3.1)$$

or equivalently,

$$u(x)=u_0(x)+u_1(x)+u_2(x)+\ldots \quad (3.2)$$

Where the elements of, $u_n(x)$, $n\geq 0$ will be identified redundantly. The mode of the Adomian decomposition method links itself with finding the elements $u_0,u_1,u_2,\ldots$ singly. The setting of these elements or components can be solved in a fair easy way through a redundant relation which includes normally simple integrals which in turn can be evaluated, simply [4].

However, Collians maintains that, firstly, we set the value of $u_0(x)$ as the term outside the integral sign of equation (2.3)

$$u_0(x)=f(x)$$

To found the redundant relation, we substitute (3.1) into the Fredholm integral equation (2.3) to obtain [5]:

$$\sum_{n=0}^{\infty}u_n(x)=f(x)+\lambda\int_{a}^{b}K(x,t)\left(\sum_{n=0}^{\infty}u_n(x)\right)dt$$

or equivalently,

$$u_0(x)+u_1(x)+u_2(x)+\ldots=f(x)+\lambda\int_{a}^{b}K(x,t)[u_0(t)+u_1(t)+\ldots]dt$$

Usman and Zubair state that, we can get the value of the components $u_0(x)$, $u_1(x)$, $u_2(x)$, ..., $u_n(x)$, ... of the unknown function $u(x)$ as follows:

$$u_0(x)=f(x)$$

$$u_1(x)=\lambda\int_{a}^{b}K(x,t)u_0(t)dt$$

$$u_2(x) = \lambda \int_a^b K(x,t)u_1(t)dt$$

$$u_3(x) = \lambda \int_a^b K(x,t)u_2(t)dt$$

$$u_{n+1}(x) = \lambda \int_a^b K(x,t)u_n(t)dt, \quad n \geq 0. \quad (3.3)$$

Then, we can get the solution $u(x)$ by

$$u(x) = u_0(x) + u_1(x) + u_2(x) + u_3(x) + \ldots$$

that converges to a closed form solution [6].

3.1. Some Applications

I have chosen these group of examples which are employed to explain the Adomian decomposition method clearly and comprehensively as compared with other modes of examples.

Example (1):

To Solve the following Fredholm integral equation

$$u(x) = e^x - x + x\int_0^1 tu(t)dt. \quad (3.4)$$

Here, Wazwaz sees that, the Adomian decomposition method assumes that, the solution $u(x)$ has a series form given in (2.1). Substituting the decomposition series (3.1) into both sides of (3.4) gives [7]

$$\sum_{n=0}^{\infty} u_n(x) = e^x - x + x\int_0^1 t\sum_{n=0}^{\infty} u_n dt. \quad (3.5)$$

or equivalently,

$$u_0(x) + u_1(x) + u_2(x) + \ldots = e^x - x + x\int_0^1 t[u_0(t) + u_1(t) + \ldots]dt$$

It is understood that, Hosseini explains that, we identify the zeroth component by all terms that are not included under the integral sign. Therefore, we obtain the following recurrence relation

$$u_0(x) = e^x - x,$$

$$u_{k+1}(x) = x\int_0^1 tu_k(t)dt, k \geq 0.$$

Hence,

$$u_0(x) = e^x - x,$$

$$u_1(x) = x\int_0^1 tu_0(t)dt = x\int_0^1 t(e^t - t)dt = \frac{2}{3}x,$$

$$u_2(x) = x\int_0^1 tu_1(t)dt = x\int_0^1 \frac{2}{3}t^2 dt = \frac{2}{9}x,$$

$$u_3(x) = x\int_0^1 tu_2(t)dt = x\int_0^1 \frac{2}{9}t^2 dt = \frac{2}{27}x,$$

$$u_4(x) = x\int_0^1 tu_3(t)dt = x\int_0^1 \frac{2}{27}t^2 dt = \frac{2}{281}x,$$

and so on [8].

Using (3.1) gives the series solution

$$u(x) = e^x - x + \frac{2}{3}x\left(1 + \frac{1}{3} + \frac{1}{9} + \frac{1}{27} + \ldots.\right). \quad (3.6)$$

It is clearly that, the infinite geometric series at the right side has $a_1 = 1$, and the ratio $r = \frac{1}{3}$. The sum of the infinite series is therefore given by

$$S = \frac{1}{1 - \frac{1}{3}} = \frac{3}{2}, \quad (3.7)$$

substituting (3.7) into (3.6) gives the exact solution

$$u(x) = e^x.$$

Example (2):

To Solve the following Fredholm inte-

gral equation

$$u(x)=\sin x-x+x\int_0^{\frac{\pi}{2}}u(t)dt \ . \quad (3.8)$$

It is knowledgeable that, Porter and Stirling maintain that, by substitute the decomposition series (3.1) into both sides of (3.8) we find

$$\sum_{n=0}^{\infty}u_n(x)=\sin x-x+x\int_0^{\frac{\pi}{2}}\sum_{n=0}^{\infty}u_n dt \ . (3.9)$$

or equivalently,

$$u_0(x)+u_1(x)+u_2(x)+\ldots=\sin x-x+x\int_0^{\frac{\pi}{2}}[u_0(t)+u_1(t)+\ldots]dt$$

Then, we set all terms that are not included under the integral sign as the zeroth component

$$u_0(x)=\sin x-x,$$
$$u_{k+1}(x)=x\int_0^{\frac{\pi}{2}}u_k(t)dt \ ,k\geq 0.$$

Hence, we obtain that,

$$u_0(x)=\sin x-x,$$
$$u_1(x)=x\int_0^{\frac{\pi}{2}}u_0(t)dt \ =x\int_0^{\frac{\pi}{2}}(\sin x-x)dt \ =x-\frac{\pi^2}{8}x,$$
$$u_2(x)=x\int_0^{\frac{\pi}{2}}u_1(t)dt \ =x\int_0^{\frac{\pi}{2}}(x-\frac{\pi^2}{8}x)dt \ =\frac{\pi^2}{8}x-\frac{\pi^4}{64}x,$$
$$u_3(x)=x\int_0^{\frac{\pi}{2}}u_2(t)dt \ =x\int_0^{\frac{\pi}{2}}(\frac{\pi^2}{8}x-\frac{\pi^4}{64}x)dt \ =\frac{\pi^4}{64}x-\frac{\pi^6}{512}x,$$
$$u_4(x)=x\int_0^{\frac{\pi}{2}}u_3(t)dt \ =x\int_0^{\frac{\pi}{2}}(\frac{\pi^4}{64}x-\frac{\pi^6}{512}x)dt \ =\frac{\pi^6}{512}x-\frac{\pi^8}{4096}x,$$

and so on [9].

Hence, by using (3.1) gives the series solution

$$u(x)=\sin x-x+\left(1-\frac{\pi^2}{8}\right)x+\left(\frac{\pi^2}{8}-\frac{\pi^4}{64}\right)x$$
$$+\left(\frac{\pi^4}{64}-\frac{\pi^6}{512}\right)x+\left(\frac{\pi^6}{512}-\frac{\pi^8}{4096}\right)x+\ldots \quad (3.10)$$

By canceling the identical terms with opposite signs in (3.10), we will obtain the exact solution

$$u(x)=\sin x.$$

Example (3):

To Solve the following Fredholm integral equation

$$u(x)=x+e^x-\frac{4}{3}+\int_0^1 tu(t)dt \ . \quad (3.11)$$

Malrknejad and Mahmoudi state that, substituting (3.1) into both sides of (3.11) gives

$$\sum_{n=0}^{\infty}u_n(x)=x+e^x-\frac{4}{3}+\int_0^1 t\sum_{n=0}^{\infty}u_n dt \ .$$

or equivalent,

$$u_0(x)+u_1(x)+u_2(x)+\ldots=x+e^x-\frac{4}{3}+\int_0^1 t[u_0(t)+u_1(t)+\ldots]dt$$

Then, we set

$$u_0(x)=x+e^x-\frac{4}{3},$$
$$u_{k+1}(x)=x\int_0^1 tu_k(t)dt \ ,k\geq 0.$$

Hence,

$$u_0(x)=x+e^x-\frac{4}{3},$$
$$u_1(x)=\int_0^1 tu_0(t)dt \ =\int_0^1 t(x+e^x-\frac{4}{3})dt \ =\frac{2}{3},$$
$$u_2(x)=\int_0^1 tu_1(t)dt \ =\int_0^1 t(\frac{2}{3})dt \ =\frac{1}{3},$$

$$u_3(x) = \int_0^1 t\, u_2(t)\,dt = \int_0^1 t(\frac{1}{3})\,dt = \frac{1}{6},$$

$$u_4(x) = \int_0^1 t\, u_3(t)\,dt = \int_0^1 t(\frac{1}{6})\,dt = \frac{1}{12},$$

and so on [10].

By using (3.1) we obtain,

$$u(x) = x + e^x - \frac{4}{3} + \frac{2}{3}\left(1 + \frac{1}{2} + \frac{1}{4} + \frac{1}{8} + \ldots.\right). \quad (3.12)$$

It is clear that, the infinite geometric series has $a_1 = 1$, and the ratio $r = \frac{1}{2}$. Therefore, the sum of the infinite series is given by

$$S = \frac{1}{1 - \frac{1}{2}} = 2.$$

The series solution (3.12) converges to the closed form solution

$$u(x) = x + e^x$$

4. The modified decomposition method

If the function $f(x)$ consists of a mixture of two or more of trigonometric functions, hyperbolic functions, polynomials, and others, the evaluation of the components $u_j, j \geq 0$ requires long time and difficult work.

Henceforth, Ali and Abdelwahid accept that, we can set the function $f(x)$ as the sum of two partial functions, such as $f_1(x)$ and $f_2(x)$. In other words, we can set,

$$f(x) = f_1(x) + f_2(x)$$

we identify the component $u_0(x)$ by one part of $f(x)$ to minimize the size of calculations. We will use the other part of $f(x)$ to find the value of the component $u_1(x)$. In other words, the modified decomposition method introduces the modified recurrence relation

$$u_0(x) = f_1(x)$$

$$u_1(x) = f_2 + \lambda \int_a^b K(x,t) u_0(t)\,dt$$

$$u_{k+1}(x) = \lambda \int_a^b K(x,t) u_k(t)\,dt . \quad (4.1)$$

We can get the exact solution $u(x)$ by correct selection of the functions $f_1(x)$ and $f_2(x)$ and by using very few iterations, and sometimes by evaluating only two or three components. The success of this method depends only on the correct choice of $f_1(x)$ and $f_2(x)$ and this can be made through experience only. A rule that may help for the correct choice of $f_1(x)$ and $f_2(x)$ could not be found until now.

We can not use this method if $f(x)$ consists of one term only, in this case the standard decomposition method can be used [11].

4.1. Some Applications

Example (1):

To Solve the Fredholm integral equation by using the modified decomposition method:

$$u(x) = e^x - 1 + \int_0^1 t\, u(t)\,dt . \quad (4.2)$$

Firstly, we will solve this equation by the "standard decomposition method" as compared with modified decomposition method.

Substituting the decomposition series (3.1) into both sides of (4.2) gives

$$\sum_{n=0}^{\infty} u_n(x) = e^x - 1 + \int_0^1 t \sum_{n=0}^{\infty} u_n dt \ . \quad (4.3)$$

or equivalently,

$$u_0(x) + u_1(x) + u_2(x) + ... = e^x - 1 + \int_0^1 t[u_0(t) + u_1(t) + ...]dt$$

we identify the zeroth component by all terms that are not included under the integral sign. Therefore, we obtain the following recurrence relation

$$u_0(x) = e^x - 1,\ u_{k+1}(x) = \int_0^1 t u_k(t) dt\ , k \geq 0.$$

Hence,

$$u_0(x) = e^x - 1,$$

$$u_1(x) = \int_0^1 t u_0(t) dt = \int_0^1 t(e^t - 1) dt$$

$$u_1(x) = \left[e^t(t-1) - \frac{t^2}{2} \right]_0^1$$

$$u_1(x) = \left[0 - \frac{1}{2} \right] - [-1] = \frac{1}{2}$$

$$u_2(x) = \int_0^1 t u_1(t) dt = \int_0^1 \frac{1}{2} t dt$$

$$u_2(x) = \left[\frac{t^2}{4} \right]_0^1 = \frac{1}{4}$$

$$u_3(x) = \int_0^1 t u_2(t) dt = \int_0^1 \frac{1}{4} t dt$$

$$u_3(x) = \left[\frac{t^2}{8} \right]_0^1 = \frac{1}{8}$$

$$u_4(x) = \int_0^1 t u_3(t) dt = \int_0^1 \frac{1}{8} t dt$$

$$u_4(x) = \left[\frac{t^2}{8} \right]_0^1 = \frac{1}{8}$$

and so on [10].

By using (3.1) we obtain,

$$u(x) = e^x - \frac{1}{2}\left(1 + \frac{1}{2} + \frac{1}{4} + \frac{1}{8} + ... \right). \quad (4.4)$$

It is clear that, the infinite geometric series has $a_1 = 1$, and the ratio $r = \frac{1}{2}$. Therefore, the sum of the infinite series is given by

$$S = \frac{1}{1 - \frac{1}{2}} = 2.$$

The series solution (4.4) converges to the closed form solution

$$u(x) = e^x$$

To solve equation (4.2) by using the modified decomposition method, Wazwaz sees that, first, we set

$$f(x) = e^x - 1$$

hence,

$$f_1(x) = e^x,\ \ f_2 = -1$$

By using (4.1) we obtain,

$$u_0 = f_1(x) = e^x$$

$$u_1(x) = -1 + \int_0^1 t u_0(t) dt\ ,$$

$$u_1(x) = -1 + \int_0^1 t e^t dt\ ,$$

$$u_1(x) = -1 + \left[e^t(t-1) \right]_0^1$$

$$u_1(x) = -1 + \left[e^1(0) - e^0(0-1) \right]$$

$$u_1(x) = -1 + [0 - (-1)]$$

$$u_1(x) = -1 + 1$$

$$u_1(x) = 0$$

It is clearly that, each component of

$u_k, k \geq 1$

is zero. So the exact solution given by [12]

$u(x) = e^x$.

Obviously, we got the solution for the equation (4.2) in a standard Adomian method after we got the value of four components. While, we were able to get the solution after we got the value of two components when we used the modified Adomian decomposition method. This mode of solution " modified Adomian decomposition method" has been employed to reduce the mathematical calculations as compared with the standard technique.

Example (2):

To Solve the Fredholm integral equation by using the modified decomposition method:

$$u(x) = 3x + e^{4x} - \frac{1}{6}(7 + 3e^{x}) + \int_0^1 t\,u(t)\,dt .$$

Almazmumy and Hendi conclude that, first, we set,

$$f(x) = 3x + e^{4x} - \frac{1}{6}(7 + 3e^{x})$$

hence,

$$f_1(x) = 3x + e^{4x}, \quad f_2 = -\frac{1}{6}(7 + 3e^{x})$$

By using (4.1) we obtain,

$$u_0 = f_1(x) = 3x + e^{4x},$$

$$u_1(x) = -\frac{1}{6}(7 + 3e^{4t}) + \int_0^1 t\,u_0(t)\,dt ,$$

$$u_1(x) = -\frac{1}{6}(7 + 3e^{4t}) + \int_0^1 t\left(3t + e^{4t}\right)dt ,$$

$$u_1(x) = -\frac{1}{6}(7 + 3e^{4t}) + \int_0^1 \left(3t^2 + te^{4t}\right)dt ,$$

$$u_1(x) = -\frac{1}{6}(7 + 3e^{4t}) + \left[\frac{3t^3}{3} + \frac{e^{4t}}{6}(4t - 1)\right]_0^1$$

$$u_1(x) = -\frac{1}{6}(7 + 3e^{4}) + \left[1 + \frac{e^{4}}{6}(3)\right] - \left[-\frac{1}{6}\right]$$

$$u_1(x) = -\frac{1}{6}(7 + 3e^{4}) + \frac{3e^{4}}{6} + \frac{7}{6}$$

$$u_1(x) = 0$$

It is clearly that, each component of

$u_k, k \geq 1$

is zero. So the exact solution given by [13]

$u(x) = 3x + e^{4x}$.

Example (3):

To Solve the Fredholm integral equation by using the modified decomposition method:

$$u(x) = \sin x - x + x\int_0^{\frac{\pi}{2}} t\,u(t)\,dt .$$

Davies states that, first, we set

$f(x) = \sin x - x$

hence,

$f_1(x) = \sin x, \quad f_2 = -x$

By using (4.1) we obtain,

$u_0 = f_1(x) = \sin x$

$$u_1(x) = -t + t\int_0^1 t\,u_0(t)\,dt .$$

$$u_1(x) = -t + t\int_0^1 t\sin t\,dt ,$$

$$u_1(x) = -t + t\left[t\sin t - t\cos t\right]_0^{\frac{\pi}{2}}$$

$$u_1(x) = -t + t\left[1 - \frac{\pi}{2}(0)\right] - [0 - 0(1)]$$

$$u_1(x) = -t + t[1 - 0]$$

$$u_1(x) = -t + t$$

$$u_1(x) = 0$$

It is clearly that, each component of $u_k, k \geq 1$ is zero. So the exact solution given by [14] $u(x) = \sin x.$

5. Conclusion

It is clear that, the integral Equations have got many applications in the fields of sciences and to help us understanding the natural phenomena in terms of design for instance. In these papers, we produce and explain new authentic and dependable method which is called (Adomian Decomposition Method) in order to solve (Fredholm integral Equations).

The researcher produced and explained accordingly, the procedural mechanism of this method in terms of its original mode as well as its modified one through variable sets of examples.

References

[1] Wazwaz A. M., "Linear and Nonlinear Integral Equations Methods and Applications", Higher Education Press, Beijing and Springer-Verlag. Berlin, (2011).

[2] Rahman M., "Integral Equations and Their Applications", WIT Press, Great Britain,(2007).

[3] Rahman M., "Applied Numerical Analysis", WIT Press, Southampton, (2005).

[4] Polyanin A. D., Manzhirov A. V., "Handbook of Integral Equations", 2nd Edition, Chapman & Hall/CRC, USA,)2008(.

[5] Collins P. J., "Differential and Integral Equations", Antony Rowe, Great Britain, (2006).

[6] Usman M., Zubair T., "A New Algorithm for Linear and Nonlinear Abel's Integral Equations", International Journal of Modern Mathematical Sciences, vol. 8, no. 2, pp. 123-129, (2013).

[7] Wazwaz A. M., "A reliable treatment for mixed Volterra-Fredholm integral equations", Applied Mathematics and Computation, vol. 127, pp. 405-414, (2002).

[8] Hosseini M. M., "Adomian Decomposition Method with Chebyshev Polynomials", Applied Mathematics and Computation, vol. 175, no. 2, pp. 1685-1693, (2006).

[9] Porter D., Stirling D. S., "Integral equations", University Press, Cambridge, (2004).

[10] Maleknejad K., Mahmoudi Y., "Taylor polynomial solution of highorder nonlinear Volterra-Fredholm integro-differential equations", Applied Mathematics and Computation, vol. 145, p. 641-653, (2003).

[11] Ali H. H., Abdelwahid F., "Modified Adomian Techniques Applied to Non-Linear Volterra Integral Equations", Open Journal of Applied Sciences, vol. 3, pp. 202-207, (2013).

[12] Wazwaz A. M., "Partial Differential Equations and Solitary Waves Theory", HEP., Springer, Beijing, (2009).

[13] Almazmumy M., Hendi F. A., "Recent Modifications of Adomian Decomposition Method for Initial Value Problem in Ordinary Differential Equations", American Journal of Computational Mathematics, vol. 2, pp. 228-234, (2012).

[14] Davies B., "Integral Transforms and Their Applications", 3rd Edition, Springer, New York, (2002).

Convergence in Possibility Measure

*Firas Hussean Maghool & **Zainb Hassan Radhy
*Department of Mathematics, College of Computer Science and Information Technology,
University of Al-Qadisiyah, Iraq,
**Department of mathematical statistic, College of Computer Science and Information Technology,
University of Al-Qadisiyah, Iraq.

Received Date: 13 / 11 / 2017
Accepted Date: 2 / 5 / 2018

الخلاصة

قياس الامكانية هي دالة مجموعة معرفة من الحقل المتكامل $\Im$ الى الفترة المغلقة [0,1] ، والمتغيرات لقياس الامكانية هي دالة قابلة للقياس من فضاء قياس الامكانية الى مجموعة الاعداد الحقيقية . في هذا البحث نسمي قياس الامكانية بقياس ρ ومتغيرات الامكانية بمتغيرات ρ .

نناقش في هذا البحث انواع من التقارب في هذا النوع من القياس وندرس العلاقة بينهم ونبرهن بعض المبرهنات المهمة.

الكلمات المفتاحية

الحقل المتكامل σ ،الفضاء القابل للقياس، قياس ρ ، التقارب، متغيرات ρ .

Vol. 9, No. 17 and 18, P. (95-102),Jun, 2019

Abstract

possibility measure as a set function $\rho : \Im \to [0,1]$ where $\Im$ is σ -field. Possibility variable is measurable function of possibility space to set of real number, in this paper we called possibility measure as ρ-measure and possibility variable is ρ-variable.

In this paper we discuss the kind of convergence in ρ-measure and study relations between them by prove some important theorem.

Keywords

σ-field, measurable space, ρ-measure, convergence , ρ-variable.

1-Introduction

Possibility theory is mathematical theory with certain kind of uncertainty and is substitutional to probability theory [1], possibility measures were introduced by Zadeh [2] in 1978.

In this paper we study the kinds of converge in ρ-measure first almost everywhere. We called almost everywhere ρ-almost everywhere . After that define almost uniformly, uniform convergence is a kind of convergence stronger than point wise convergence. It is clear from these definitions that uniform convergence imply pointwise convergence for every, and define converge in

ρ- measure many author discuss converge in measure (see [3,4,5]) in this paper we discuss converge in another measure is called ρ - measure .

In [6] discussion convergence in another measure.

After that discussion of kinds of converge in possibility variable as converge almost surely, converge in mean and converges in distribution, and prove some properties theory.

2.Preliminaries

2.1. Definition [1]

A family $\Im$ of subsets of a set X is called a σ-field on a set X if

(1) $X \in \Im$

(2) If $A \in \Im$, then $A^c \in \Im$

(3) If $A_n \in \Im, n = 1,2,...$ then $\bigcup_{n=1}^{\infty} A_n \in \Im$

$(X, \Im)$ is a measurable space, where X is a set and $\Im$ is σ-field on X

a subset A of X is called measurable to the σ-field $\Im$, for all $A \in \Im$ is called a measurable set.

2.2. Definition [5]

Let $(X, \Im)$ is a measurable space, the set function $\rho : \Im \to [0,1]$ is called ρ- measure if it is holds the following axioms:

(1) $\rho(X) = 1$, $\rho(\phi) = 0$

(2) For every sequence $\{A_n\}$ in F, we have

$$\rho(\bigcup_{n=1}^{\infty} A_n) = \max_{1 \le n \le \infty} \{\rho(A_n)\}$$

a space is a tripe $(X, \Im, \rho)$ where X is a set, $\Im$ is σ- field, ρ- measure on $\Im$.

2.3. Definition [3]

Let $(X, \Im, \rho)$ is a ρ- measure. A function $\xi : X \to R$ is said

a ρ-variable if X is a Borel measurable . i.e.

$\xi^{-1}(A) = \{X \in A \} = (\{x \in X : \xi(x) \in A \} \in$

Let ξ be a ρ-variable on $(X, \Im, \rho)$. The ρ- distribution ϑ defined as $\vartheta_x : R \to [0,1]$ of any ρ-variable $\vartheta_x(x) = \rho\{w \in X : \xi(w) \le x\}$ for any $x \in R$.

2.4. Definition [3]

Let X is a ρ- variable on $(X, \Im, \rho)$, then the expected value of X is defined as

$$E(X) = \int_0^{+\infty} \rho\{X \ge r\} dr - \int_{-\infty}^{0} \rho\{X \le r\} dr$$

2.5. Theorem

Let $(X,\Im,\rho)$ be ρ-measure space, then

(1) $0 \le \rho(A) \le 1$.

(2) $\rho(A_1 \cup A_2) \le \rho(A_1) + \rho(A_2)$

(3) If $A_1, A_2 \in F$ and $A_1 \subset A_2$ then $\rho(A_1) \le \rho(A_2)$.

(4) If $A_1, A_2 \ldots, A_n \in F$, then $\rho(\bigcup_{k=1}^{n} A_k) \le \max_{1\le k\le n}\{\rho(A_k)\}$.

(5) $\rho(\bigcup_{k=1}^{\infty} A_k) \le \sum_{i=1}^{\infty} \rho(A_k)$

(6) $\rho(A_1 \cap A_2) \le \min\{\rho(A_1)\ \rho(A_2)\}$

(7) $(2_A \cap 1_A)\rho \ge 1-(2_A)\rho+(1_A)\rho$

(8) If $A_1, A_2 \in F$, then . $\rho(A_1\text{-}A_2) \ge \rho(A_1)\text{-}\rho(A_2)$

In the following definition we define the kind of converge by ρ- measure by using the definition in [1]and [6] that was use converge another measure

2.6. Definition

Let $(X,\Im,\rho)$ ρ-measure space, sequence (f_n) of real–valued measurable function on X said be

1- converge ρ-almost everywhere to *a.e* real –valued measurable function f denoted by $f_n \xrightarrow{a.e} f$ if for each $\varepsilon > 0$ and $x \in X$ exist a set $E \in \Im$ and a natural number N such that $\rho(E) < \varepsilon$ and $|f_n(x) - f(x)| < \varepsilon$, $x \in E^c$ and each $n \ge N$.

2- converge ρ-almost uniformly to an a.e real –valued measurable function f denoted by $f_n \xrightarrow{a.u} f$ if for each $\varepsilon > 0$ there is a set $E \in \Im$ and a natural number N such that $\rho(E) < \varepsilon$ and $\|f_n - f\|_\infty = \sup_{x\in E^c}|f_n(x) - f(x)| < \varepsilon$, $n \ge N$.

3- converge in ρ-measure to an a.e real –valued measurable function f denoted by $f_n \xrightarrow{\rho} f$ if for each $\varepsilon > 0$ $\lim_{n\to\infty} \rho(x \in X : |f_n(x) - f(x)| \ge \varepsilon) = 0$.

2.7. Definition [7]

Let $(X,\Im,\rho)$ ρ-measure space is called complete if $\Im$ contains all subsets of measure zero. That is, if $H \in \Im, \rho(H) = 0$ and $A \subset H$ then $A \in \Im$.

2.8. Proposition

Let $(X,\Im,\rho)$ complete ρ-measure space and $f = g$ a.e if f is measurable on $H \in \Im$ as well g.

Proof

Let $\psi \in R$ and $N = \{x \in H : g(x) \ne f(x)\}$ then $N \in \Im$ and $\rho(N) = 0$

Now

$$\{x \in H : g(x) > \psi\} = \{x \in H \mid N : g(x) > \psi\} \cup \{x \in N : g(x) > \psi\}$$

$$= \{x \in H \mid N : f(x) > \psi\} \cup \{x \in N : g(x) > \psi\}$$

2.9. Proposition

Let $(X,\Im,\rho)$ complete ρ- measure space , f_n is sequence of measurable function on $H \in \Im$ is converges to f a.e , then f is measurable on H.

2.10 .Theorem

Let $(X,\Im,\rho)$ is ρ-measure space and f_n is sequence of

real-valued measurable functions on X, if a sequence f_n converge

ρ- almost uniformly , then it is converge in the ρ-measure to f.

Proof

$\because$ the sequence f_n converges ρ-almost uniformly to f,

there exist measurable set H and a natural number N such that

$\rho(E) < \varepsilon$ and , $\varepsilon > 0$

and

$|f_n(x) - f(x)| < \varepsilon$, $\forall$ $x \in X \mid H$ and $n \geq N$.

now , for all $n \geq N$.

$\{x \in X : |f_n(x) - f(x)| \geq \varepsilon\} \subset H$

Then $\forall$ $n \in N$

$\rho(\{ x \in X : |f_n(x) - f(x)| \geq \varepsilon\}) < \varepsilon$.

2.11. Theorem

Let $(X, \Im, \rho)$ ρ-measure space , f_n is a sequence of a.e real-valued measurable function on X , if a sequence f_n converges ρ-almost uniformly, then it is converges ρ-almost everywhere.

Proof

Let f_n converges ρ- almost uniformly to f, then for each $n \in \mathrm{N}$ there is

a measurable set A_n for $\rho(A_n) < \frac{1}{n}$ such that $f_n \to f$ uniformly of

$X \mid A_n$, Let $A = \bigcup_{n=1}^{\infty} (X \mid A_n)$ then

$$\rho(X \mid A) = \rho(\bigcap_{n=1}^{\infty} A_n) \leq \rho(A_n) = \frac{1}{n} \to 0$$

That is $\rho(X \mid A) = 0$

Then , for each $x \in A, f_n(x) \xrightarrow{a.e} f(x)$ as $n \to \infty$ we gate $f_n \to f$

2.12. Theorem

Let $(X, \Im, \rho)$ is a finite ρ-measure space and f_n is a sequence of a.e real-valued measurable function on X. If the sequence f_n converges

ρ-almost everywhere to f, then it is converges ρ-almost uniformly to f.

2.13. Theorem

Let $(X, \Im, \rho)$ is a ρ-measure space and f_n is a sequence of a.e

real-valued measurable function on X, if a sequence f_n converge in

ρ-measure to f, then there exist a subsequence f_{n_k} to f_n is converges ρ-almost everywhere to f.

Proof

Let $n_1 \in N$ such that for all $n \geq n_1$

$\rho(\{ x \in X : |f_n(x) - f(x)| \geq 1\}) < \frac{1}{2}$

Now , choose $n_2 \in N$ such that $n_2 \geq n_1$ and for all $n \geq n_2$

$$\rho(\{ x \in X : |f_n(x) - f(x)| \geq \frac{1}{2}\}) < \frac{1}{2^2}$$

Next , choose $n_3 \in N$ such that $n_3 \geq n_2$ and for all $n \geq n_3$

$$\rho(\{ x \in X : |f_n(x) - f(x)| \geq \frac{1}{3}\}) < \frac{1}{2^3}$$

Continue this process obtaining an increasing sequence (n_k) of natural numbers

$$\rho(\{ x \in X : |f_n(x) - f(x)| \geq \frac{1}{k}\}) < \frac{1}{2^k}$$

For each $k \in N$, let

$$A_k = \{x \in X : |f_n(x) - f(x)| \geq \frac{1}{k}\}$$

$\because$ for all $k \in \mathrm{N}$, $\rho(A_k) < \frac{1}{2^k}$ have

$\sum_{k=1}^{\infty} \rho(A_k)$ converges

Then have $\rho(\limsup A_k) = 0$

$$A = \limsup A_k = \bigcap_{k=1}^{\infty} \bigcup_{j=k}^{\infty} A_j$$

Choose $x \in X \mid A$, then $\exists\, j_x \in N$, $x \in X \mid A_{j_x}$ then

$$X \mid A_{j_x} = X \mid \bigcup_{k=j_x}^{\infty} \{x \in X : |f_k(x) - f(x)| \geq \frac{1}{k}\}$$

$$\bigcap_{k=j_x}^{\infty} [X \mid x \in X : |f_k(x) - f(x)| \geq \frac{1}{k}\}$$

$$\bigcap_{k=j_x}^{\infty} [x \in X : |f_k(x) - f(x)| \geq \frac{1}{k}\}$$

Then for $k \geq j_x$, $|f_k(x) - f(x)| < \frac{1}{k}$

Let $\varepsilon > 0$, $k_o \geq j_x$ such that $\frac{1}{k_o} < \varepsilon$ then for all $k \geq k_o$

$$|f_k(x) - f(x)| < \frac{1}{k} < \varepsilon$$

Therefore , for all $x \in X \mid A$, $f_k(x) \to f(x)$

Then $f_k \to f$ almost everywhere.

3. Relation between converge concept:

3.1 .Definition

Let $(X, \Im, \rho)$ is ρ-measure space

1- a sequence ζ_n is said to be convergent ρ-almost surely (a.s) to

ρ- variable ζ if exists an event β with $\rho\{\beta\} = 1$ such that $\lim_{n\to\infty} |\zeta_n(x) - \zeta(x)| = 0$, for all $x \in \beta$.

2- a sequence ζ_n is said to be convergent in ρ-measure to a ρ-variable ζ if $\lim_{n\to\infty} \rho\{|\zeta_n(x) - \zeta(x)| \geq \varepsilon\} = 0$, for all $\varepsilon > 0$.

3- a sequence ζ_n is called convergent in mean to ζ

if $\lim_{n\to\infty} E[|\zeta_n(x) - \zeta(x)|] = 0$, such that $\zeta, \zeta_1, \zeta_2, \ldots$ be ρ- variables with finite expected values.

4- a sequence ζ_n is said to be convergent in distribution to ζ if $\varphi_n \to \varphi$, at any point φ such that $\varphi, \varphi_1, \varphi_2, \ldots$ be ρ- distribution of ρ-variable $\zeta, \zeta_1, \zeta_2, \ldots$, respectively.

3.2. Proposition

Let $\zeta, \zeta_1, \zeta_2, \ldots$ be ρ- variable then ζ_n converges a.e to ζ if and only if for any $\varepsilon > 0$ we have $\rho\left(\bigcap_{m=1}^{\infty} \bigcup_{n=m}^{\infty} \{x \in X \| \zeta_n(x) - \zeta(x)| \geq \varepsilon\right) = 0$.

3.3. Definition

Let $\zeta_n, \zeta, n \geq 1$ be ρ- variable defined in the possibility measure space $(X, \Im, \rho)$. The sequence ζ_n is said converges ρ-uniformly a.s to ζ if exist $\mathrm{A}_k, \rho(\mathrm{A}_k) \to 0$ such that ζ_n converges ρ- uniformly to ζ in $\Im - \mathrm{A}_k$ for any k.

3.4. Proposition

Let $\zeta, \zeta_1, \zeta_2, \ldots$ be ρ-variable then ζ_n converges ρ- uniformly to ζ if and only if $\lim_{n\to\infty} \rho\left(\bigcup_{n=m}^{\infty} (x \in X \mid |\zeta_n(x) - \zeta(x)| \geq \varepsilon\right) = 0$

Proof

Let ζ_n be converges ρ-uniformly a.s to ζ then for $\gamma > 0$ there exist β such that $\rho\{\beta\} < \gamma$ and

ζ_n converges uniformly to ζ on $\Im \mid \beta$.

Then for any $\varepsilon > 0$ there exists $m > 0$ s.t $|\zeta_n(x) - \zeta(x)| < \varepsilon$ where $n \geq m$ and $x \in \Im \mid \beta$ that $\bigcup_{n=m}^{\infty}\{(x \in X \mid |\zeta_n(x) - \zeta(x)| \geq \varepsilon\} \subset \beta$

Then

$$\rho(\bigcup_{n=m}^{\infty}(\{ x \in X \mid |\zeta_n(x) - \zeta(x)| \geq \varepsilon) \leq \rho(\beta) < \gamma$$

Thus

$$\lim_{n\to\infty} \rho\left(\bigcup_{n=m}^{\infty}(x \in X \mid |\zeta_n(x) - \zeta(x)| \geq \varepsilon\right) = 0$$

In the second hand

Let

$$\lim_{n\to\infty} \rho\left(\bigcup_{n=m}^{\infty}(x \in \mathrm{X} \mid |\zeta_n(x) - \zeta(x)| \geq \varepsilon\right) = 0$$

For any $\varepsilon > 0$ then for any $\gamma > 0$, $k \geq 1$ there exists m_k

$$\rho\left(\bigcup_{n=m}^{\infty}(x \in X \mid |\zeta_n(x) - \zeta(x)| \geq \frac{1}{k}\right) < \frac{\gamma}{2^k}$$

Let $\bigcup_{k=1}^{\infty}\bigcup_{n=m_k}^{\infty}\{x \in X \mid |\zeta_n(x) - \zeta(x)| \geq \frac{1}{k}\}$

Then $\rho\{\beta\} < \gamma$ we have $\sup_{x\in X\mid\beta} |\zeta_n(x) - \zeta(x)| < \frac{1}{k}$ for any k=1,2,…, and $n > m_k$.

3.5. Theorem

Let $\zeta, \zeta_1, \zeta_2, \ldots$ be ρ-variable if ζ_n converges ρ- uniformly a.s to ζ then ζ_n converges a.s to ζ.

Proof

Since ζ_n converges ρ- uniformly a.s to ζ then

$$\lim_{n\to\infty} \rho\left(\bigcup_{n=m}^{\infty}(x \in X \mid |\zeta_n(x) - \zeta(x)| \geq \varepsilon\right) = 0$$

From proposition 3.3.

$$\rho\left(\bigcap_{m=1}^{\infty}\bigcup_{n=m}^{\infty}\{x \in X \|\zeta_n(x) - \zeta(x)| \geq \varepsilon\right)$$

$$\leq \rho\left(\bigcup_{n=m}^{\infty}(x \in X \mid |\zeta_n(x) - \zeta(x)| \geq \varepsilon\right)$$

Taking the limit of $m \to \infty$

$$\rho\left(\bigcap_{m=1}^{\infty}\bigcup_{n=m}^{\infty}\{x \in X \|\zeta_n(x) - \zeta(x)| \geq \varepsilon\right) = 0$$

Then ζ_n converges a.s to ζ.

3.6 .Theorem

Let $\zeta, \zeta_1, \zeta_2, \ldots$ be ρ-variable if ζ_n converges ρ- uniformly a.s to ζ then ζ_n converges in ρ- measure to ζ.

Proof

Since ζ_n converges ρ- uniformly a.s to ζ then

$$\lim_{n\to\infty} \rho\left(\bigcup_{n=m}^{\infty}(x \in X \mid |\zeta_n(x) - \zeta(x)| \geq \varepsilon\right) = 0$$

From proposition 3.3.

$$\rho\{x \in X \mid |\zeta_n(x) - \zeta(x)| \geq \varepsilon\}$$

$$\leq \rho\left(\bigcup_{n=m}^{\infty}(x \in X \mid |\zeta_n(x) - \zeta(x)| \geq \varepsilon\right)$$

then ζ_n converges in ρ-measure to ζ.

Reference

[1] R. B. Ash, "Real Analysis and probability", university of lllinois, Academic press, (1972).

[2] L. A. Zadeh, "Fuzzy sets as a basis for a theory of possibility," Fuzzy Sets and Systems, vol. 1, pp. 3–28, (1978).

[3] H. K wakernaak, "Fuzzy random variables Definition and theorem", Information Sciences 1-15, (1978).

[4] B. Liu, Y. Liu, "Expected value of fuzzy variable and fuzzy expected value Models", IEEE Transactions on Fuzzy Systems 10 (4) ,445-450, (2002).

[5] B. Liu, "Uncertainty Theory", 2nd ed., Springer-Verlag, Berlin, (2007).

[6] Cuilian You," On the convergence of uncertain sequences", Mathematical and Computer Modelling 49, 482–487, (2009).

[7] Mr. Andrew L Pinchuck, " Measure Theory Notes ", (2010).

The Effect of Annealing Temperature on The Structural and Optical Properties of Fe2O3Thin Films

Mustafa Shakir Hashim
Amira Jawad Kadhim
Esraa Akram Abbas
Reem saadi Khaleel
Physics department, Education College, Almustansiriya University, Iraq.

Received Date: 22 / 11 / 2016
Accepted Date: 19 / 2 / 2019

الخلاصة

أستخدم الرش الكيمياوي الحراري لترسيب أغشية أوكسيد الحديد على قواعد زجاجية مُسخَّنة مسبقاً بدرجة (200) ^{0}م. لُدِّنت العينات بدرجات (300)، (400) و(5000)م بمحيط جوي. وُظِفَت تقنية حُيود الأشعة السينية لدراسة تأثير التلدين على تركيب أغشية اوكسيد الحديد. ان تركيب الأغشية المرسبة تركيب عشوائي تحول الى مُتعدد التبلور بالتلدين على درجة (300) ^{0}م باتجاه مُتسيد [104]. تحسَّن التركيب البلوري مع زيادة درجة حرارة التلدين. مع المعاملة الحرارية زاد حجم الحبيبات البلورية النانوية من (23.3) الى (29.3) نانوميتر للغشاء المُرَسَّب والمُلَدَّن بدرجة (500) ^{0}م على التوالي. مَعْلَمات تركيبية أخرى كالمطاوعة الميكروية، كثافة الإنخلاعات وعدد الحُبيبات البلورية لوحدة المساحة حُسِبَت ورُبِطت مع تغيرات درجات التلدين. أستعمل مطياف الأشعة فوق البنفسجية والأشعة المرئية لدراسة تأثير التلدين على الخواص البصرية لا غشية اوكسيد الحديد. زادت فجوة الطاقة البصرية مع التلدين من (2.105) الى (2.159) الكترون فولت نتيجة نقصان الحالات المتموضعه داخل فجوة الطاقة من (0.396) الى (0.162) الكترون فولت.

الكلمات المفتاحية

التلدين، Fe_2O_3 , الحجم الحبيبي، التبلور، فجوة الطاقة، عرض الذيول.

Abstract

Chemical spray pyrolysis was used to deposit Fe_2O_3 thin films on pre-heated glass substrates at (200)^{0}C. The films were annealed at (300), (400) and (500)^{0}C at ambient atmosphere. X ray diffraction (XRD) technique was utilized to study the effect of annealing on the structure of Fe_2O_3 thin films. XRD technique was utilized to study the effect of annealing temperature on structural properties of Fe_2O_3 thin films. It was found that the as deposit thin film has amorphous structure but it became polycrystalline structure by annealing at (300) ^{0}C with dominant orientation along [104] direction. with dominant orientation along [104] direction. Crystallinity of Fe_2O_3 thin films was improved with increasing annealing temperature (Ta). Crystallite size increased with heat treatment from (23.3) to (29.3) nm for as deposit and annealed sample at (500) ^{0}C respectively. Other structural parameters like micro strain (η), dislocation density and number of crystallites per unit area were calculated and correlated with the variation of Ta. UV-Visible spectrophotometer was used to study the annealing effects on optical properties of Fe_2O_3 thin films. With increasing of Ta; optical energy gap (Eg) values increased from (2.105) to (2.159) eV due to decreasing of localized states inside the band gap from (0.396) to (0.162) eV.

Keywords

annealing, Fe_2O_3, grain size, crystallinity, energy gap, band tail.

1.Introduction:

Transition metal oxide thin films have great interest for their variable applications. Iron oxide is one of these materials with multiple applications [1]. Size reduction alters chemical and physical properties of materials and has intense recent research. Metal oxides with microstructures like nanorods, nanotubes, and nanoparticles as building blocks have been attracted great interest [2]. In applications of thin films field, Iron oxide has several employments. As a result, to its fast response Fe_2O_3 thin film is using to sense flammable gas [3]. Due to its high absorption coefficient and small energy gap it is utilized as solar cell [4]. This material is low cost, nontoxic, has environmentally friendly properties, high chemical stability, high corrosion resistance and easy to fabricate [5]. Spray pyrolysis method is a simple, versatile and low cost technique. Large number of different thin films types can prepare by this technique. By this method mixed and doped thin films are deposited [6]. Also without the need of an ultra-high vacuum by using this method it can produce large area films and it can be controlled easily [7]. Annealing process is a simple method utilized to get multiple advantageous for example it is used to improve crystallinity and minimized defects and dislocations.

In this contribution an attempt is done to study the effect of annealing on structural and some optical properties of Fe_2O_3 thin film.

2.Experimental part:

Fe_2O_3 thin films deposit on preheated glass substrates. The best examined conditions of deposition were: substrate temperature (200) ^{0}C, the time of spraying (5) s, distance between substrate and nozzle was (30±1) cm and carrier gas was filtered air. The used solution consists from $FeCl_3.6H_2O$ (1.6221) g powder as a precursor of Fe dissolved in distilled water (100) ml. To ensure the complete dissolving of powder inside the solution it was left under magnetic stirrer for (30) minute. The thickness of deposit films was determined by weight method; it was (45020±) nm. Shimadzu X-ray diffractometer is utilized to determine the orientations of Fe_2O_3 miller indices. To characterize the optical properties of the samples UV-Visible (1800) spectra photometer is used.

3.Results and discussions:

Fig. (1) shows XRD pattern of as deposit and annealed Fe_2O_3 thin films. In general; as deposit sample has amorphous structure but there is a beginning to form a peaks along (104) and (110) planes. After annealing the structure transform to polycrystalline with dominant direction at [104] beside several peaks. According to standard card (JCPDS) with number (00033-0664) annealed samples have hexagonal phase. The sharpness of all peaks increases with increasing of Ta.

After annealing at (500) ºC; the dominant peak (104) becomes sharper and higher intensity. This result attributed to the increasing of sample's crystallization and reduction of defects. The rearrangements of atoms positions inside Fe_2O_3 lattice are achieved when Ta reach to (500) ºC [8].

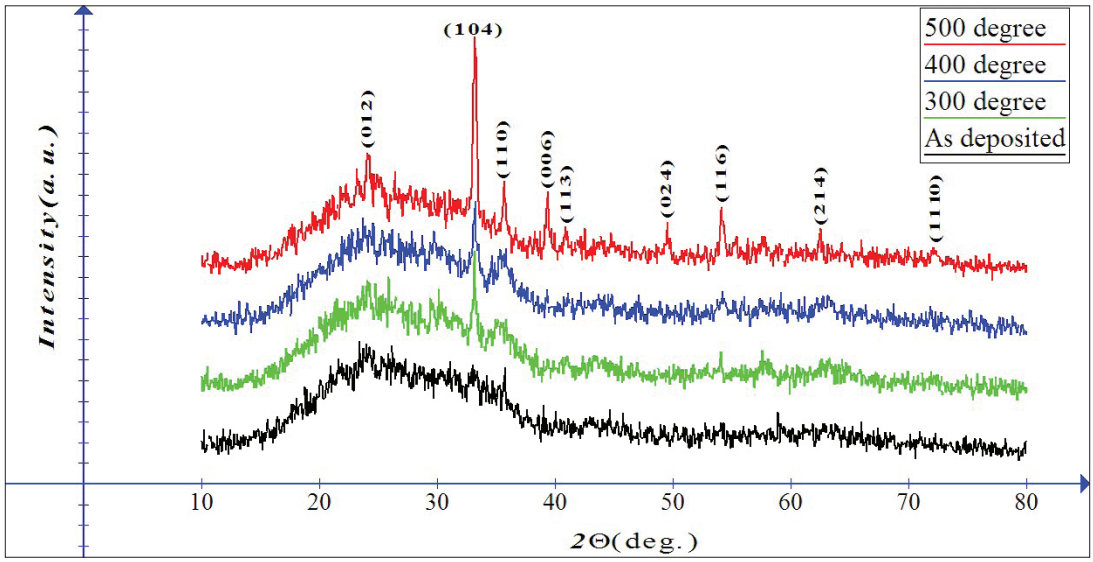

Fig. (1): XRD of as deposit and annealed samples.

For (104) peak of standard, as deposit and annealed Fe_2O_3 Table 1 shows interplanar spacing (d_{hkl}) and peak position (2Θ).

Table (1): (104) peak data at different Ta.

Sample type	2Θ (degree)	d_{hkl} (Å)	FWHM (radian)
Standard Fe_2O_3	33.152	2.7	-
As deposit	33.0798	2.70582	0.0076
Annealed at (300) °C	33.1872	2.69731	0.0075
Annealed at (400) °C	33.1897	2.69711	0.0073
Annealed at (500) °C	33.1957	2.69663	0.0061

In comparison with standard value it was found that all annealed samples have shifted positions to right and this shift increases with Ta. On the other hand, the values of interplanar spacing (d_{hkl}) for annealed samples are less than that of standard one. The behavior of 2Θ and d_{hkl} is a direct result to Bragg law. Crystallite size is calculated by using Scherrer's equation [9].

$$Crystallite\ size(\xi) = \frac{0.94\lambda}{\beta cos\theta} - - - - - -(1)$$

Where λ is x-ray wavelength, β is the broadening of the hkl diffraction peak measured at half of its maximum intensity (in radians) and θ is Bragg diffraction angle (°). Crystallite size increase with Ta until it reached to (500) °C which it exhibited a maximum size. This result is in agreement with previous reports [10].

Also Fig. (2) illustrates the decreasing of full width at half maximum (FWHM) with Ta indicating to the enhancement of the crystalline quality of the films. It is known that an increase in Ta leads to an increase in kinetic energy of the atoms and molecules making it easier for them to correct their occupancy in the lattice and then increase the size of the crystallites [8].

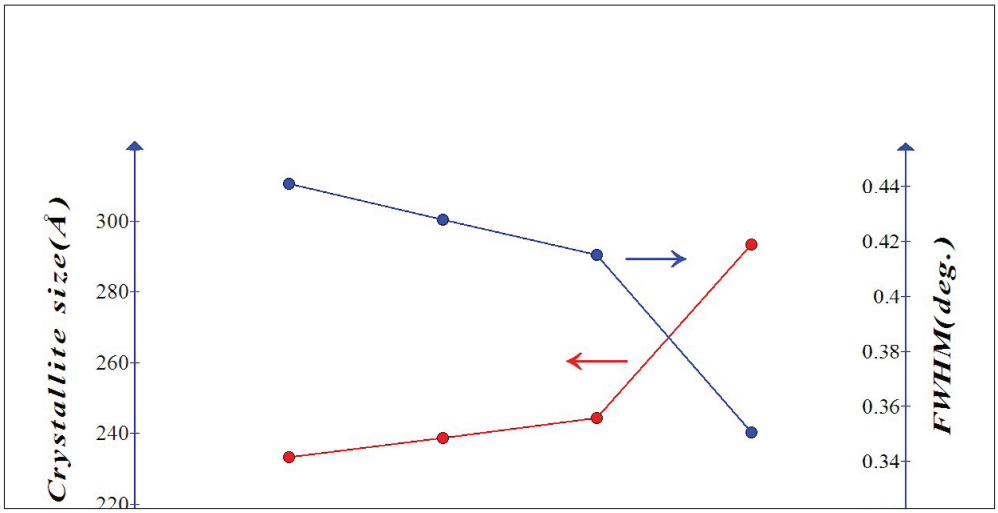

Fig. (2): crystallite size and FWHM as function to Ta.

XRD pattern is utilized again to calculate lattice constants (a_o and c_o) by using equation 2 [11].

$$\frac{1}{d^2} = \frac{4}{3}\left(\frac{h^2 + hk + k^2}{a_o^2}\right) + \frac{l^2}{c_o^2} \quad ------(2)$$

Where h,k,l are miller indices. The results of are tabulated in Table 2.

Table (2): Lattice constants for as deposit and annealed samples.

Lattice constant (Å	Standard (JCPDS)	As deposit	(Ta (°C		
			300	400	500
a_o	5.035	5.04	5.051	5.063	5.027
c_o	13.74	13.79	13.70	13.68	13.73

Table (2) confirms the recrystallization of all annealed samples due to the change in c_o parameter compared with that of as deposit sample. Current lattice constants close to that obtained by Shinde *et al.* [12]. After annealing at (300) and (400) ^{0}C (a_o) increases but it decreases at (500) ^{0}C. (c_o) has reverse behavior as equation (2) impose. For as deposit and annealed samples; Table (3) shows the values of micro strain (η), dislocation density and number of crystallites per unit area by using equation (3,4 and 5): [8].

$$\eta = \frac{|c_o(JCPDS) - c_o(XRD)|}{c_o(JCPDS)} * 100\% \quad -------(3)$$

$$N_d = \frac{1}{\xi^2} \quad ---------- (4)$$

$$Nc = \frac{t}{\xi^3} \quad ---------- (5)$$

Where t is thin film thickness [13].

Table (3): Some physical parameters of Fe_2O_3 thin films

Sample	Micro strain % (η)	Dislocation density $*10^{11}(cm^{-2})$	Number of crystallites per unit area $*10^{9}(cm^{-2})$
As deposit	0.36 -	1.83	3.4
Annealed at $(300)^0C$	0.29	1.75	3.6
Annealed at $(400)^0C$	0.43	1.67	2.97
Annealed at $(500)^0C$	0.72	1.16	1.9

A strain can define as following: it is measure of deformation representing the displacement between particles in the body relative to a reference length. For as deposited film non-uniform strain in the films is responsible on broadening in XRD profile, these strain is caused during the growth of thin film [14]. From Table 3 and Fig. (2) it is clear that the increasing of micro strain is related to the increasing of crystallite size which increases with Ta. This may due to decrease of mechanical surface-free energy with annealing. The dislocation density, defined as the length of dislocation lines per unit volume [15]. Table 3. shows the decreasing of dislocation density with Ta, the sample annealed at (500) ^0C has minimum dislocation density this can attributed to its minimum crystallite size of this sample.

Finally, the number of crystallites per unit area decreases with increasing of Ta. This result may explained by the mobility of crystallites along the surface of substrate [16]. Fig. (3) shows the variation of transmission (T%) against wavelength. There is no difference in (T%) between that of as deposit and annealed one at (300) ^0C; this may due to the substrate temperature (200) ^0C at spray time. (T%) of all samples is approximately the same beyond (600) nm. The falling of (T%) toward short wavelength at spectral region of fundamental absorption is sharper for annealed sample at (500) ^0C; this behavior may relate with the recrystallization at this temperature.

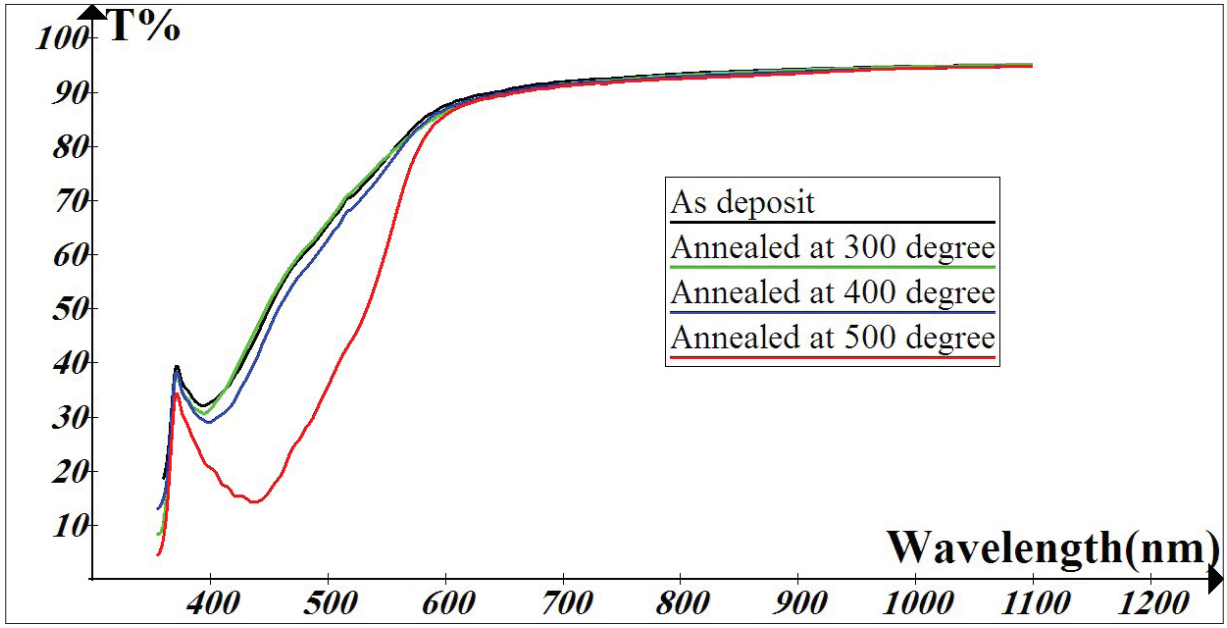

Fig. (3): T % as a function of wavelength for deposit and annealed Fe_2O_3 thin films.

For all samples (except that annealed at (500) ^{0}C there is no sharp absorption near absorption edge; this is attributed to the existence of sub-band gap levels which relate with defects. This result is expected due the minimum dislocation density of annealed sample at (500) ^{0}C as in Table (3). Fig. (4) shows the evaluation of energy gap (Eg) values for all samples. Table (4) shows the values of Eg.

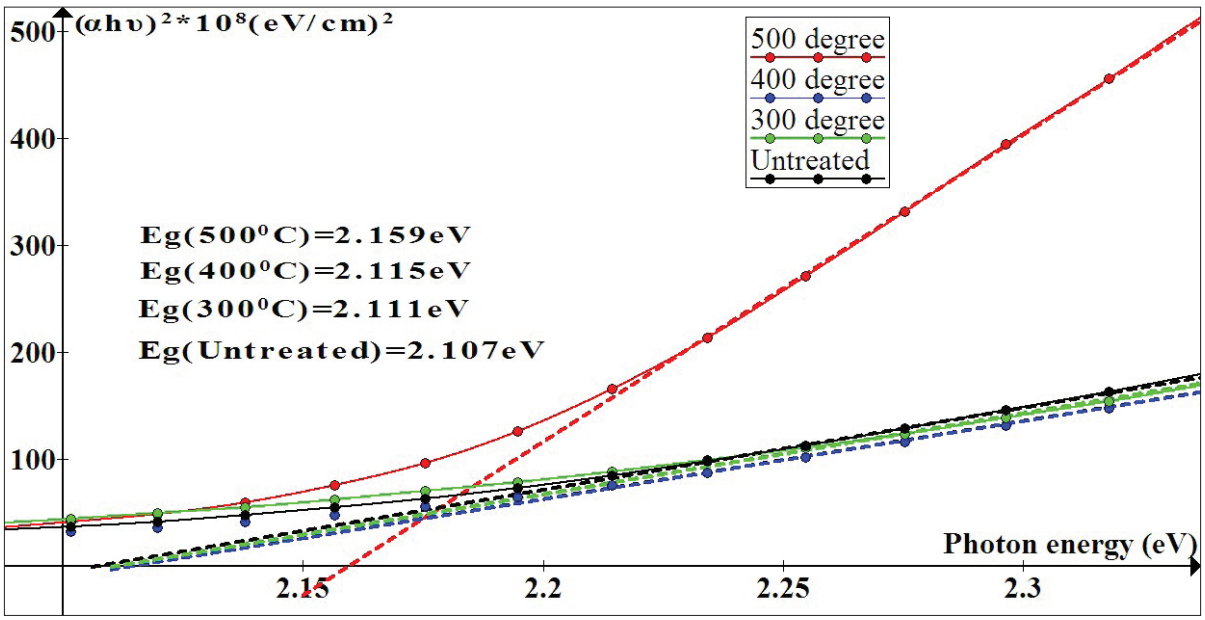

Fig. (4): energy gap (Eg) values for deposit and annealed samples.

Table (4): Eg values for all samples.

Sample type	Eg (eV)
As deposit	2.107
Annealed at (300) ^{0}C	2.111
Annealed at (400) ^{0}C	2.115
Annealed at (500) ^{0}C	2.159

The Eg values increase with Ta; this is attributed to decreasing of energy levels inside energy gap that relates with defects and dislocations [17]. Fig. (5.A) illustrates relation between lnα and photon energy for as deposit and annealed Fe_2O_3 thin films, where α is absorption coefficient. With increasing of Ta localized states in the band gap decrease as Fig. (5.B) shown. This result explains the increasing of Eg in Fig. (4) This result is in agreement with that obtained by Mubarak *et al*. [18]

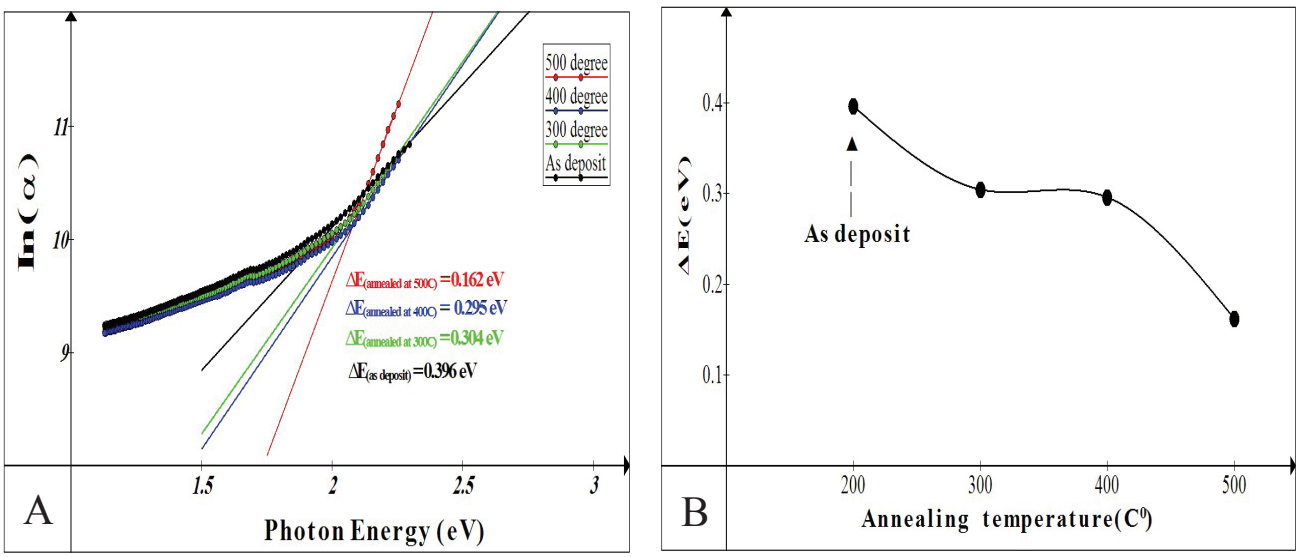

Fig. (5): A-Determination of localized states width (ΔE) (band tail energy or Urbach energy). B-ΔE verses Ta.

Fig. (6) shows the variation of α with photon energy. It is clear that the absorption coefficient increases with increasing of Ta and slightly shifted to lower photon energies. The high values of α refer to the allowed direct transition for all thin films. This result is in agreement with that obtained by Khalid [19].

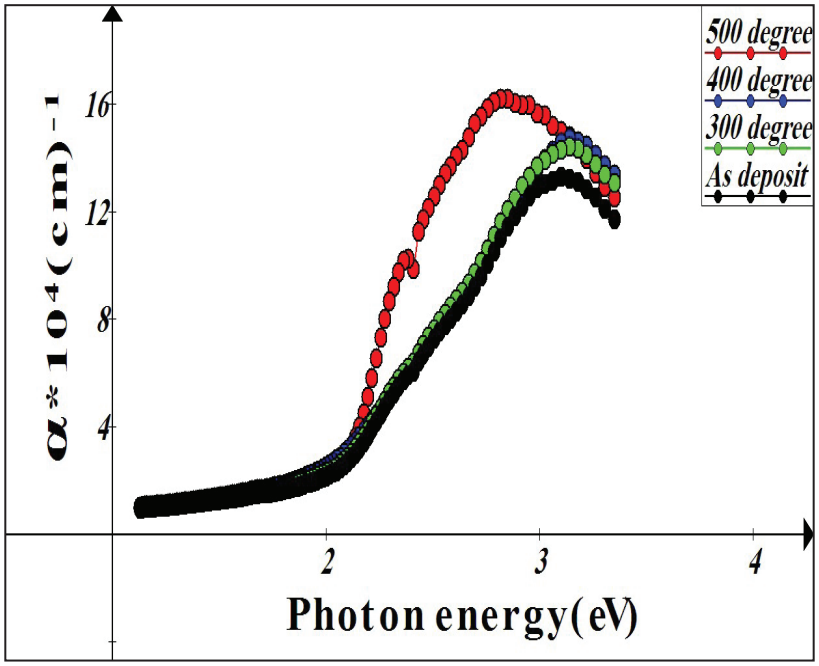

Fig. (6): absorption coefficient variation with photon energy.

4. Conclusions:

Increasing of Ta changed structural and optical properties of Fe_2O_3 thin film; crystallite sizes are increased and the crystallinity of it is improved. The annealing process reduces dislocation density and the number of crystallites per unit area but it enhances the micro strain. The Eg and the absorption coefficient values increase with annealing due to decreasing of localized states in the band gap.

References:

[1] P., Mallick, and B. N. Dash. Nanoscience and nanotechnology. 3(5),130-134, (2013).

[2] Song, Ha-Chul, Seong-Hun Park and Young-Duk Huh. Bull. Korean Chem. Soc. 28(3), 477-480, (2007).

[3] Siroky, Karel, Jana Jirešová and Lubomír Hudec. 245(1-2), 211-214, (1994).

[4] Kennedy, J.H. and D.J.Dunnwald. Electrochem. Soc. 130, 2013-2016, (1983).

[5] Hahn, Nathan T., Heechang Ye, David W Flaherty, Allen J Bard and C Buddie Mullins. Acs Nano. 4 (4),1977-1986, (2010).

[6] Akl, A., Applied Surface Science 221,319–329, (2004).

[7] Seeber, W.T., M.O. Abou-Helal, S. Barth, D. Beil, T. Höche, H.H. Afify, and S.E. Demian. Materials Science in Semiconductor Processing. 2 (1), 45–55, (1999).

[8] Mishjil, Kh., Asaad A. Kamil and Ahmed N. Jasim. Diyala journal for pure sciences.11(3),1-13, (2015).

[9] Saini, Isha, Rozra, J., Chandak, N., Aggarwal, S., Sharma, P. K. and Sharma A. Materials Chemistry and Physics 139(2-3),802-810, (2013).

[10] Jandow, N., Iraqi journal of applied physics,IJAP. 10 (3),17-22, (2014).

[11] Mitra, P., and Khan, J. Materials Chemistry and Physics. 98(2-3), 279-284, (2008).

[12] Shinde, S. S., R. A. Bansode, C. H. Bhosale, and K. Y. Rajpure. Journal of Semiconductors. 32(1),1-8, (2011).

[13] Kariper, I. Afsin. J mater res technol.5(1),77-83,

(2016).

[14] Berkum, J. G. Van, A. C. Varmcuch, R. Delhen, Th. H. Dinkeijser, and E. J. Hemeijer. J. Appl. Crys. 27,345-357, (1994).

[15] Sarma, H., Dhruba Chakrabortty and K.C. Sarma. International Journal of Innovative Research in Science Engineering and Technology. 3 (10),16957- 16964, (2014).

[16] Givargizov, E.I., Oriented crystallization on amorphous substrates, springer science, (1990).

[17] Habobi, N. Fadel, Reem S.Kh.and Muhammad H.A. Proceeding of 6 th Sci. of Karbala University. (2010).

[18] Mubarak, T.H., M. H. Abdul-Allah and W.H. Abass. J. of education college, 3, 161-168, (2012).

[19] Abass,Kh. Haneen. International Letters of Chemistry, Physics and Astronomy. 6,24-31, (2015).

Double Quantum Dot Solar Cell

*Farooq Mumtaz, *Ali Hadi Al-Batat and
**Amin Habbeb AL-Khursan
*Dept. of Physics, College of Education, Al-Mustansiriya University, Baghdad, Iraq.
**Nassiriya Nanotechnology Research Laboratory (NNRL)، Science College, Thi-Qar University, Nassiriya, Iraq.

Received Date: 5 / 12 / 2017
Accepted Date: 2 / 5 / 2018

الخلاصة

تم وضع نموذج لخلية شمسية مكونة من زوج من النقط الكمية باستخدام معادلة استمرارية الحاملات الثانوية مع نظرية مصفوفة الكثافة. هذا النموذج جعل ممكنا الأخذ بالحساب مساهمة المستوي الأرضي للنقط الكمية، الطبقة الرطبة، والحاجز تم اختبار مساهمة معدلات الاسترخاء المختلفة، والكفاءة الكمية للخلية. لقد وجد إن أعلى المعدلات يخص الإلكترونات من طبقة الحاجز إلى الطبقة الرطبة في حزمة التكافؤ، لذا فإنه للحصول على كفاءة كمية عالية لابد أن يكون هذا المعدل عالياً.

الكلمات المفتاحية

النقطة الكمية، الخلية الشمسية، الطبقة الرطبة، نظرية مصفوفة الكثافة.

Abstract

Double quantum dot solar cell system was modeled and studied by coupling the minority carrier-continuity equation with the density matrix theory. This makes it possible to take into account the contribution from ground state in quantum dot (QD) in addition to wetting layer (WL) and barrier. The contribution of different rates and the quantum efficiency are examined. It is shown that the highest rate was that from barrier-to-WL in the conduction band, thus, to get high QE one needs that this rate was high.

Keywords

Quantum–dot, Solar cell, Wetting layer, Density matrix theory.

1. Introduction

Solar cells (SCs) suffer from low conversion efficiency (~ 40%) due to the limited range of photons that can be absorbed from solar spectrum. Many approaches are used to increase efficiency, like; hot carrier relaxation, quantum cascade structure, and intermediate band structure. Nanostructures, especially QDs, has shown to cover these approaches [1, 2]. Hot carriers can be cooled in QDs by fast relaxation, cascading is possible in QDs by their inter-sub band transitions, and finally, QDs can work as an intermediate band corresponding to the bulk band gap [3-5].

Due to their promising results, In As/GaAs QDs was extensively studied as a quantum dot solar cells (QDSCs). This comes from their possibility in band gap engineering and the concept of the intermediate band solar cell (IBSC) due to increase the power conversion efficiency of QDSCs [6].

Quantum coherence can be realized in QDs by manipulating their electron-hole (e-h) transitions. This can be done by designing QD geometry to obtain localized states at the desired energies energy states. This resulting in a controlled de-phasing times [7]. This opens the way to desire a QD collections to realize the required application such us SC. Double quantum dot (DQD) structures can now be grown by self-assembling technique [8, 9].

Gioannini et. al. introduces a set of articles that models QDSCs by connecting drift-diffusion equations of bulk carriers with QD carrier dynamics to study the effect of thermal-assisted processes [10, 11-13]. Joelly et. al. compares the influence of inter-sub band optical absorption with thermal inter-sub band optical absorption [1]. Using the model presented in [10], Cedola et. al. studied the effect of excitonic carrier escape on QDSC performance [14]. In [11] Cappelluti et. al. studied the QDSC under selective doping where they predicts that high doping dominates the emission from wetting layer (WL). Plasmonic QDSCs were examined by Foroutan and Baghban in [12].

Although of these examples, which is a very few part of QDSC researches, but the use of DQD as a QDSCs was not examined to now and we examine DQDSC for the first time.

2. DQD structure

Considering a QD molecule synthesized from double dots. Each QD was an In As QD of a quantum disk shape with radius of a and height of h. QD sizes are (h= 2 nm, a =14 nm) for the first dot and (h=3.5 nm, a =13 nm) for the second dot. Each QD have one conduction and valence sub-band, while the WL conduction and valence sub-band are the reservoir states for both dots. Thus, three conduction sub-band and three valence sub- band were considered. Barrier conduction and valence bands were also considered. A sketch of energy band diagram for DQDSC structure was shown in Fig. (1).

3. The dynamical equations of DQD system

Considering the system Hamiltonian of

DQD system

$$H=\sum_{j=0}^{7}\hbar w_j\left|j\right\rangle\left\langle j\right|+\sum_{\ell\neq m}\Omega_{\ell m}e^{-iw_\ell t} \quad (1)$$

Note that $\hbar w_j$ is the energy of the j[th] state. ℓ and m any two sub band in the system and $\Omega_{\ell m}=\frac{\mu_{\ell m}E_\ell}{2\hbar}$ is the Rabi frequency and $\mu_{\ell m}$ is the momentum matrix element for the transition between ℓ and m states. Note that $\mu_{\ell m}$ is calculated considering orthogonalized plane wave between WL and QD states [5,15]. w_ℓ is the frequency corresponds to Rabi field $\Omega_{\ell m}$ as in Fig. (1).

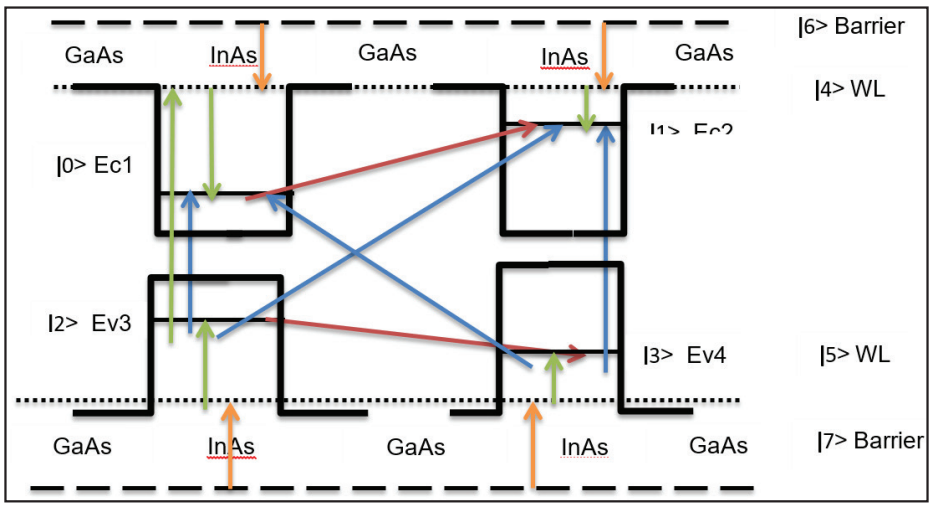

Fig. **(1):** Schematic energy diagram for DQD system with WL and barrier bands.

The dynamical approach for DQD system is written as follows [16],

$$\frac{d\rho}{dt}=-\frac{i}{\hbar}[H,\rho] \quad (2)$$

Substituting the Hamiltonian H into the above density matrix equation, two types of dynamical equations can be written for DQD system with WL and barrier shown in Fig. (1),

$$\dot{\rho}_{jj}=(\Gamma-\gamma_{jj}\rho_{jj})+i\sum_{\ell'=0}^{7}(\Omega_{j\ell'}\rho_{\ell' j}-\rho_{j\ell'}\Omega_{\ell' j}) \quad (3)$$

$$\dot{\rho}_{\ell j}=-(\mathrm{R}_{\ell j}\rho_{\ell j}+i\omega_{\ell j}\rho_{\ell j})+i\sum_{\ell'=0}^{7}(\Omega_{\ell\ell'}\rho_{\ell' j}-\rho_{\ell\ell'}c) \quad (4)$$

Note that ℓ and j are refers to the states $|0\rangle,|1\rangle,.....|7\rangle$ with $|4\rangle,|5\rangle$ are conduction and valence band WL states, and $|6\rangle,|7\rangle$ are refers to conduction and valence bands in the barrier layer. Other states are DQD states, see Fig. (1). Also, ρ_{jj} refers to the occupation of state j, the off-diagonal density matrix elements $\rho_{\ell j}$ are correspond to transitions between states ℓ and j, while γ_{jj} refers to the relaxation from state j. The Rabi frequency was $\Omega_{\ell j}=E_{\ell j}\mu_{\ell j}/2\hbar$ with $\omega_{\ell j}$ is the frequency of transitions energy $\hbar\omega_{\ell j}$. Note that $J_{n(p)}$ was the or electron (hole) diffusion photocurrent defined in the following section.

4. Relaxation rates

The relaxation rates are defined as

$$R_{ij}=[\rho_{ij}(1-\rho_{jj})/\tau_{ij}^{0}] \quad (5)$$

So for example $R_{10}=[\rho_{10}(1-\rho_{00})/\tau_{10}^{0}]$.

This includes the following rates: R_{10} (R_{23})

is the inter-DQD electron (hole) relaxation rate, QD electron (hole) capture rate from WL; R_{41} , QD hole emission rate from QD to WL; R_{35}, Inter-DQD recombination rates are R_{30} and R_{21} , and QD recombination rates are R_{31} and R_{02}.

5. Derivation of QE in solar cell

Beginning from the minority carrier-continuity equation and applying the boundary conditions on each side of the junction for holes on the n-side and electrons on the p-side, one can write [17, 18],

$$D_p \frac{\partial^2 \delta p_n}{\partial x^2} - \frac{\delta p_n}{\tau_p} + G_L = 0, \qquad (6)$$

$$D_n \frac{\partial^2 \delta n_p}{\partial x^2} - \frac{\delta n_p}{\tau_n} + G_n = 0, \qquad (7)$$

where the excess hole (electron) concentration due to external excitations is expressed as $\delta p_n = p_n - p_{n0}$, $(\delta n_p = n_p - n_{p0})$, with $p_n(n_p)$ is the total hole (electron) concentration in the n-region (p-region), and $p_{n0}(n_{p0})$ is the hole (electron) concentration without any injection. τ_p and τ_n are the hole and electron lifetimes, respectively. D_p and D_n are the diffusion coefficients for the hole and electron. The electron-hole generation rate as a function of the distance is given by [18],

$$G(x) = (1-R)\alpha(x)\Phi e^{-\alpha x} \qquad (8)$$

where R is the optical reflectivity between the air and semiconductor, $\alpha(x)$ is the coefficient absorption (as a function of the distance x) of the optical intensity, and Φ is the illuminated photon number. In Eq. (22), $G(x) = G_L$, and the generation rate is at steady state. For the p-side, the generation rate was [17]

$$G_n = (1-R)\alpha_n \Phi \exp\left\{-\left(\alpha_n x_j + \alpha_d W + \alpha_p \left[x - x_j - W\right]\right)\right\}, \qquad (9)$$

where α_p , α_n , α_d are the absorption coefficients of the $p-$, $n-$, and depletion layers, respectively, x_j is the depletion depth, and W is the depletion width. Eqs. (6) and (7) are solved by summing the homogeneous and particular solutions. After some manipulations, the relation of the hole density is derived. It is given by

$$\delta P_n = \frac{\alpha_n \phi(1-R)\tau_p}{(\alpha_n^2 L_p^2 - 1)} \left\{ \frac{\cosh(x/L_p)}{\sinh(x_j/L_p)} \left[e^{-\alpha_n x_j} - \frac{(D_p \alpha_n^2 - S_p)}{([D_p/L_p^2] - S_p)} e^{(x_j/L_p)} \right] + \frac{(D_p \alpha_n^2 - S_p)}{([D_p/L_p^2] - S_p)} e^{(x/L_p)} - e^{-\alpha_n x} \right\} \qquad (10)$$

Note that S_p is the surface recombination velocity at the p-layer. $L_p (= \sqrt{\tau_p D_p})$ is the hole diffusion length. The hole diffusion photocurrent on the n-side is dominated by the diffusion and is given by

The electron density in the p-region can be derived in a similar way to that used for the hole density. It is written as shown below,

$$\begin{aligned} \delta n_p(x) = \frac{\alpha_p \phi (1-R)\tau_n}{(\alpha_p^2 L_n^2 - 1)} e^{-(\alpha_n x_j - \alpha_d W)} \{ & e^{-(x - x_j - W/L_n)} \\ & + \frac{\sinh(x - x_j - W/L_n)}{\sinh(H'/L_n)[\frac{D_n}{L_n^2} - S_n]} [(\alpha_p^2 - S_n) e^{-\alpha_p H'}] \\ & - [\frac{D_n}{L_n^2} - S_n] e^{-H'/L_n} - e^{-\alpha_p (x - x_j - W)} \} \end{aligned} \qquad (11)$$

Note that $H' = H - x_j - W$.

After obtaining the photocurrent density in p-region from Eq. (10) using;

$$J_p \approx -qD_p \frac{\partial}{\partial x} \delta P_n. \qquad (12)$$

and a similar one for J_n .

The drift photocurrent density from the depletion region is defined by [17].

$$J_{dr} = q\phi(1-R) e^{-\alpha_n x_j} \left(1 - e^{-\alpha_d W}\right) \qquad (13)$$

while the QE is defined by the relation [17]

$$QE = \frac{\left(J_p + J_n + J_{dr}\right)}{q\phi(1-R)} \qquad (14)$$

6. Computational skills

The dynamical equations, Eqs. (3)-(4) are solved by using the 4th order Rang-Kutta method under Matlab after coupling it with the derivatives of the current densities obtained from Eqs. (10) and (11). The QE was calculated using Eq. (14). QD energy sub band are calculated under quantum disk model [19], momentum matrix elements under orthogonalized plane wave approximation were calculated [5, 15].

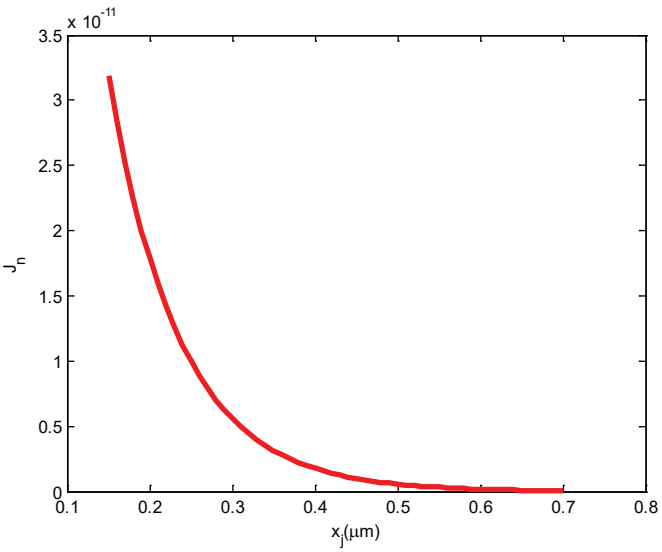

Fig. **(2):** (a) The hole current density (J_P) and (b) The electron current density (J_n) versus junction depth.

7. Results and discussion

Fig. (2-a) shows the hole current density (J_P) versus junction depth where the current density was reduced with increasing depth. Fig. (2-b) shows the electron current density (J_n) versus junction depth where the current density was reduced with increasing depth. It is shown that electron current density lowers that of holes in Fig. (2-a) by three orders.

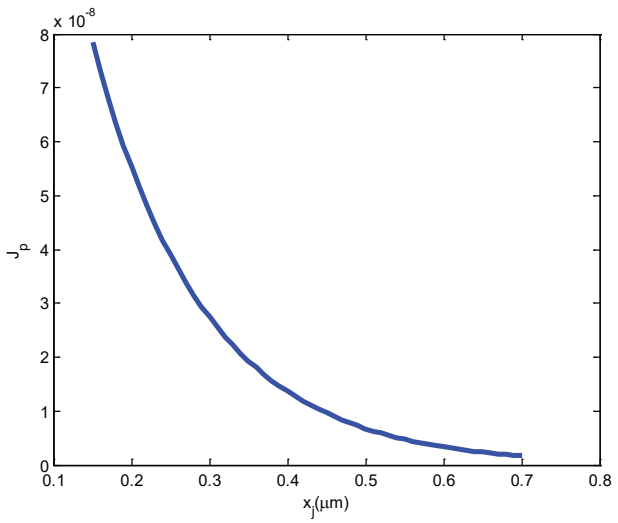

7.1. Effect of DQD rates

A comparison between e-h model with exciton model was done in this section. Fig. (3) shows the variation of occupation probability vs the inter-DQD capture rate R_{10}. It is shown that ρ_{00} occupation in the exciton model exceeds the separate e-h model, in the contrary to the case of ρ_{11} occupation. In the e-h model, while ρ_{00} increasing with R_{10}, ρ_{11} descending. The bistability behavior was shown in both ρ_{00} and ρ_{11} at low R_{10} rate. In the exciton model the occupations are constant with changing R_{10} rate.

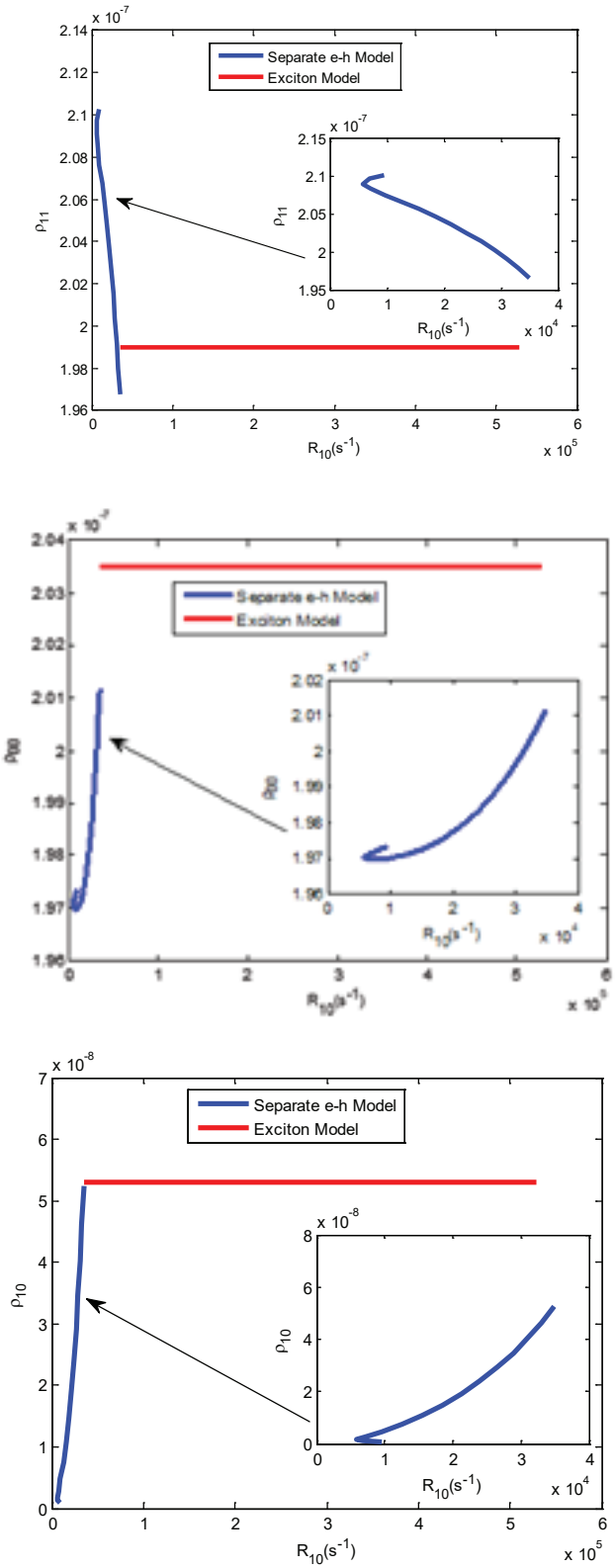

Fig. **(3):** The variation of occupation probabilities vs the inter-DQD capture rate R_{10}: (a) ρ_{00}, (b) ρ_{11}, (c) ρ_{10}.

Fig. (4) shows the variation of occupation probability vs the interdot transition rate R_{20}. Also ρ_{00} occupation in the exciton model exceeds the separate e-h model, in the contrary to the case of ρ_{22} occupation. In the e-h model, while ρ_{00} increasing with R_{20}, ρ_{22} descending. Also occupations are constant with changing R_{20} rate in the exciton model. The rate R_{20} was greater than R_{10}.

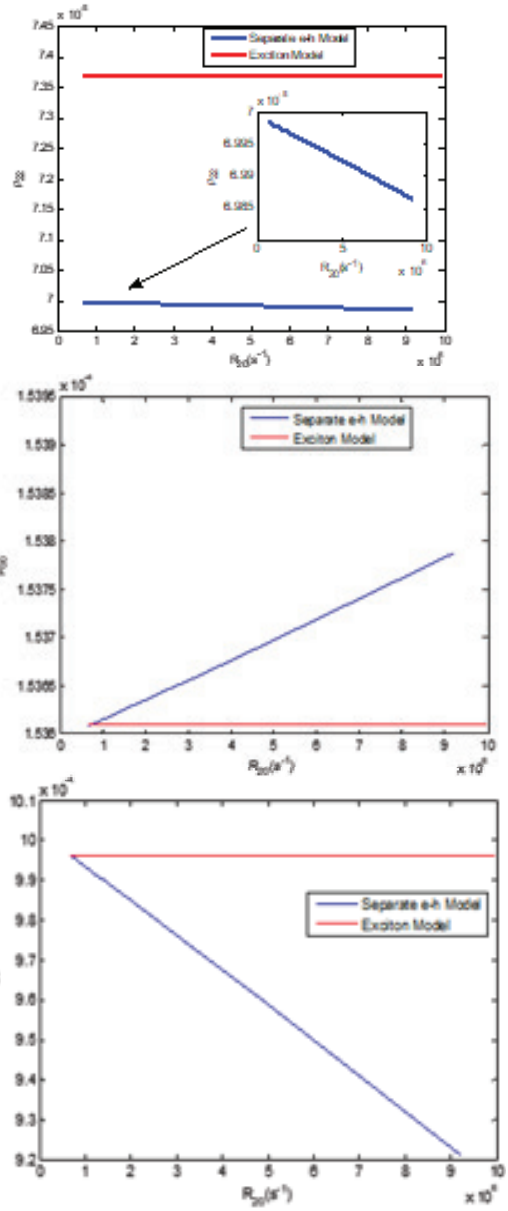

Fig. **(4):** The variation of occupation probabilities vs the interdot transition rate R_{20}. R_{10}: (a) ρ_{00}, (b) ρ_{22}, (c) ρ_{20}.

Fig. (5) shows the variation of occupation probability vs the QD capture rate R_{40} from WL. Here, the occupations in the exciton model lower than that in the separate e-h model. In the e-h model, the rate R_{40} in the e-h model was less by one order than the exciton model. The capture rate R_{40} was smaller than both R_{20} and R_{10} which is due to the difference between continuum WL and completely quantized QDs. Note that one must refers to the lowest momentum matrix element for transitions between WL and QDs.

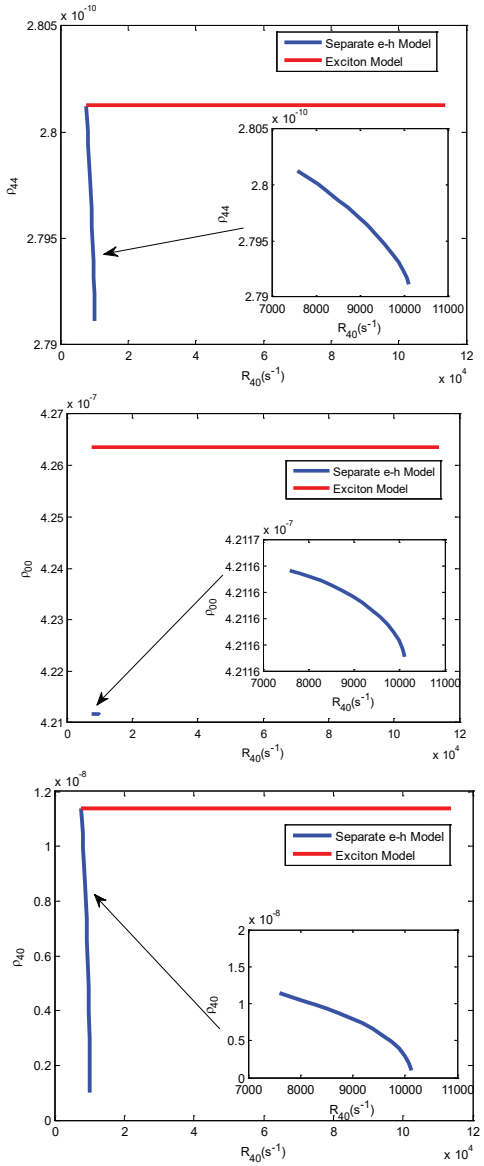

Fig. (5): The variation of electron occupation probability vs the QD capture rate R_{40}. (a) ρ_{00}, (b) ρ_{44}, (c) ρ_{40}.

Fig. (6) shows an important property of using DQD structure. While the capture rate R_{40} from WL to QD was the least compared with QD-QD transition rates, the captur rate R_{41} from WL to another QD was high. The separation between WL and QD energy state was one of important parameters controlling the momoentum matrix element. This can speed up the processes in DQD structure. Multistability behavior in both ρ_{11} and ρ_{44} occupations was obvious in the insets of figures.

Fig. (7) shows the electron capture rate from barrier to WL R_{64} vs carrier occupations ρ_{44}, ρ_{66}, and ρ_{64}. Compared with the above figures, it is shown that this WL capture rate R_{64} was the highest rate in this DQDSC struture. While WL carrier occupation ρ_{44} was very low, the carriers in the barrier layer ρ_{66} are very high. Except the case of $R_{10}-\rho_{11}$ (Fig. 2 (b)) where the occupation ρ_{11} in e-h model exceds that in exciton model at some rates, all other occupations in the exciton model exceeds their values in e-h model. Here, ρ_{66} in e-h model exceeds that in the exciton model at all R_{64} rate. From Figs. (3-7), it is shown that the highest rate was that from barrier-to-WL in the conduction band (R_{46}).

Fig. (8) shows the hole capture rate from QD to WL R_{25} vs carrier occupations ρ_{22}, ρ_{55}, and ρ_{25}. For these three occupations, the values of exciton model exceeds e-h model.

7.2. Effect of junction depth

Let us examine the carrier occupations of

structure states versus the junction depth x_j. Fig. (9) shows electron occupations ρ_{00}, ρ_{11} in the QDs. Occupations in the exciton model exceeds that in the e-h model.

Fig. (10) shows hole occupations ρ_{22}, ρ_{33} in the QDs where they are in the same range of QD electron occupations in Fig. (10). For ρ_{33}, e-h model exceeds the exciton model.

Fig. (11) shows electron occupations of WL (ρ_{44}) and barrier (ρ_{66}) vs junction depth. Low WL occupation, as also seen in Fig. (7), with high electron occupation in the barrier. While the carriers are ascending with junction depth x_j in WL, they are descending with x_j. Carriers in WL using exciton model exceeds that calculated from e-h model while both models are conicides in $\rho_{66} - x_j$ curves for barrier layer.

Fig. (12) shows hole occupations of WL (ρ_{55}) and barrier (ρ_{77}) vs junction depth. Hole occupation was also low in WL and high in the barrier. Hole are constant with junction depth x_j in WL, while they are descending with x_j in the barrier. Carriers in WL using exciton model exceeds that calculated from e-h model while both models are conicides in $\rho_{77} - x_j$ curves for barrier layer.

7.3. Quantum efficiency of DQDSC

Fig. (13) shows QE vs inter-DQD capture rate R_{10}. QE appears at R_{10} rate in exciton model higher than that of e-h model. This is a result from the occupation of CB QD states shown in Fig. (3). The same behavior was also shown for CB-CB, and CB-VB QD states. As an example Fig. (14) shows QE vs rates of CB-VB QD states. This behavior then changes for WL-QD rate R_{40} as in Fig. (15) where QE appears at low rate for exciton model. For WL-barrier, QE appears at the same rate R_{64} as in Fig. (16).

From Figs. (14-16), it is shown that the rates in the exciton model are more efficient in changing QE while the rate R_{64} was efficient in both models. This returns to the importance of both WL (ρ_{44}) and barrier (ρ_{66}) occupations as shown in Fig. 13. Thus, to get high QE one needs to have high R_{64}. This also comes from our recent conclusion that WL washes out the modes due to its long capture time compared with that of inter-dots [20]. Practically one can chosse a barrier material that having a long relaxation time to WL compared with relaxation between dot state.

8. Conclusions

By coupling the minority carrier-continuity equation with the density matrix theory, DQD solar cell system was modeled and studied for the first time. The momentum contributions for QD-QD, QD-WL, and barrier-WL where used to calculate the contribution from ground and excited states in QD in addition to WL and barrier. The contribution of different rates and the quantum efficiency are examined. It is shown that the highest rate was that from barrier-to-WL in the conduction band (R_{46}). Thus, to get high QE one needs to have high R_{46}.

References

[1] Greg Jolley, Lan Fu, Hao Feng Lu, Hark Hoe Tan and Chennupati Jagadish "The role of inter-sub band optical transitions on the electrical properties of InGaAs/GaAs quantum dot solar cells", Prog. Photovolt: Res. Appl. 21, 736–746, (2013).

[2] A. J. Nozik,"Quantum dot solar cells", Physica E 14 115–120, (2002).

[3] [3] Amin H. Al-Khursan, M. K. Al-Khakani, K.H. Al-Mossawi, "Third-order non-linear susceptibility in a three-level QD system", Photon and Nanostruct – Fundamentals Appl. 7, 153–160, (2009).

[4] Amin H. Al-Khursan "Intensity Noise Characteristics in Quantum-Dot Lasers: Four-Level Rate Equations Analysis", Journal of Luminescence, 113, 129-136, (2005).

[5] Ektefaa Rehman and Amin H. Al-Khursan,"All-Optical Processes in Double Quantum Dot Structure", Applied Optics 55, 7337-7344, (2016).

[6] A. Luque, "Increasing the efficiency of ideal solar cells by photon induced transitions at intermediate levels", Phys. Rev. Lett. 78, 5014–5017, (1997).

[7] J. M. Villas-Boas, A. O. Govorov, and Sergio E. Ulloa, "Coherent control of tunneling in a quantum dot molecule", Physical Review B 69, 125342, (2004).

[8] S. Michael, W. W. Chow, and H. C. Schneider, "Group-velocity slowdown in a double quantum dot molecule" Physical Review B 88, 125305, (2013).

[9] H. S. Borges, L. Sanz, J. M. Villas-Boas, O. O. Diniz Neto, and A. M. Alcalde, "Tunneling induced transparency and slow light in quantum dot molecules", Physical Review B 85, 115425, (2012).

[10] M. Gioannini, A. Cedola, N. Di Santo, F. Bertazzi and F. Cappelluti "Simulation of quantum dot solar cells including carrier inter-sub band dynamics and transport IEEE J. Photovoltic 3, 1271, (2013).

[11] F. Cappelluti, M. Gioannini, A. Khalili, "Impact of doping on InAs/GaAs quantum-dot solar cells: A numerical study on photovoltaic and photoluminescence behavior", Solar Energy Materials & Solar Cells 157209–220, (2016).

[12] M. Gioannini, A. Cedola, F. Cappelluti, "Impact of carrier dynamics on the photovoltaic performance of quantum dot solar cells", IET Optoelectronics 9, 69-74, (2015).

[13] A. Cedola1, F. Cappelluti and M. Gioannini, "Dependence of quantum dot photocurrent on the carrier escape nature in InAs/GaAs quantum dot solar cells", Semicond. Sci. Technol. 31, 025018, (2016).

[14] A. Cedola, M. Cappelletti, and E. L. Peltzer, and Y. Blancá, " Study of Excitonic Carrier Dynamics in Quantum Dot Solar Cells by Numerical Simulations", Argentina conference of micro-nano electronics, technology and applications, (2016).

[15] Haneen Akram and Amin H. Al-Khursan, "Second-order nonlinearity in ladder plus-Y configuration in double quantum dot structure", Applied Optics 55, 9866-9874,

(2016).

[16] S. L. Chuang, Physics of Photonic devices, John-Wiley, (2009).

[17] S. N. Dwara and Amin H. Al-Khursan, "Quantum Efficiency of InSbBi Quantum Dot photodetector", Applied Optics 54, 9722-9727, (2015).

[18] S. N. Dwara and A. H. Al-Khursan, "Two-window InSbBi quantum-dot photodetector", Applied Optics 55, 5591-5595, (2016).

[19] H. Al-Husaini, Amin H. Al-Khursan and S. Y. Al-Dabagh,"III-N QD Lasers", Open Nanoscience J. 3, 1-11,(2009).

[20] Hussein B. Al Husseini, Kais A. Al Naimee, Amin H. Al-Khursan and Ali. H. Khedir, "External Modes in Quantum Dot Light Emitting Diode with Filtered Optical Feedback", Journal of Applied Physics, 119, 224301, (2016).

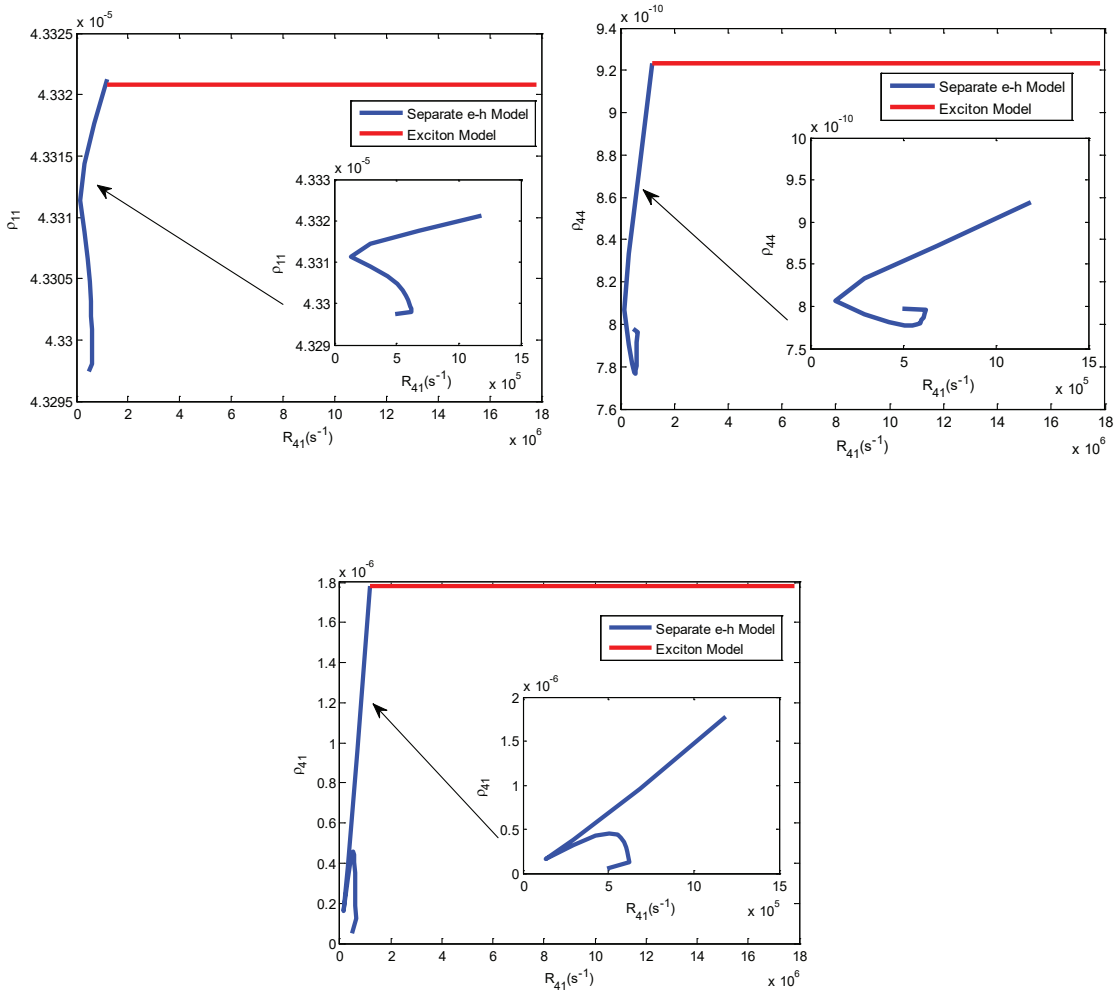

Fig. 6: The variation of electron occupation probability vs the QD capture rate R_{41}. (a) ρ_{11}, (b) ρ_{44}, (c) ρ_{41}.

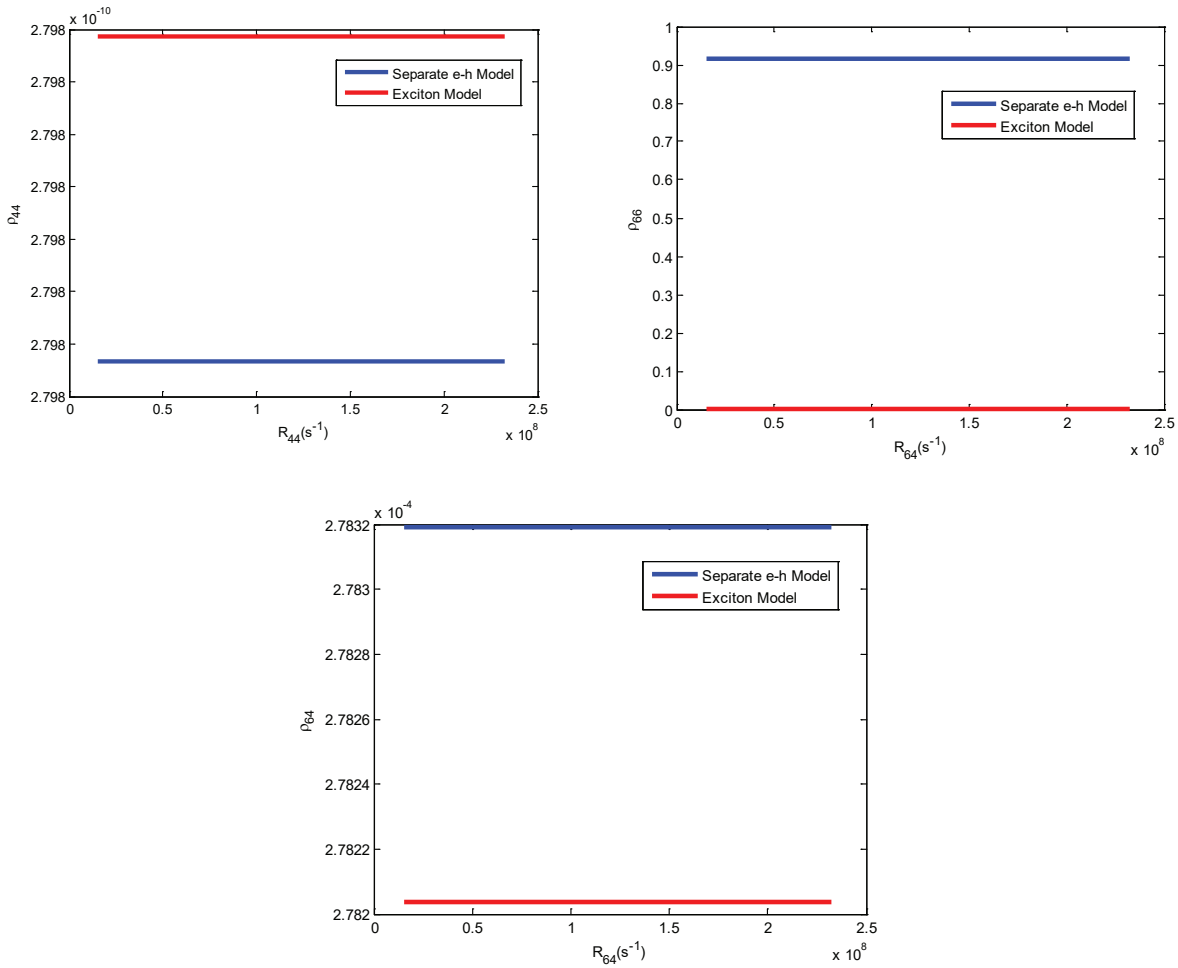

Fig. 7: The electron capture rate from barrier to WL R_{64} vs electron occupations (a) ρ_{44}, (b) ρ_{66}, (c) ρ_{64}.

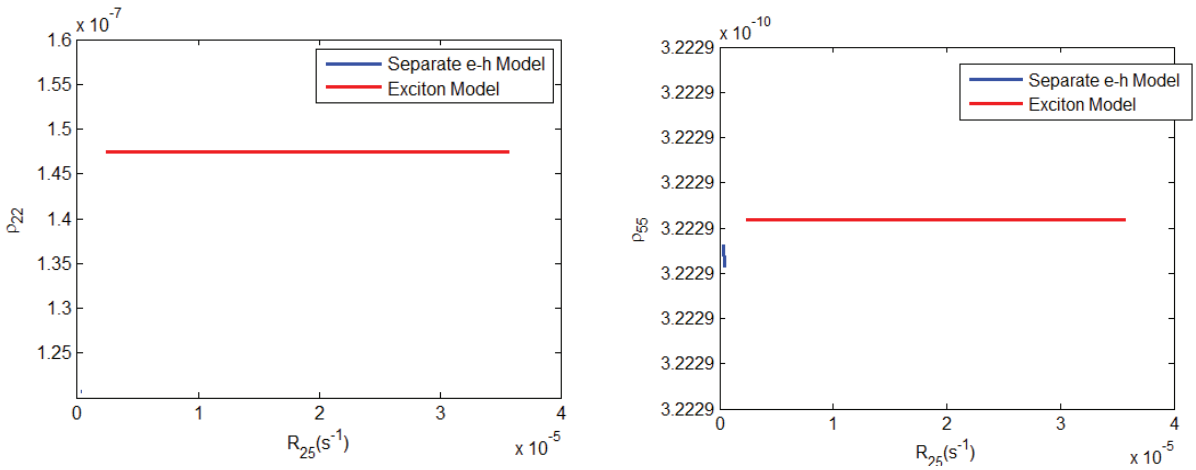

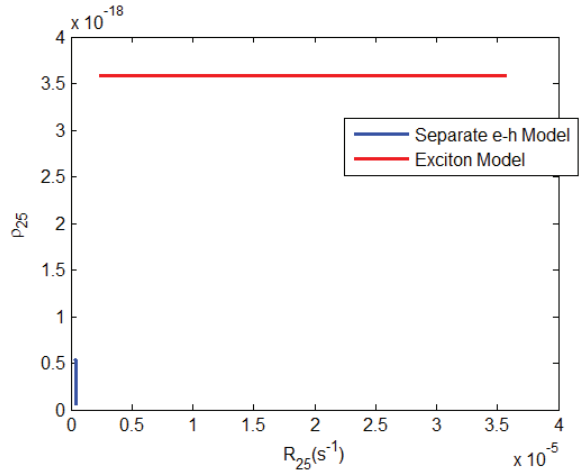

Fig. 8: The hole capture rate from QD to WL R_{25} vs hole occupations (a) ρ_{22}, (b) ρ_{55}, (c) ρ_{25}.

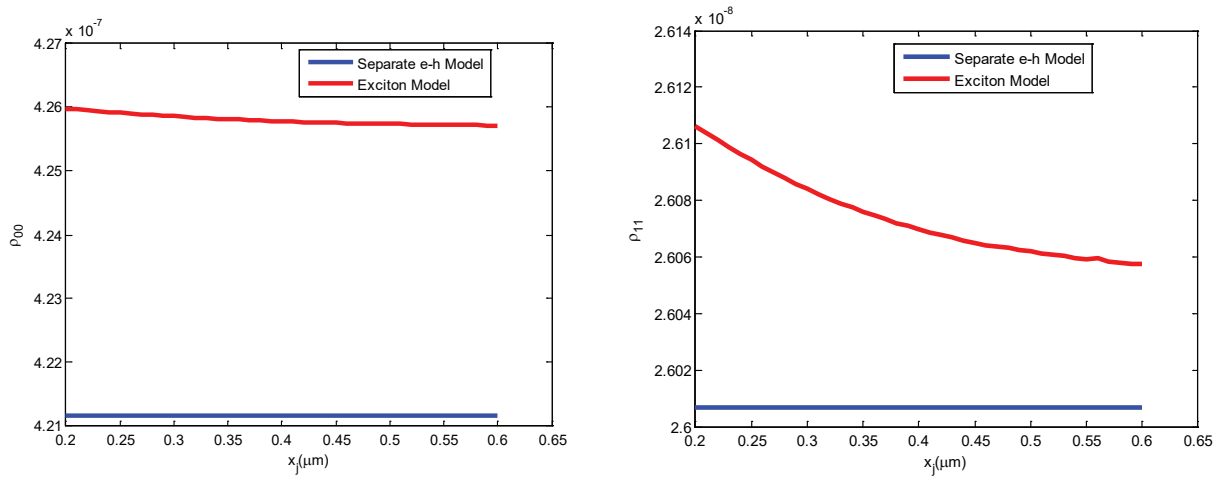

Fig. 9: Electron occupations ρ_{00}, ρ_{11} in the QDs versus the junction depth x_j.

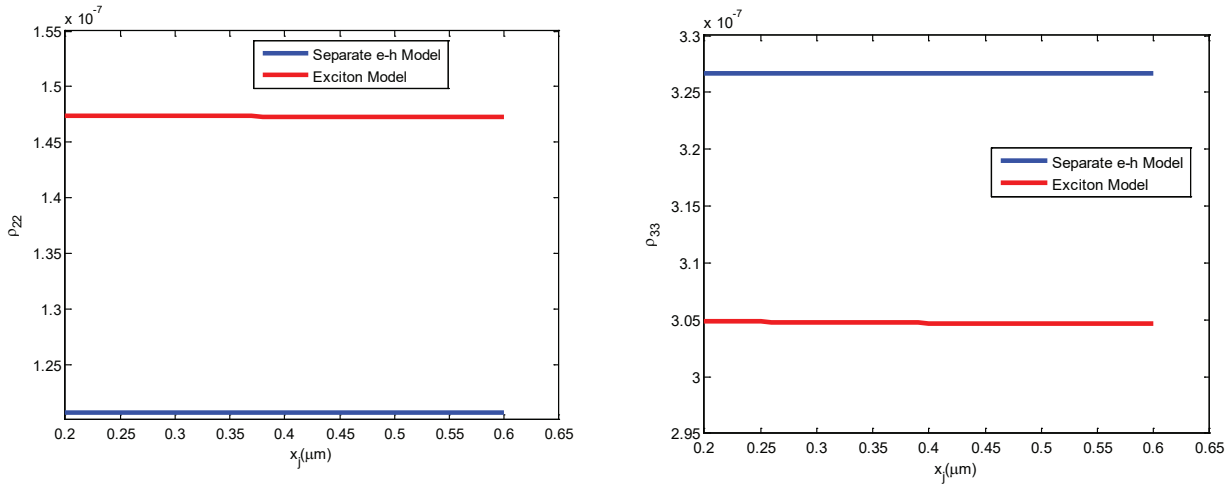

Fig. 10: Hole occupations ρ_{22}, ρ_{33} in the QDs versus the junction depth x_j.

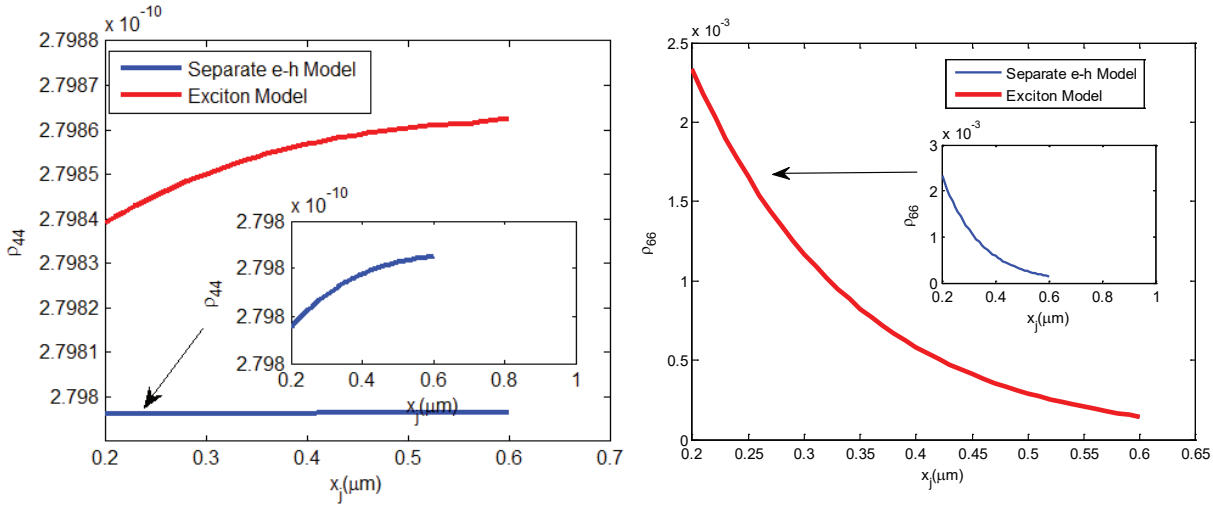

Fig. 11: Electron occupations of WL (ρ_{44}) and barrier (ρ_{66}) versus the junction depth x_j.

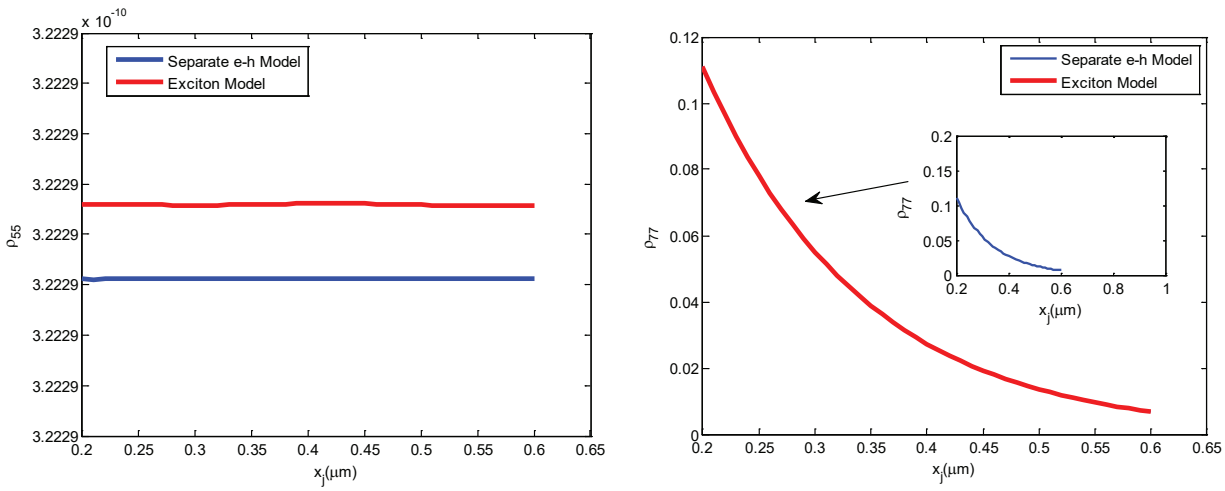

Fig. 12: Hole occupations of WL (ρ_{55}) and barrier (ρ_{77}) versus the junction depth x_j.

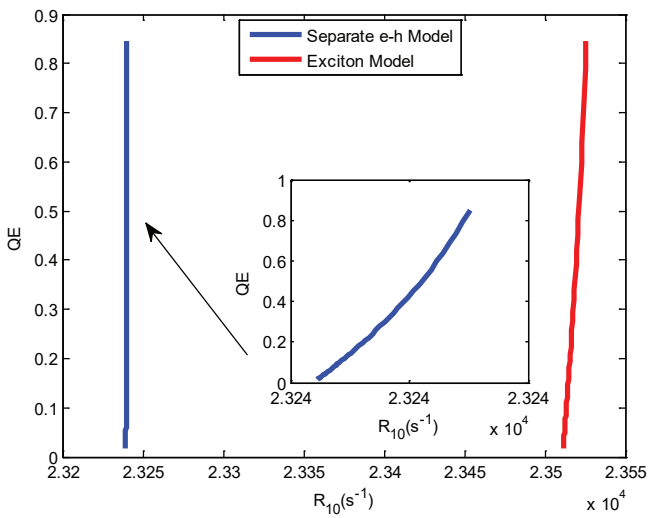

Fig. 13: QE vs inter-DQD capture rate R_{10}.

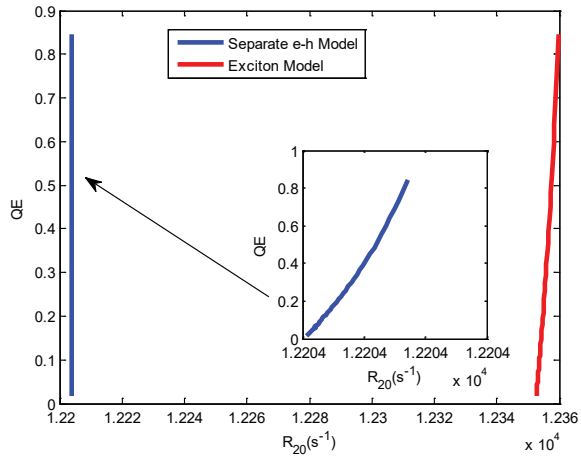

Fig. 14: QE vs rates of CB-VB QD states.

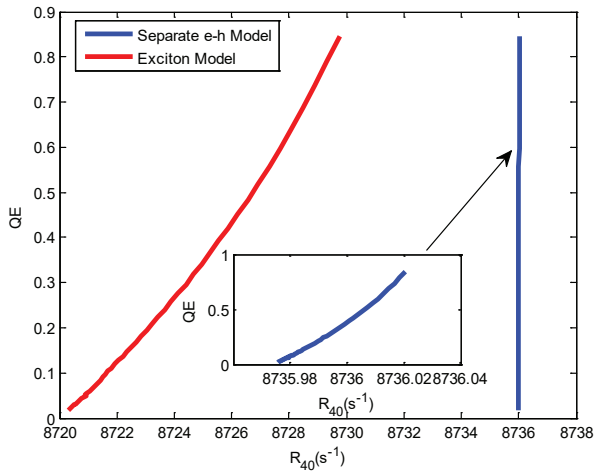

Fig. 15: QE vs WL-QD rate R_{40}.

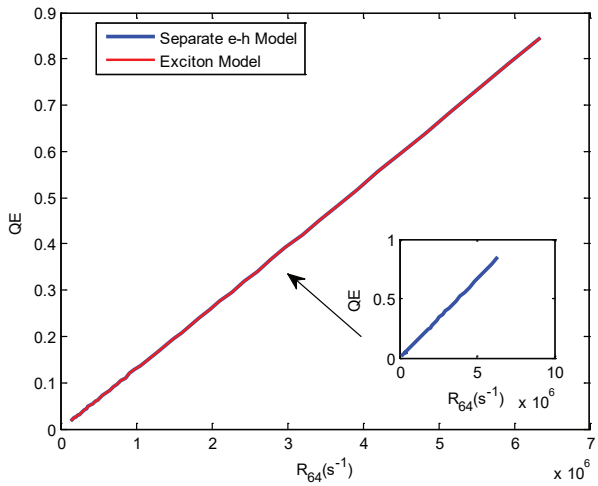

Fig. 16: QE vs WL-barrier rate R_{64}.